AD-A154 133 A SURVEY OF THE TURBULENCE IN THE MARINE SURFACE LAYER FOR THE OPERATION O..(U) VIRGINIA POLYTECHNIC INST AND STATE UNIV BLACKSBURG DEPT OF E.. H W TIELEMAN MAR 85 VPI-E-85-10 N00014-83-K-0658 F/G 4/2 1/2 NL

UNCLASSIFIED

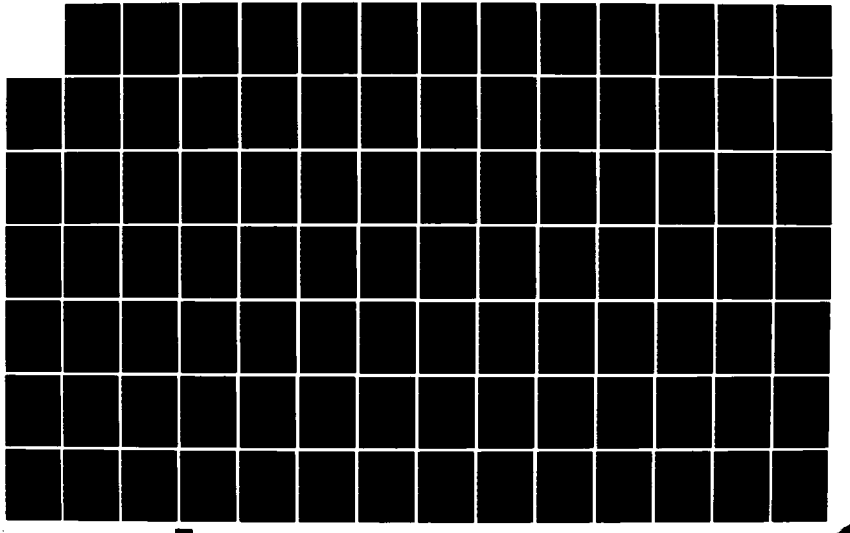

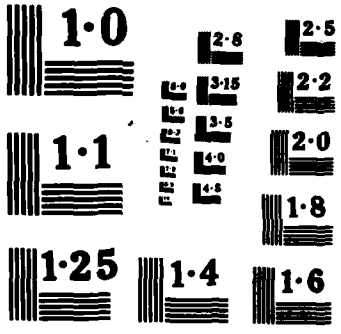
1·0
1·1
1·25
1·4
1·6
1·8
2·0
2·2
2·5
2·8
3·15
3·5
4·0
4·5

COLLEGE ENGINEERING

VPI-E-85-10

A Survey of the Turbulence in the Marine Surface Layer for the Operation of Low-Reynolds Number Aircraft

H. W. Tieleman
Department of Engineering Science and Mechanics
Virginia Polytechnic Institute and State University
Blacksburg, Virginia 24061

March 1985

VIRGINIA POLYTECHNIC INSTITUTE AND STATE UNIVERSITY
BLACKSBURG, VIRGINIA

VPI-E-85-10

A Survey of the Turbulence in the Marine Surface Layer for the Operation of Low-Reynolds Number Aircraft

H. W. Tieleman
Department of Engineering Science and Mechanics
Virginia Polytechnic Institute and State University
Blacksburg, Virginia 24061
March 1985

Prepared for the
Department of the Navy
Office of Naval Research

ONR Contract No. N00014-83-K-0658

Acknowledgements

Financial assistance for preparation of this report from the U.S. Department of the Navy through Contract No. 00014-83-K-0658 is gratefully acknowledged.

The following persons are gratefully acknowledged for making available data reports and articles which have been used in this manuscript:

Dr. S. D. Smith
Bedford Institute of Oceanography
Dartmouth, Nova Scotia, Canada

Dr. S. Pond
University of British Columbia
Department of Oceanography

Dr. M. A. Lemone
National Center for Atmospheric Research
Boulder, Colorado

Dr. S. SethuRaman
North Carolina State University
Raleigh, North Carolina

Dr. D. H. Lenschow
National Center for Atmospheric Research
Boulder, Colorado

Dr. T. V. Blanc
Department of the Navy
Naval Research Laboratory, Washington, D.C.

Dr. J. Wieringa
Royal Netherlands Methorological Institute
De Bilt, Netherlands

Also Mr. Richard Swanson is being acknowledged for his expert contribution to the numerical analysis and the graphical presentation of the data. A special thanks goes to Mrs. Vanessa McCoy for her willing cooperation and preseverance in the typing of this report.

TABLE OF CONTENTS

List of Symbols

Symbol	Definition
$( )_{avg}$	Arithmetic mean or average value
A_α	Slope of the linear regression relation through the origin $\sigma_a = A_\alpha U^*$
b_α	Intercept of the linear regression relation $\sigma_\alpha = m_\alpha U + b_\alpha$
C	Constant of integration (15)
C	Wave phase velocity
c_p	Specific heat
E	Mean turbulent energy
F( )	Function
f( )	Function
f_m	Peak reduced frequency
f	Coriolis parameter
G	Geostrophic wind vector
g( )	Function
g	Gravitational constant
H_o	Surface heat flux
h	Depth of ABL
K	Thermal conductivity (3)
K	von Karman constant
k	Roughness parameter (8)
k	Radian wave number
L	Morin-Obukhov length
$L_\alpha^x, L_\alpha^y, L_\alpha^z$	Turbulence integral scales
m_α	Slope of the linear regression relation $\sigma_\alpha = m_\alpha U + b_\alpha$
m'_α	Slope of the linear regression relation through the origin $\sigma_\alpha = m'_\alpha U$

Symbol	Definition
n_m	Peak cyclic frequency
P	Pressure
p	Pressure fluctuation
Q_o	Kinematic surface heat flux
R	Radiation
R_f	Flux Richardson Number
Ri	Gradient Richardson Number
$R_\alpha(y')$	Space correlation coefficient
SD	Standard deviation (used in tables)
S_α	Standard deviation of turbulence components (used in figures only)
T	Temperature
T	Integral time scale
T_v	Virtual temperature
t	Time
U	Mean velocity
U*	Friction velocity, $\sqrt{-\overline{uw}}$
U_o^*	Profile friction velocity or $\sqrt{\tau_o/\rho}$
u,v and w	Turbulence velocity components in x, y and z directions respectively
x,y and z	Mean wind coordinate directions
x',y' and z'	Separation distances in x, y and z direction respectively
W^*	Scaling velocity for the mixed layer
z_i	Altitude of the lowest inversion, often taken as the depth of the ABL
z_o	Roughness length
α	Subscript for the velocity components α = u, v or w
δ	Boundary layer depth

Symbol	Definition
ε	Viscous dissipation
θ	Temperature fluctuation
κ	Kolmogoroff constant
λ_m	Peak wave length in the logarithmic velocity spectrum
μ	Absolute viscosity
ν	Kinematic viscosity
ρ	Density
σ_α	Standard deviation of turbulence
τ	Time delay
τ_o	Surface shear stress
$\phi_\alpha(k)$	Spectral density function
$\psi(z/L)$	Universal function in the surface layer wind profile

List of Figures

List of Figures

List of Figures

List of Tables

A Survey of the Turbulence in the Marine Surface Layer for the Operation of Low-Reynolds Number Aircraft

1.0 Introduction

The motivation for the preparation of this report is the need for low-level wind input, required for the design and operation of remotely piloted aircraft at low-Reynolds numbers an at extremely low altitudes above the ocean. Surface winds and gusts are known to have a strong influence on the operation of aircraft near the surface and can cause serious control problems. In general, cross winds, wind shear and gusts encountered by low-flying aircraft pose significant problems in their operation.

However, most analytical and experimental work on the atmospheric boundary layer over the ocean has been directed toward the understanding of the processes dealing with the transport of mass, momentum and energy. The majority of surface wind measurements has been collected by meteorologists who study these processes, and has not been collected with the needs of the aeronautical engineer in mind. Although numerous experimental studies have been made in the surface layer and boundary layer over the ocean, the ability to apply the available information to the design and operation of aircraft is limited.

Notwithstanding this limitation, this report reviews the current experimental knowledge of the marine atmospheric surface layer and discusses the nature and quality of the reported data as well as their applicability as input to the design and operation of low-flying aircraft.

2.0 General Discussion of the Problem

For aeronautical applications at high altitudes, local wind speed is relatively small and for design purposes the velocity is taken as that of the aircraft. For low altitude situations, particularly with the speed of the aircraft being of the same order as the wind speed, the relative velocity between the aircraft and the wind should be used. For aircraft flying at extremely low ground speeds of approximately 10 m/s at altitudes of 50m or less, the atmospheric winds will not only affect the overall operation and control of the aircraft but also affect the airfoil performance. Under these conditions the relative wind velocity as experienced by the aircraft will alter dramatically as the aircraft moves through the highly variable wind field.

The vertical turbulence, cross-winds, lateral wind shear and gusts encountered by this type of aircraft will undoubtedly affect its performance. However there does not seem a complete understanding how wind and gusts enter into the design, operation and control of any aircraft. Consequently, it is not totally clear what information of the ground winds is needed to aid the aeronautical engineer in the design of these unusual aircraft.

In addition, the atmospheric turbulence can have a direct affect in many different ways on the airfoil performance at chord Reynolds numbers of the order of 100,000. Under these conditions angle of attack, separation and transition from the laminar to the turbulent regime of either the foil boundary layer or wake have a pronounced effect on the lift and drag of the airfoil. Especially when the chord Reynolds number decreases below 100,000 can abrupt performance changes be expected [1].

It is the concensus among aeronautical engineers that the overall performance of the aircraft is much affected by the vertical force spectrum and pitching moment spectrum due to u and w turbulence, yawing moments due to v turbulence and rolling moments due to spanwise variations in u and w turbulence (Fig. 1). This is specifically a problem for low Reynolds number flight at ground velocities of the same order as the wind speed and at low altitudes where there is little room for error.

Of course, the fluctuations of the rolling, pitching and yawing motion of the aircraft are primarily caused by turbulent eddies of a scale comparable to the dimension of the aircraft [3]. On the other hand the performance of the airfoil, controlled by the boundary layer flow over the foil, is primarily governed by turbulence, fluctuations of much smaller scale, of the order of the boundary layer thickness. However detailed information of the turbulence at these small scales and of the non-uniformity of the gusts over the dimensions of the aircraft (cross-correlations) is extremely scarce especially for the atmospheric flow over the ocean.

Existing data obtained over the ocean are either from instruments mounted on floating platforms primarily below 20m or from instrumented aircraft above 20m. Moreover, the marine environment is not very conducive to the acquisition of multipoint turbulence measurements, and available turbulence data obtained from floating platforms are usually limited to a single level. Only a limited amount of multipoint turbulence data is available from micrometeorological towers located on land close to the water for on-shore winds.

The results presented in this report are obtained from many different sources dealing with mean wind and turbulence measurements in the atmospheric surface layer over the ocean. Particular emphasis is placed on the identification and analysis of the low-altitude turbulence measurements that have the greatest influence on the operation of the low Reynolds number aircraft in the marine surface layer.

3.0 General Discussion of the Atmospheric Boundary Layer

The atmospheric or planetary boundary layer (A.B.L. or P.B.L.) is the result of the interaction of the atmospheric flow over the underlying land or sea surface. This layer is characterized by a turbulent transfer of momentum, heat and mass (water vapor) and their associated gradients. Non-uniform boundary conditions, nonstationarities, variable stability and thermal conditions as well as Coriolis effects are conditions which are typical for the A.B.L. but not common to wind tunnel or laboratory boundary layers. Moreover, under extreme inversion and convective conditions, the latter including the passage of fronts, squall lines, thunderstorms and other mesoscale phenomena, the surface flow cannot be classified as typical boundary layer flow.

During daytime under generally convective conditions the boundary layer depth is assumed to correspond to the altitude of the lowest inversion, z_i, typically about 1000 m [4]. Away from the surface the large scale buoyancy-generated turbulence promotes the transport and mixing of heat and momentum. As a result of this vigorous mixing the mean profiles in the upper 90% of the A.B.L. below the inversion are almost uniform (mixed layer), while above the inversion base the

velocity and potential temperature increase with height. Another factor which complicates the nature of the A.B.L. is the downward flux of momentum and heat due to entrainment into the convective boundary layer.

During nighttime, thermal conditions are often stable near the surface and the depth of the surface inversion is considered to correspond to the A.B.L. (typically about 100 m [4]). Under these conditions the surface cools down resulting in a stable temperature stratification just above the surface where the buoyancy forces will inhibit the vertical motion and suppress the turbulent mixing. Above the A.B.L. the flow is considered frictionless and primarily governed by pressure forces, Coriolis forces and horizontal temperature gradients.

The surface layer, approximately the lowest 10% of the A.B.L., is characterized by the mechanically produced turbulence from the surface roughness and friction, with nearly constant vertical fluxes of momentum, heat and mass. The height of this layer may vary over a wide range but is typically of the order of 50 m [4]. In the lower most part of the surface layer, commonly referred to as the roughness layer, the flow is affected by the individual roughness elements and is nonhomogeneous and three-dimensional in nature. Several roughness heights above the mean surface, this three-dimensionality of the flow disappears and the flow is usually considered to be horizontally homogeneous. In the marine roughness layer various properties of the sea surface, primarily the travelling surface waves affect the flow. However, the observation of these wave effects have been hindered by the motion of the instrument platform induced by the wind and waves as well as by the presence of the platforms (towers, buoys, ships) in the flow field.

There exists a strong interaction between the oceanic and atmospheric motions. The atmospheric flow is responsible for the ocean currents, bringing layers of water of different temperature to the surface, which in turn affects the air temperature and the water vapor content and thus affects the atmospheric motion. The trade winds drive the ocean currents north and south of the equator, while a combination of high-pressure and low-pressure cells cause the warm sea currents like the Gulf Stream and cold sea currents.

4.0 The Governing Equations

The basic conservation laws of mass momentum and energy are used for the description of the motion of the atmosphere. The momentum equation should include body and buoyancy forces, Coriolis forces in addition to the pressure and viscous forces. The use of this set of equations may be greatly simplified by adopting the Boussinesq approximation. In this approximation the atmosphere is assumed to be a perfect gas, while pressure, density and temperature vary only slightly from the neutrally stable atmosphere (hydrostatic equilibrium). Temperature variations are considered to be sufficiently small so that viscosity and heat conductivity can be considered constant. Also it is assumed that the velocity of the flow is sufficiently small so that variations in density due to variations in dynamic pressure are small. However, the variations in density due to variations in temperature, as the fluid parcels change elevation and adapt themselves to the new environment, cannot be ignored. These variations in temperature and density produce a non-equilibrium between buoyancy and gravitational forces. The net amount of work done by these forces may be positive (turbulent production) or negative (turbulent suppression). Although

generally speaking the A.B.L. flow is purely turbulent, in stable air non-turbulent gravity waves will also produce velocity fluctuations.

Considering the flow to be turbulent and with Reynolds averaging of the instantaneous equations, the continuity equation for the mean flow becomes

$$\frac{\partial U_i}{\partial x_i} = 0 \quad \text{(Incompressible flow)} \tag{1}$$

Here capital letters denote averages and lower case letters denote fluctuations. Similarly, the mean momentum equation becomes

$$\frac{DU_i}{Dt} = -\frac{1}{\rho_o}\frac{\partial P'}{\partial x_i} + \frac{1}{\rho_o}\frac{\partial}{\partial x_j}\left[\mu\frac{\partial U_i}{\partial x_j} - \rho_o\,\overline{u_i u_j}\right] + \frac{g}{T_o}T'\delta_{3i} \tag{2}$$

Here the subscript o indicates properties associated with the reference state, and the primes indicate deviations from this reference state. This form of the momentum equation includes the Reynolds stress term and the resultant between the gravitational and buoyancy force. The thermal energy equation becomes

$$\frac{DT'}{Dt} = -\frac{1}{c_p\rho_o}\frac{\partial}{\partial x_j}\left[-K\frac{\partial T'}{\partial x_j} + c_p\rho_o\,\overline{\theta u_j} + R\right] \tag{3}$$

which include the conduction (usually negligible), the turbulent heat flux and the heat flux due to radiation. Because of the presence of the turbulent flux terms this set of equations can no longer be considered to be a closed set.

So far the effect of moisture fluctuations on the density has been neglected, which might be quite reasonable for A.B.L. flow over land. However over water and specifically over warm water (tropical oceans) the effect of moisture is not negligible. Under these conditions the variations in specific humidity can be incorporated in the governing

equations by replacing the temperature and heat flux by virtual temperature and virtual heat flux [5]. The virtual temperature is defined as the temperature dry air would have in order to obtain the observed density and pressure of the moist air in which the observations are being made.

Equations for the turbulent terms and specifically the turbulent kinetic energy $e = \frac{1}{2} u_i u_i$ can also be obtained. With Reynolds averaging and the neglection of the small viscous term and the assumption of horizontal homogeneity, the equation of mean turbulent energy, E becomes

$$\frac{DE}{Dt} = \underset{1}{-\overline{uw}\frac{\partial U}{\partial z}} + \underset{2}{\frac{g}{T_o}\overline{\theta w}} \underset{3}{- \varepsilon} \underset{4}{- \frac{\partial}{\partial z}\left(\frac{\overline{ew}}{2} + \frac{\overline{pw}}{\rho_o}\right)} \qquad (4)$$

Each of the terms on the righthand side has the following physical interpretation:

1. The mechanical production of turbulence.
2. The rate of turbulence production $\overline{\theta w} > 0$ for unstable atmosphere, or the rate of suppression of turbulent energy $\overline{\theta w} < 0$ for a stably stratified atmosphere.
3. The viscous dissipation.
4. The diffusion of turbulent energy.

The ratio of terms 2 and 1 represents a measure of the buoyancy production or suppression of turbulence relative to the mechanically produced turbulence, and is referred to the flux Richardson number

$$R_f = \frac{g}{T_o} \frac{\overline{\theta w}}{\overline{uw}\frac{dU}{dz}} \qquad (5)$$

For vanishing R_f the atmospheric flow is considered to be neutrally stable, for $R_f < 0$ with $\overline{\theta w} > 0$ (upward heat flux) the atmosphere is

thermally unstable and for $R_f > 0$ with $\overline{\theta w} < 0$ (downward heat flux) the atmosphere is thermally stable.

With the introduction of turbulent diffusivities or transport coefficients and assumption that these coefficients are equal, the gradient Richardson number can be defined as

$$Ri = \frac{g}{T_o} \frac{dT/dz}{(dU/dz)^2} \tag{6}$$

Since no detailed solution of the turbulent flow can be expected from the above set of equations, they can only provide a framework for the interpretation and description of observations and a basis for the modelling of the flow.

5.0 Similarity Theories

The description of turbulent boundary layers has been based primarily similarity arguments. Using this approach, the statistical flow parameters are described in terms of empirical functions which require a number of basic parameters which control the flow in different parts of the boundary layer. Specific empirical relations have been derived from experimental data, by organizing the data in accordance with the established turbulent boundary-layer model.

5.1 Wind Tunnel Boundary Layers

5.1.1 Smooth Boundary

Based on dimensional analysis and experimental results from turbulent boundary layers in the laboratory two basic laws emerged. The "law of the wall" describing the mean flow near:

a. smooth wall $U/U_o^* = f(\frac{z}{\nu/U_o^*})$ (7)

b. rough wall $U/U_o^* = f(z/k)$. (8)

and the "velocity defect law" governing the mean flow in the outer layer for either rough or smooth walls

$$(U - U_o)/U_o^* = g(z/\delta). \quad (9)$$

Millikan showed that the existence of an overlap region of the two laws requires a logarithmic velocity profile without introducing eddy viscosity, mixing length and without assuming the existance of a constant stress layer.

Using the method of asymptotic matching Tennekes and Lumley [6] showed the existence of the logarithmic velocity profile for smooth flat-plate boundary layers provided the Reynolds number is large ($U_o^*\delta/\nu \to \infty$). Under these conditions the velocity profiles are self-preserving and the normalized velocity defect, $(U - U_o)/U_o^*$, and the normalized turbulent stresses are universal functions of z/δ, independent of downstream distance or any other parameter. As $U_o^*\delta/\nu$ or $\delta/(\nu/U_o^*) \to \infty$, the law of the wall can be matched with the velocity defect law in the overlap region where simultaneously $z >> \nu/U_o^*$ and $z << \delta$. In this region the nondimensional velocity gradients obtained from either the law of the wall or the velocity defect law must be equal and also independent of any other variables and therefore equal to a universal constant. Integration of both velocity gradients and evaluation of the constants from experimental results lead to

$$U/U_o^* = 2.5 \ln (U_o^* z/\nu) + 4.9 \quad (10)$$

and

$$(U - U_o)/U_o^* = 2.5 \ln (z/\delta) - 2.5 \quad (11)$$

5.1.2 The Effect of Roughness

The effect of wall roughness on the flow in the boundary layer can only be treated in general terms because of the variation in geometrical shapes and distribution of the roughness elements. The roughness does not directly affect the velocity defect law except through the value of the wall shear or friction velocity, U_o^*, provided the size of the uniform roughness elements, k, is much smaller than the boundary layer thickness, δ. The friction velocity, U_o^*, can no longer be considered to be a local value but instead must be interpreted as an average value over an area which includes a sufficient number of roughness elements. On the other hand, the velocity distribution close to the boundary is affected directly by the roughness, so that the law of the wall may be written as

$$U/U_o^* = f(\frac{z}{k}, \frac{U^*k}{\nu}) \tag{12}$$

In the overlap region where $z >> k$ and $z << \delta$, the nondimensional velocity gradients must be equal to the same universal constant as in the smooth-wall case. Integration leads to

$$U/U_o^* = 2.5 \ln (z/k) + F(\frac{U_o^*k}{\nu}) \tag{13}$$

where F is not a universal constant but for a given roughness size also depends on the shape, distribution and density of the roughness elements even if $k >> \nu/U_o^*$, fully rough wall. Also note that the logarithmic profile is valid only in the overlap region where $z >> k$. In the region where z and k are of the same order (roughness layer) the above criterion is not satisfied, and the logarithmic profile should not be expected to apply.

5.2 Atmospheric Boundary Layer

5.2.1 Neutral Atmospheric Boundary Layer

Consider the flow in the A.B.L. as being steady and horizontally homogeneous without the effect of any buoyancy forces and over a flat homogeneous surface whose roughness can be represented by a roughness length-scale, z_o. Above the A.B.L., the pressure gradient force must be balanced with the horizontal component of the Coriolis force and

$$f\vec{k} \times \vec{G} = -\frac{1}{\rho} \vec{\nabla} p \qquad (14)$$

where f is the Coriolis parameter $f = 2\omega \sin\lambda$, with ω being the earth's angular velocity and λ the geographic latitude and $\vec{G}$ being the geostrophic wind. The vertical component of the Coriolis force is negligible in comparison with gravity. The external parameters which control the flow are f, G and z_o. Other flow parameters which enter are the friction velocity U_o^* and the height of the neutral A.B.L., h. In the absence of buoyancy forces, the turbulence is purely of mechanical origin and the friction velocity, U_o^*, is the only characteristic velocity scale for the turbulence [7]. The height h, which is proportionally to U_o^*/f, and z_o must be the characteristic length scales for the flow in the outer and inner layer respectively. In the limit as $U_o^*/fz_o \to \infty$ the two similarity laws one for the surface layer and one for the outer layer must match in the overlap region where both laws are valid simultaneously. In this region with $z/z_o \to \infty$ and $zf/U_o^* \to 0$ the nondimensionalized velocity gradients should be equal to the same universal constant as before. Integration leads again to the well known logarithmic velocity profile

$$\frac{U}{U_o^*} = \frac{1}{K} \ln (z/z_o) + C \qquad (15)$$

Although at the present time some controversy exists over the numerical value of the value of K (the von-Karman constant), a value of K = 0.4 based on wind tunnel experiments is most commonly accepted. As before C is not a universal constant but must depend on the nature of the roughness and the roughness Reynolds number $U_o^* z_o/\nu$. The constant of integration, C, is often incorporated into z_o in the above expression

$$U/U_o^* = \frac{1}{K} \ln (z/z_o) \qquad (16)$$

For any natural roughness it is impossible to assign a single numerical value for z_o, without taking into account the variation in roughness size, shape, distribution and density. For all practical situations a "profile roughness length" can be obtained from velocity observations only in the range for which (16) is expected to be valid, or for $z >> z_o$. Also the friction velocity U_o^* is certainly not a local value but is based on the wall shear stress τ_o, averaged over a sufficiently large upstream fetch. Using this derivation of the logarithmic wind profile in the neutral A.B.L. does not require the assumption of constant stress layer.

5.2.2 Non-Neutral Atmospheric Boundary Layer

So far the discussion has been limited to a neutral atmospheric boundary layer and laboratory boundary layers with adiabatic temperature profiles and therefore without vertical heat flux. However the A.B.L. nearly always has some vertical heat flux either in the form of sensible or latent heat. In addition to the mechanically produced turbulence, turbulent energy is either produced or suppressed depending on whether the heat flux is upward (unstable) or downward (stable). Consequently

the mean flow as well as the turbulence in the diabatic surface layer are different from those in the neutral surface layer.

Stable conditions are usually encountered during night or when warmer air flows over a colder water surface and are characterized by a suppression of the turbulence. Under extreme stable conditions, the air in the different layers becomes uncoupled as a result of reduced mechanical mixing, and jet-like flows either near the surface or at higher elevations may be observed. Additional complications may occur when turbulence and gravity waves co-exist. Under these conditions the flow seldom reaches a state of quasi-steadiness, because conditions vary rather rapidly, and consequently no simply boundary-layer model is available for the description of the flow.

With daytime heating of the earth's surface resulting in an upward heat flux, the mechanical turbulence production is augmented with buoyant energy production. Near the surface the mechanical energy production dominates but decreases rapidly with height, while on the other hand the buoyant production is almost constant through the surface layer. Outside the surface layer, the unstable or convective A.B.L. undergoes strong vertical mixing due to upward buoyancy and the production of large-scale convective turbulence. In addition, downward fluxes of momentum and heat due to entrainment into the convective boundary layer across the overlying inversion complicate matters a great deal. Near the surface the turbulent fluxes exist as a result of gradients, however in the mixed layer the fluxes are maintained by buoyancy effects and entrainment. No single internal parameter as the friction velocity, U_o^*, is available to scale the mean and turbulent flow in both layers and consequently the method of asymptotic matching cannot

be used. Instead we have to resort to separate similarity theories in the surface and the outer layer.

5.2.3 Surface Layer Similarity

Monin and Obukhov [8] proposed that the flow (mean or turbulence) in the surface layer is uniquely determined by the surface stress, U_o^*, the kinematic surface heat flux $Q_o = H_o/\rho c_p$, the buoyancy parameter g/T_o and the height z. With this approach, flow quantities are not directly dependent on the roughness but are influenced by it indirectly through the magnitude of the momentum flux or U_o^*. Then by dimensional analysis, properly nondimensionalized flow variables should be universal functions of the stability parameter z/L where L is the buoyancy length scale known as the Monin-Obukhov stability length.

$$L = - \frac{U_o^{*3}}{K(g/T_o)Q_o} \tag{17}$$

Accordingly, the dimensionless wind shear should be a universal function of z/L, which can be integrated to give

$$U/U_o^* = \frac{1}{K} [\ell n\ z/z_o - \psi(z/L)] \tag{18}$$

where z_o is introduced as a constant of integration and can only be obtained by extrapolation of velocity observations above the roughness layer down to the axis where U = 0. Here, the function ψ is an empirically derived universal function of z/L with the limit $\psi \to 0$ for the aproach of neutral stability for which $L \to \infty$ and $z/L \to 0$.

5.2.4 Outer Layer Similarity

In the outer layer the mean and turbulent flow, besides depending on the height z and on the surface fluxes of heat and momentum, also

depend on the boundary layer height, h, the Coriolis parameter, f, entrainment and wind shear at the top of the boundary layer. The form of the universal functions describing the dependence of the flow characteristics on these parameters can only be obtained from observations and numerical modelling. However, most of the mean wind and turbulence observations have been limited primarily to the lower 100 m over land and to the lower 20 m over water. Simultaneous observations of the mean flow and turbulence throughout the depth of the A.B.L. are extremely sparse and limited to observations from instrumented airplanes and from tethered balloons either with or without surface layer observations. Moreover, it is practically impossible to study the effect of only one of the above parameters on the flow characteristics while holding the remaining parameters constant. Most of the existing similarity schemes are restricted by including only one or two of the above parameters in the analysis.

For a far more comprehensive treatment of the atmospheric boundary layer and atmospheric turbulence the reader is advised to consult References 4, 5, 9, 10 and 11.

6.0 Discussion of Experimental Procedures

6.1 General Observations

Recent improvements in the quality of data acquisition, data handling and data processing systems have resulted in an increased number of experimental research programs dealing with the structure and dynamics of the turbulence in the A.B.L. Most of these investigations have been performed over land, using meteorological towers instrumented at several levels for observations generally at elevations below 200m,

and instrumented airplanes as well as instrumentation suspended from balloon tethers for observations at higher elevations. These kind of observations over water and specifically over the open ocean, where conditions are not amenable to experimental investigations, are much fewer in numbers.

Difficulties in obtaining quality measurements of the turbulence over water are generally compounded by the contradictory requirements that the anemometers should be sensitive enough to measure the high-frequency fluctuations and at the same time be rugged enough to withstand the extreme marine environment. Because of this problem wind observations over water can generally be classified into two groups: those based on mean flow observations from which certain turbulence characteristics associated with the mixing processes are being deduced, and those which measure mean wind and turbulence simultaneously. Only data sets belonging to the latter category have been used for analysis in this report. In addition, observations over water are often limited to one level, frequently at a height of about 10m or lower. Wind measurements acquired so close to the water surface may have been taken in the roughness layer, especially at the higher wind velocities for which wave amplitudes may be 1m or more. Consequently, data acquired at these levels vary considerably and are not only influenced by wave height but also by the direction and the speed at which the waves are being propagated [12,13,14 and 15]. It has been observed that the wave influence on mean wind and turbulence occurs to a height equivalent to at least three wave heights [14].

Only with many hours of observations and averaging of the results can a representative "average" picture of the flow over water be

obtained. Much of the observed scatter of the data may not be random but may be due to variation in thermal stability or due to varying wind and wave conditions. The water surface roughness and hence the turbulence characteristics above it seem to depend on surface-wave parameters which by themselves are the result of local wind conditions both past or present, but are also dependent on the location of the observations with respect to the large weather patterns.

Many of the mean wind and specifically turbulence observations suffer from experimental error such as contamination by water spray, inadequate calibration control, platform oscillation, platform motion and flow distortion due to platform blockage. Results from a carefully executed comparison experiment between two different sonic anemometer systems show systematic differences in measured turbulence quantities by as much as 40% [16]. Another comparison experiment with three different type of sensors (gust anemometer, acoustic anemometer and a propeller anemometer system) show variations of at least 10% even after corrections for response limitation and for calibration differences were applied [17]. Despite continued improvements in sensor design and in data acquisition and data handling systems, one must expect remote observations of the turbulence in the atmospheric surface layer over the ocean to exhibit considerable scatter.

A good deal of the scatter may be of a strictly statistical nature, meaning that the turbulence characteristics in the A.B.L. are by no means constant. Time plots of the turbulent velocity component show relatively large fluctuations in relation to the average value. Consequently with finite-time averaging, the presence of low-frequency fluctuations will lead to a considerable scatter of the averaged

quantities. In addition, turbulence quantities measured at a given location can not be interpreted as being an accurate estimate of what the turbulent flow is at any other location in a large area of several hundred kilometers in dimension. Therefore, the turbulence measurements at a given location at a given instant can only be expected to be a small sample out of a set of infinite samples which makes up the process of atmospheric turbulence.

Actually, the conditions of steady state and spatial homogeneity, which are necessary requirements for similarity theory, are seldomly satisfied for 100 percent. Consequently, the data presented in this report can only be considered as estimates based on a limited number of observations. In view of this and with all the other uncertainties of instrumentation performance, data analysis, platform motion, etc., it would be impossible to expect the results presented in this report to show perfect uniformity.

For an excellent review of the different methods and their limitations for the measurement of turbulence fluxes in the atmospheric surface layer over water, the reader should consult Reference 18.

6.2 Turbulence Stress and Friction Velocity

An abundance of turbulent flux coefficients are presented in the open literature, however, they are usually referenced to a height of 10m. These results are primarily acquired from instrumentation mounted on masts on floating platforms, on fixed towers in relatively shallow coastal waters, lakes or on beaches, or from instrumentation mounted on ships or airplanes over the open ocean. For most of these investigations the turbulence observations are limited to the turbulent

stress and heat fluxes (sensible and or latent). There are several ways to measure the turbulent fluxes of momentum, heat and moisture in the marine surface layer. Concentrating on the momentum flux or turbulent stress ($-\rho\overline{uw}$), or the friction velocity, $U^* = \sqrt{-\overline{uw}}$, one can obtain values of these parameters as follows.

The first method is the profile or gradient technique in which the profile friction velocity, U_0^*, is estimated from mean velocity measurements at several levels above the roughness layer, but still in the overlap region where the logarithmic velocity law (18) with the appropriate stability correction is valid. The recommended stability corrections as derived from land observations are $\psi = -5\ z/L$ for stable air [11], and are given by Paulson [19] for unstable conditions. However the stability parameter z/L itself requires the knowledge of the friction velocity U*. By using additional empiricism, z/L can be estimated from the gradient Richardson number [11], the latter requiring the measurement of the mean velocity and the virtual potential temperature at two levels above the roughness layer. In addition to the stability correction to the profile there is also an uncertainty about the value of the vonKarman's constant ($0.35 \leq K \leq 0.41$), which obviously will affect the values of the profile friction velocity. Blanc [20] provides estimates for the uncertainty of the profile-flux measurements by scaling of the results from one experiment to another. This analysis showed that the variation for typical values of the turbulent stress and the roughness length fell in the range from 10 to 40% and 25 to 100% respectively. To say the least, the profile method is quite empirical and both Krügermeyer et al. [14] and Wieringa [21] conclude that the aerodynamic stress can not be estimated with

sufficient accuracy from wind profile measurements close to the water surface.

The second method for obtaining the friction velocity, U*, is by the dissipation technique, for which the measurement of the downwind velocity spectrum at a single elevation is required. Successful application of this method requires delicate instrumentation with very small sensors and a high frequency response up to 2000 Hz. The method is based on the assumption that the production of mechanical energy is equal to the dissipation for near neutral stability conditions or

$$-\overline{uw}\,\frac{dU}{dz} = \varepsilon. \tag{19}$$

With the assumption of the existence of the logarithmic velocity profile, in differentail form

$$\frac{dU}{dz} = \frac{U_o^*}{Kz} \tag{20}$$

and assuming that the turbulent stress is constant with height and equal to the profile stress

$$-\overline{uw} = (U^*)^2 = (U_o^*)^2 \tag{21}$$

one obtains

$$(U^*)^2 = (K\varepsilon z)^{2/3} \tag{22}$$

The value of the dissipation, ε, can be obtained from the measured velocity spectrum which in the inertial subrange should follow

$$\phi_u(k) = \kappa\, \varepsilon^{2/3} k^{-5/3}, \tag{23}$$

where κ is the Kolmogoroff constant ($\kappa = 0.5$) and $k = \frac{2\pi n}{U}$, is the radian wave number. The values of both the vonKarman constant, K, and the Kolmogoroff constant, κ, are still somewhat controversial. In the equilibrium subrange the turbulence is assumed to be locally isotropic which requires the value of the ratio $\phi_w(k)/\phi_u(k)$ to be 4/3. However measurements 8m above the water surface, by Schmitt et al. [22] show

values of this ratio instead to be close to unity, indicating a condition of anisotropy of the turbulence in the inertial subrange. Also under non-neutral stability conditions expression (22) must be modified requiring an estimate of the stability parameter z/L as discussed before. Besides requiring delicate instrumentation for the measurement of the velocity spectra at sufficiently high frequencies, this method is likely to suffer from the fact that basic assumptions may not be satisfied.

The third and possibly the most frequently used method for measuring the momentum flux is the eddy-correlation technique which requires the direct measurement of the covariance of the vertical and downwind velocity components. This method is also used for the measurement of the variances of all three velocity components, requiring delicate sensors capable of measuring these components up to a frequency of at least 10 Hz. The variances and covariances can be obtained by multiplication of the instantaneous values and consequent time integration or may be obtained by integration of the spectra and cospectra respectively. Both methods suffer from the same problem, namely that the contribution of the low-frequency fluctuations to the variances and covariances is not well established. For the majority of the reported observations, only fluctuations between 0.001 Hz and 1 Hz are included in the evaluation of these quantities. Inspite of the delicate sensor requirement, limited frequency band-width, large amount of raw data acquisition as well as the sensitivity of the momentum flux to sensor alignment, most research programs dealing with turbulence measurement have used this method. Certainly the eddy correlation method for measuring the momentum flux requires fewer assumptions than

the profile and dissipation methods. Consequently, the majority of the turbulence data included in this report used the eddy-correlation method for analysis, and were obtained primarily by either sonic anemometer or thrust anemometer, although in some of the referenced research programs, propeller or cup anemometers were used. In the case fluxes obtained from two different methods were available, the preference was given to those measured by the eddy-correlation technique.

7.0 Discussion of Experimental Results

The flow in the atmospheric boundary layer is usually considered to be horizontally homogeneous and steady. Ignoring the effects of entrainment, cloud cover, Coriolis acceleration and baroclinity, the ABL can be divided into 2 distinct regions each with its own governing parameters. In the surface layer the mean flow and turbulence are governed by the surface stress, τ_o, the elevation above the surface, the buoyancy parameter g/T_v, surface heat flux H_o and the flow properties ρ_o and c_p. Consequently, flow parameters nondimensionalized with the shear velocity, $U^* = \sqrt{\tau_o/\rho_o}$, should be universal functions of the stability parameter, z/L, where the Monin-Obukhov length, $L = -U^{*3}/K(g/T_v)(H_o/\rho_o c_p)$.

In the outer layer the flow is often no longer influenced by the shear but is usually driven by buoyancy. Under strong convective conditions when the buoyancy forces promote strong mixing, a so-called mixed layer is formed where the turbulence is governed by z_i, the height of the mixed layer, g/T_v, H_o, ρ_o and c_p. The velocity scale for this regime is the convective velocity, $W^* = [(g/T_v)(H_o/\rho_o c_p)\ z_i]^{1/3}$. Consequently, turbulence parameters nondimensionalized with W* are

expected to be universal functions of z/z_i only. Over land where the heat fluxes are usually much larger than over the oceans, the surface layer and mixed layer are separated by a region where neither U* nor z_i are important and free convection scaling might apply, with z, g/T_v and $H_o/\rho_o c_p$ as the governing variables. However over the oceans the surface heat flux is much smaller than over land, consequently the flow in the large region between the surface layer and mixed or convective layer is governed not only by those parameters but also U* and z_i as well. Using the U* as scaling velocity, the dimensionless turbulence parameters should then depend on two independent parameters, z/z_i and z_i/L. As one examines the literature, turbulence data rom the A.B.L. are usually presented in both surface layer and mixed layer scaling schemes.

7.1 Mean Wind Profiles

7.1.1 Observations Above the Surface Layer

The flow in the larger part of the ABL above the surface layer depends not only on the elevation, z, and the surface fluxes of momentum and virtual heat, but also on the ABL height z_i, Corriolis effects, atmospheric conditions above the ABL and entrainment. Several similarity schemes have been introduced but none of them have included all these parameters. Figures 2, 3, 4 and 5 show mean wind profiles taken under different stability conditions. Obviously the observations at higher elevations above the surface layer can only be made by balloon soundings or instrumented aircraft, and therefore are not made simultaneously. The velocity profiles shown in Figures 3 and 4 are averages of several soundings. Under thermally unstable conditions, trade-wind velocity profiles show velocity maxima to occur well within

the ABL (Figs. 2 and 3), while profiles measured at larger latitudes do not seem to exhibit these maxima (Fig. 4). In the presence of low-level inversions with warmer air blowing over cooler water, mean wind profiles show well defined maxima at very low elevations (Figs. 5, 6). Under these conditions, as the turbulence is suppressed, Coriolis effects become important and conditions vary rapidly as the observations of Figure 5 indicate.

From these observations one can conclude that a mixed layer with near-uniform velocity, as is often observed over land surface, is seldom present over the ocean, and instead wind shears often exist throughout the ABL. It has been suggested that the effect of baroclinicity (horizontal temperature gradient), not included as a governing parameter in the mixed layer similarity scheme, may be responsible for the observed mean wind maxima in the ABL [28].

7.1.2 Observations in the Surface Layer

In the lowest part of the ABL (Surface Layer) the flow is characterized by a rapidly decreasing mean velocity and turbulence toward the earth's surface. Near the surface the mechanically produced turbulence dominates the flow while thermal stratification has an important effect on the turbulence only in extreme situations. Generally speaking, the surface layer flow over land surfaces is affected by the large variations in surface heat flux during day and night. This heat flux (upward during the day) is responsible for the generation of convective turbulence, but creates stable conditions (downward heat flux) during night when turbulence is suppressed. Over the ocean these diurnal variations are much less pronounced and the heat

flux is generally much smaller than over land. Also the heat flux over the ocean is dominated by the flux of latent heat (water vapor) rather than sensible heat.

In addition, it has been observed that the ocean surface is aerodynamically speaking extremely smooth. Even under strong wind conditions U > 12 m/s in the presence of large waves, the roughness length z_0 is less than 1mm [29]. For flow over a land surface this value of z_0 would be equivalent to that of flat desert terrain [11]. The influences of heat flux and roughness on the mean velocity profile are shown schematically in Figure 7.

Close to the water surface the flow must be influenced by the waves themselves. The extent of the influence of the waves on the air flow directly above is not exactly established but must include among other things, the wave amplitude, which itself is governed by the wind speed.

Similarity theory applicable to the surface layer requires the assumptions of steady state, horizontal homogeneity and the fluxes to be inependent with height. Under the condition of neutral stability in the absence of any vertical heat flux, the theory leads to the well known logarithmic wind profile.

$$\frac{U}{U^*} = \frac{1}{K} \ln(z/z_o) \qquad (24)$$

where, z_0, the roughness length must be characteristic of the underlying roughness, in this case the water waves. In practice, z_0 is determined by measuring mean velocity, U, at several elevations and extrapolating a straight line through a plot of the velocity observations versus $\ln z$ down to the axis where the mean velocity is zero. However, when the extrapolation is performed on a set of velocity observations obtained

within the layer where the waves influence the flow directly, the values of z_o may not be representative of the actual roughness.

In the case of non-neutral thermal stratification, the logarithmic profile equation needs to be modified to

$$\frac{U}{U^*} = \frac{1}{K} \left(\ell n \frac{z}{z_o} - \psi \right), \tag{25}$$

where ψ is a universal function based on the stability parameter z/L (see Section 6.5 of Reference 11). Many of the values of z_o presented in the literature are based on velocity measurements below 10m and assuming neutral stability. This practice leads to tremendous scatter of z_o. For instance, values of z_o obtained from more than 1000 velocity profiles acquired over the Baltic Sea and North Sea [29] are scattered between 1×10^{-4} mm and 100 m. Even when the results were limited to only those profiles for which the thermal stratification was near neutral, values of z_o still show a considerable scatter and moreover exhibit a clear dependence on either the shear velocity or mean velocity at a given reference height [29,31].

In a later paper Krügermeyer et al. [14] show that close to the water surface (within three wave heights), wind profiles are distorted to lower wind speeds in comparison to velocity profiles over a comparable rigid surface. Consequently, they conclude that the determination of the stress and roughnes length by the profile method must be based on velocity observations above this layer of wave height influence. Other investigators, including Fujita [32], who have made multilevel mean velocity measurements close to the sea surface observed appreciable departures from the logarithmic profile especially under strong wind conditions with wave heights in excess of 2m. Many of the

profiles show a single velocity maximum below 10m, while under strong wind conditions two velocity maxima have been observed (Fig. 8).

Based on these observations, the mean wind profile in the ABL over the ocean can vary in extreme fashion depending on the sea state, the virtual heat flux, conditions at the upper edge of the boundary layer as well as the general atmospheric conditions in the free atmosphere. Consequently no simple similarity model is available at the present time to describe the ABL flow, and be able to predict the mean velocity profile with any certainty.

7.2 Velocity Variances and Momentum Flux

In general the atmospheric motions are categorized as macroscale, mesoscale and microscale, where the latter is considered the turbulent part of the flow. Obviously it is the turbulence in the ABL that affects the operation of low-velocity, low-altitude aircraft. Since the turbulence is a random phenomenon it is best studied by variances, spectra and scales. In the ABL the mechanically produced (small scale) turbulence dominates the flow near the surface but decreases rapidly with height as the large-scale convective turbulence becomes more important (Fig. 9).

Above the ocean the convective turbulence created through buoyancy effects is relatively weak. Not withstanding, a well-mixed boundary layer can exist as a result of large-scale motions such as roll vortices which are primarily responsible for the upward transport of turbulent and moist air. As this moist air is moved upward it cools and will eventually condense and form the typical cloud streets associated with these roll vortices (Fig. 10). These large-scale structures including

gravity waves, which are frequently observed in the ABL under thermally stable conditions [34], cannot be considered turbulence. These low-frequency motions are nearly two-dimensional affecting the vertical turbulence component very little. Other large-scale phenomena include thunderstorms and squalls, etc., which are usually of short duration and characterized by a sudden increase in windspeed and turbulence followed by a sudden decrease as shown in Figure 11.

The turbulence characteristics of the ABL discussed in the following sections will apply primarily for stationary flow-observations or for those observations where the large-scale fluctuations are removed from the data through some form of high-pass filtering.

7.2.1 Observations Above the Surface Layer

In Figures 12 and 13 the standard deviations of the velocity component and the turbulent stress are presented for two different stability cases. The values of σ_α (α = u,v and w) have also been normalized by the friction velocity, U*, conforming to surface-layer similarity and by the convective velocity, W*, for comparison in the convective outer layer of the ABL. The observations in the ABL below the cloud base are quite similar for the two cases but considerable differences for both the standard deviations and the stress exist above the ABL. Near the surface, σ_u increases rapidly as the surface is approached, σ_v and σ_w increase also but much less rapidly. For the near neutral case, the surface values of the ratios σ_u/U^*, σ_v/U^* and σ_w/U^* are 2.3, 1.6 and 1.25 respectivey, in reasonable accordance with the values observed over flat terrain [11]. For the more unstable case (Fig. 13) with increased cloudiness, the surface values of σ_α/U^* are

3.8, 2.3 and 1.8 respectively which are systematically higher than those for the near neutral case. Above 100m the standard deviations decrease but become nearly constant in the upper 1/3 of the ABL, where the values of σ_α/W^* are 0.95, 0.55 and 0.4 respectively for the near neutral case. In both the near-neutral and the more unstable case the turbulence components do not vanish at the edge of the boundary layer. In the near-neutral case the standard deviations of the 3 velocity components just below the cloud base are approximately 70% of their respective surface values. On the other hand in the more unstable case with the presence of clouds, the standard deviations of the three velocity components are approximately equal at the edge of the boundary layer.

Figures 12 and 13 also show the distribution of the turbulent stress $-\overline{uw}$ in the ABL which in both cases varies linearly with height decreasing to about zero at the edge of the boundary layer.

Measurements made during the GARP Atlantic Tropical Experiment in the summer of 1974 reveal that the distribution of σ_w is quite dependent on stability (Fig. 14), and that the normalization with the convective velocity certainly does not collapse the data. The shape of the σ_w/W^* distribution resembles that of Figure 12, although the values of the bulk stability parameter, z_i/L, except for day 218 are all considerably smaller than -10. The observations at the lowest level (approximately z = 20m) show average values of z/L of -0.5, -1.5, -1.5 and -1.2 respectively for the four days, with average values of σ_w/U^* for these days all in excess of 2.0.

Measurements of the standard deviations and stress made over the North Sea on February 26, 1975 [36] show remarkable similarity with the trade wind observations (Fig. 15). Later observations over the North

Sea around Great Britain [25] under a variety of meteorological conditions are shown in Figure 16. This multiple data set was subdivided in two categories, class A with $z_i/L < -1.9$ (average -3.9, 46 runs) and the near neutral class for which $z_i/L > -1.5$ (average -0.9, twenty eight runs). The distributions of σ_α/U^* shown in Figure 16 for the two classes show clearly the variation with stability, especially for the lateral velocity component. The standard deviation of the vertical component σ_w/U^* seems to be independent with stability in the surface layer ($z/z_i < 0.1$), but shows considerable variation with stability above the surface layer. The maximum value of σ_w/U^* at $z/z_i \approx 0.5$ and the distribution of σ_w/U^* are similar to the results shown in Figure 14. The lateral component, σ_v/U^*, depends rather strongly on the stability parameter z_i/L for all heights. Figure 16 also shows for comparison purposes the average values of σ_α/U^* measured in the surface layer over water by eight different investigators. The stress distribution seems relatively independent with stability as the results of Figure 16 indicate and also decreases uniformly with height as was the case with previous observations (Figs. 12, 13, 15).

7.2.2 Observations in the Surface Layer

Observations of the atmospheric flow in the surface layer over water are much more numerous and are available for a large variety of atmospheric and stability conditions. Since the detailed knowledge of the mean and turbulent flow in the lower 50 m is required for the operation of low-velocity aircraft near the ocean surface, the remainder of the analyzed data is primarily based on observations made below this height.

Table 1 provides the reader with a summary of all the references used in this report, from which turbulence and mean velocity data have been obtained, including specific information as to the location, instrumentation and platform used during the experiment. Also the height of the observations above the water surface as well as the range of stability conditions and the mean velocity range and the number of observations analyzed are listed in this table. Average values of the variance ratios σ_α/U and/or σ_α/U^* were taken directly from the text for eight different references. However, for the majority of the listed references, the number of observations of the mean velocity, shear velocity and the standard deviation of the turbulence components are presented in this table.

The majority of the low-level observations were made below 15 m, of which some were made above shallow water on fixed masts. However, most of the observations over the open ocean and below 15 m were either acquired from the stable platform operated by the Bedford Institute of Oceanography or from the resarch platform F.L.I.P (Floating Instrument Platform) operated by the Marine Physical Laboratory of the Scripps Institute of Oceanography (Fig. 17). For higher elevations the results are primarily based on observations made with instrumented aircraft and on observations made with F.L.I.P. at the 30 m level and on the observations acquired from the miorometeorological tower on the beach at Wallops Island, Virginia.

7.2.2.1 General Turbulence Observations

Because of the variations in thermal stability, atmospheric conditions, instrumentation and data analysis, discrepancies between the

different sets of data are unavoidable. Average values of σ_α/U^* and σ_α/U are presented for each elevation in Tables 2 through 7 and Figs. 18 through 23. Also values of the constants A_α and m'_α obtained from least squares curve fitting of σ_α versus U* and U respectively, are presented in these tables. Where ever possible, values of the friction velocity, U*, obtained with the direct measurement of $\overline{uw}$ were compared with values of the friction velocity as obtained with either the mean velocity profiles or with the inertial dissipation technique. However based on the discussion in Section 6.2 of this report, and since most of the observations of the friction velocity were obtained with the use of the direct measurement method of $\overline{uw}$, preference was given in this report to those values of the friction velocity obtained with this method.

For several data sets enough observations were available to study the effect of stability and wind speed on the measured turbulence quantities. For the analysis of the turbulence data only local values of U* and U were used for normalization, no attempt was made to correct these velocities to the often used reference height of 10 m. The average values of σ_α/U and σ_α/U^* as listed in Tables 2 through 7 are also plotted in Figs. 18 through 23. The plots of σ_α/U show considerable scatter primarily due to variation in stability. The solid lines in Figs. 18, 19 and 20 which were drawn through the data should provide the reader with reasonably accurate estimates of the average turbulence intensities under near neutral conditions. The scatter of the results is also enhanced by the fact that above a certain critical mean velocity, turbulence intensities increase with wind speed as a result of increased wave height and aerodynamic roughness under strong wind conditions. However the data presented in Figs. 18, 19 and 20 are

averaged turbulence intensities for which the mean velocities fall generally below this critical wind speed. Consequently, the scatter of the results in these figures must be primarily due to variation in thermal stability. Below a height of 20 m above the water surface the average turbulence intensities, $(\sigma_u/U)_{avg}$, vary between 6 and 12 %, $(\sigma_v/U)_{avg}$ between 5 and 12 % and $(\sigma_w/U)_{avg}$ between 3 and 7 %.

The distribution of the average values of σ_α/U^* are shown in Figs. 21, 22 and 23. Especially the scatter for the horizontal velocity components is appreciably, while on the other hand the scatter of $(\sigma_w/U^*)_{avg}$ is much more limited. It is of note to observe in these figures that the average values of σ_α/U^* over flat and uniform terrain ($\sigma_u/U^* = 2.39$, $\sigma_v/U^* = 1.29$, $\sigma_w/U^* = 1.25$, Ref. 11) are systematically lower than those observed over water.

7.2.2.2 Variation of σ_α and U* with Mean Velocity, U

Figures 24 through 28 show clearly how the slope of the plots of σ_α (α = u, v and w) and U* versus U change at a mean velocity of approximately 10 m/s. For mean velocities below this level the straight line fitted through the data goes approximately through the origin. However, for velocities above 10 m/s lines of best fit through the data intersect the ordinate (σ_u-axis) well below the origin. Consequently, the turbulence intensities, σ_α/U, and the ratio U*/U and therefore the drag coefficient, U^{*2}/U^2 are velocity dependent above some critical mean velocity, which is approximately 10 m/s for observations at a height of 10 m above the water surface.

The data from References 17, 47, 48, 49, 50, 51, 53 and 62 all show a similar behavior. Between wind speeds of 10 m/s and 20 m/s the

average increase for σ_u/U is 38% while increases of 35%, 28% and 33% are observed for σ_v/U, σ_w/U and U^*/U respectively. The data from References 17 and 48 both taken on Sable Island show an excessive increase in σ_v/U of 88% in the same wind speed range and therefore have not been included in the average value of the other data sets of 35%. Similarly, the drag coefficient $C_D = U^{*2}/U^2$ increases by an average of 75% based on the data of References 17, 58 and 53. SethuRaman [49] attributed the abrupt increase of the velocity variance with mean wind speed above the critical wind speed to the presence of large roll vortices, since only the variances of the horizontal velocity components were affected. However, carefull analysis of the observations from other sources show that σ_w versus U-plots also exhibit abrupt changes in slope at a mean velocity of approximately 10 m/s. Moreover, identical variations can be observed from the data acquired over Lake Flevo in the Netherlands [47], a location where roll vortices are unlikely to exist. In addition, similar abrupt changes in the covariance $\overline{uw}$, and therefore the friction velocity as defined by $U^* = \sqrt{-\overline{uw}}$, exist for the observations from References 17, 48 (Fig. 27) and 53. These observations seem to furnish more evidence for the increased-roughness hypthesis than for the existence of roll vortices as an explanation for this phenomenon. In Table 8 a summary is presented of the variation of σ_α with mean velocity below and above the critical wind speed, while in Table 9 the average turbulence intensities in the high-velocity range in excess of 10 m/s are listed. The results clearly indicate the increase in intensity with mean velocity for the horizontal components and also a slight increase in intensity for the vertical component.

Figures 28 through 31 show the variation of σ_α and U* with mean velocity for three different stability categories based on the results listed in Reference 53. Since most of the results are for strong wind conditions (U > 10 m/s) the lines of best fit do not go through the origin but well below it. In addition, the plots exhibit a difinite stability dependence which is not negligible especially in case of the two horizontal components. The effect of stability in the case of the σ_w and U* versus U plots [Figs. 30, 31] is much less pronounced and consequently the scatter of the data is much less than for the lateral and streamwise components. Based on these observations it must be concluded that the turbulence intensities, σ_α/U, as well as the ratio U^*/U (and therefore also the drag coefficient U^{*2}/U^2) vary in varying degrees with mean wind speed (U > 10 m/s) as well as thermal stability.

The thermal stability dependence of the turbulence intensities and the velocity ratio, U*/U, can also be ascertained from the results plotted in Figs. 32 through 35. Here the data of Reference 53 were classified according to nine stability groups, $z/L < -0.10$, $-0.10 \leq z/L < -0.05$, $-0.05 \leq z/L < -0.025$, $-0.025 \leq z/L < -0.01$, $|z/L| < -0.01$, $0.01 \leq z/L < 0.025$, $0.025 \leq z/L < 0.05$, $0.05 \leq z/L < 0.10$ and $z/L \geq 0.10$. For each stability category the average stability, $(z/L)_{avg}$ and the straight line of best fit of σ_α and U* versus U were determined. From the latter the turbulence intensities σ_α/U and the ratio U*/U were calculated for given mean wind speeds between 10 m/s and 20 m/s. These results generally exhibit an increase with mean velocity and a decrease with stability. It is surprising to note that σ_w/U is relatively insensitive to stability but increases with mean wind speed. Also of note is the rather eratic behavior of U*/U with stability. The results

plotted in the Figs. 32 through 35 show the following variation due to velocity and stability, 7.5% < σ_u/U < 12%, 6% < σ_v/U < 11%, 4% < σ_w/U < 6% and 0.032 < U^*/U < 0.043.

A different way of analyzing the data is to group the turbulence intensities and the shear ratio U^*/U in velocity categories of 1 m/s intervals. As an example, all the available data between the mean wind speeds of 11.0 and 12.0 m/s are plotted versus z/L in Fig. 36. These results show a clear stability dependence for σ_u/U and σ_v/U, both increasing with decreasing stability, while the ratios σ_w/U and U^*/U are relatively insensitive with stability over the stability range shown. Similar plots for the other velocity categories between 11.0 and 20.0 m/s show identical behavior, although for mean wind speeds approaching 20 m/s, the stability range for the available data is much narrower and the stability dependence is less obvious. For mean wind speeds above 20 m/s the results show actually a slight decrease with decreasing stability over the stability range $|z/L| < 0.05$ (Fig. 37). The general stability dependence can be established by the fitting of straight lines to the data in each velocity category. The values of σ_α/U and U^*/U for zero stability (z/L = 0) are plotted against the average velocity for each velocity category (Fig. 38). Average values of σ_α/U for four different mean wind speeds and three stability values, z/L = 0.2, z/L = 0.0 and z/L = +0.2, based on the data of Reference 53 are also presented in Table 10.

7.2.2.3 Variation of σ_α with U^*

Special emphasis is placed in this article on the behavior of velocity ratios σ_α/U^* and on the coefficients A_α in the expression

$\sigma_\alpha = A_\alpha U^*$, with stability, specifically under near neutral conditions. Monin-Obukhov similarity theory predicts that in the surface layer velocity ratios σ_α/U^* are functions of the stability parameter z//L, independent of the roughness of the underlying surface and wind speed. Based on observations over uniform terrain and primarily under convective conditions, the Monin-Obukhov theory is adequate to explain the behavior of the vertical velocity component. However in Reference [61] it is pointed out that ratios of the standard deviations of horizontal velocity components to the friction velocity, U*, depend on z_i/L, where z_i is the height of the lowest inversion. However, for most of the available data no values for z_i are given and approximately 40% of the data have no values for z/L listed. The ratios σ_α/U^* or the coefficients A_α should be constants for near-neutral thermal stability, usually assumed to occur under sufficiently strong wind conditions when z/L and z_i/L both approach zero and convection in the surface layer is relatively unimportant.

First we will investigate if the velocity ratios σ_α/U^* vary with wind speed as was the case for the velocity ratios σ_α/U and U*/U. The plots of σ_α versus U* did not indicate any change from a linear relationship and always extrapolated towards the origin. In order to study the effect of wind speed more closely, all available values of σ_α/U^* were divided in velocity categories of 1 m/s interval, and a straight line relation $\sigma_\alpha/U^* = m(z/L) + b$ was fitted to the data from which values of σ_α/U^* at neutral stability, z/L = 0, for each velocity category were obtained. The results of this analysis are shown in Fig. 39, clearly indicating the independency of the ratios σ_α/U^* with wind

speed. The average values of these results which are $\sigma_u/U^* = 2.71$, $\sigma_v/U^* = 2.22$ and $\sigma_w/U^* = 1.39$ fit the results over the entire velocity range quite well. Comparable values under near-neutral conditions obtained from observations at a number of locations over uniform land terrain are $\sigma_u/U^* = 2.39$, $\sigma_v/U^* = 1.92$ and $\sigma_w/U^* = 1.25$ [11]. Comparison of these results show clearly that the average values obtained above water surfaces are systematically higher by approximately 15%.

The stability dependence of the turbulence ratios σ_α/U^* re shown in Fig. 40, where the data of Reference 53 were classified according to the same 9 stability groups as before in article 7.2.2.2. The average value of σ_α/U^* for each group was then plotted versus the average stability. The results show that σ_u/U^* and σ_v/U^* both increase under increasing thermally unstable conditions. Both σ_w/U^* and $U^{*2}/\sigma_u\sigma_w$ are quite independent with stability. Based on a linear regression analysis of these results, the values at neutral stability, $z/L = 0$, are $\sigma_u/U^* = 2.71$, $\sigma_v/U^* = 2.25$, $\sigma_w/U^* = 1.42$ and $U^{*2}/\sigma_u\sigma_w = 0.266$. These results compare favorably with the results of Fig. 39. In Fig. 41 all the data between $z = 8$ m and $z = 13.5$ m are classified in discrete stability categories and average values of σ_α/U^* are plotted versus average values of z/L. For this set of data the stability dependence is quite similar to that observed in Fig. 40, and the neutral values of σ_α/U^* are 2.66, 2.19 and 1.33 for $\alpha = u$, v and w respectively. The data from Reference 51 which were acquired over the open ocean and which are summarized in Fig. 42, the latter taken directly from this reference, show identical

behavior and neutral values of σ_α/U^* of 2.63, 2.19 and 1.25 respectively for α = u, v and w.

Figures 43, 44 and 45 show plots of all individual observations of σ_α/U^* versus stability up to a height of 150 m. Figure 43 shows a strong stability dependence for the data below a height of 20 m (normally the height of the surface layer) and in the stability range $|z/L| \leq 0.5$. Similar conclusions can be drawn for the results in Fig. 44 where the σ_v/U^* observations at z = 30 m do not seem to fit in with the observations between z = 2.3 m and z = 13.5 m. Also the same observations can be made for the σ_w/U^* data in Fig. 45.

The plots of the individual observations of σ_α/U^* versus z/L and restricted to the surface layer ($z \leq 20$ m) in Figs. 46, 47 and 48 show a clear stability dependence as far as the horizontal turbulence components is concerned.

The plotted data as well as the linear regression line clearly indicate a greater stability dependence for the lateral velocity component. On the other hand, the stability dependence of the vertical component is less clear and actually shows an increase under stable conditions and a near constant value under unstable conditions. The results published by DeLeonibus, Fig. 13 in Reference 63, show clearly a quite similar behavior. The average values for σ_α/U^* in the stability range $|z/L| < 0.1$ for these data sets are 2.64, 2.17 and 1.37 respectively for α = u, v and w. In Table 11 the average values at neutral conditions and obtained by different methods are listed together with the near-neutral land values from Panofsky and Dutton [11]. The values of σ_α/U^* for data acquired over water are 12%, 15% and 10% higher as compared for the land values for α = u, v and w respectively.

It has been observed that in the surface layer over land surfaces the turbulence ratios σ_u/U^* and σ_v/U^* are increased drastically due to the presence of large-scale fluctuations of the order z_i in the convective boundary layer and/or mesoscale terrain features in the case of complex terrain, and that in both cases σ_w/U^* is relatively unaffected [11]. Consequently it seems reasonable to assume that the increase in σ_w/U^* over water is primarily due to the travelling waves which certainly affect the turbulent flow just above the water surface. Davidson [13] has pointed out that turbulence ratios σ_α/U^* not only vary with stability but also with the wind-wave coupling parameter C/U^*. Here C is the phase velocity of the peak energy-containing components of the wave spectrum. Antonia and Chambers [15] observed that increases in σ_α/U^* are the combined effect of increases in σ_α and a decrease in the turbulence stress, provided $C/U^* > 40$. While for $C/U^* \leq 40$ values of σ_u/U^* and σ_w/U^* are in reasonable agreement with those measured over land for the same value of the stability parameter z/L. During the Davidson observations, May 1969, above the Atlantic Ocean approximately 200 miles northeast of Barbados, conditions prevailed for which $C/U^* > 40$. However, the presented values of σ_α/U^* are relatively small undoubltedly as a result of the short averaging time of 10.9 minutes. Since the data set presented in this report lacked information on wave speed, one can only assume that during these experiments conditions prevailed for which $C/U^* > 40$ and observed values of σ_α/U are expected to be in excess of those observed over land.

7.2.2.4 Turbulence Integral Scales

Longitudinal velocity scales are usually obtained from the integral time scale

$$T = \int_0^\infty R(\tau)d\tau, \tag{26}$$

from which the corresponding length scale can be obtained by multiplying this time scale by the mean velocity in accordance with Taylor's frozen wave hypothesis. This kind of integral scale is very sensitive to the presence of low-frequency velocity fluctuations and consequently on the method by which the turbulence is separated from the mean velocity. Lateral and vertical scales can be obtained by integration of the space-correlation coefficients with lateral and vertical separation distances respectively. In order to obtain reasonable estimates of these scales it is assumed that these correlation coefficients decay exponentially according to

$$R_\alpha(y') = \exp[-y'/L_\alpha^y]$$

and (27)

$$R_\alpha(z') = \exp[-z'/L_\alpha^z]$$

where y' and z' are the separation distances in either the lateral or vertical direction. Lateral integral scales can then be obtained from a least-squares fit of expression 27 on the measured correlation coefficients for various separation distances y' and z'. Some of these scales have been measured with instrumented towers located on land close to the water [60, 64 and 65]. The results from the two expermental sites show a reasonable agreement. The variation in the longitudinal

integral scales measured at Wallops Island is primarily due to the presence of large scale low-frequency velocity fluctuations.

An alternate method for obtaining the length scale of the energy-containing eddies is by determining the wavelength, λ_m, corresponding to the peak of the logarithmic spectrum which is related to the integral scale as follows [66],

$$L_x = \frac{1}{2\pi} \lambda_m = \frac{1}{2\pi} \frac{U}{n_m} = \frac{1}{2\pi} \frac{z}{f_m}, \tag{28}$$

where n_m is the peak cyclic frequency and f_m the peak reduced frequency. However often, primarily under convective conditions the logarithmic spectral functions are quite flat near their maximum and no distinct peak can be discerned except for the vertical velocity spectra. Typical values for the peak reduced frequency for the w-spectra are $f_m = 0.25$ for unstable conditions and $f_m = 0.5$ for stable conditions [59]. With expression 28 this leads to values of $L_x^w = 25$ m and $L_x^w = 13$ m respectively at a height of 40 m which is in reasonable agreement with the value of $L_x^w = 32$ m from Reference 65 (Table 12).

So far our discussion of integral scales has been based on observations made from stationary platforms. Spectra measured from moving platforms such as aircraft flying in the along-wind direction are related to those obtained from stationary platforms with the aid of Taylor's frozen wave hypothesis. The along-wind u and v spectra contain the low-frequency fluctuations similar to the spectra obtained from a stationary plat form, while the w spectra have a well defined peak in both cases [36,67]. The across-wind u and v spectra lack the low-frequency contribution especially under near-neutral conditions. Integral scales obtained from the peak wave length of the along-wind

spectra must be interpreted as longitudinal integral scales like L_x^a, while the lateral integral scales L_y^a are related to the across-wind spectra. The results presented in Table 12 show that the along-wind and across-wind integral scales from aircraft spectra compare quite well with the integral scales obtained from the correlation coefficients from an array of stationary wind measuring instruments.

8. Summary and Conclusions

8.1 General Observations and Remarks

The purpose of this report has been to provide detailed information of the atmospheric flow in the surface layer above the ocean, say below 30 m. This information is required as input for the design and operation of remotely piloted aircraft at low velocities and low altitudes above the water surface. In this report most of the available experimental data are reviewed and brought together in order to provide this information.

Many of the flow observations in the surface layer over the ocean suffer from experimental error and lack of calibration control etc. Despite continuous improvements of the measurement techniques, the data handling and the data analysis, one must expect a considerable scatter of the results. Some of this scatter is experimental in nature, some is due to the variable conditions encountered at the sea-air interface. Above all the atmospheric flow must be considered as being random in time and space and consequently the results presented in this report must be interpreted as averages based on a limited number of observations. What the probability is that the average results will actually occur at any given time and at any instant is difficult to ascertain. In order to get some idea of the variability of the

observations, standard deviations of the presented data have also been included in the tables.

There is a number of important differences between the atmospheric flow over water and over land. The most obvious difference is that of the surface which is fixed over land and is in motion over water, examplified by travelling waves generated by the atmospheric flow. The influence of the atmospheric flow on the disturbed water surface and vice versa the influence of the disturbed water surface on the flow is extremely complex and not well understood. Analysis of the data in this report show that mean wind profiles and turbulence are extremely variable below 10 m. Most likely as a results of wave effects.

8.2 Conclusions for the Mean Velocity Profile

The variability of the mean flow in the ABL is evident of the data presented in Figures 2, 3a and 4 and 5, while the mean flow variability near the water surface is well demonstrated in Figures 6 and 8. Despite a stability dependence, the variability of the mean velocity profile is clearly exemplified by the scatter of the profile roughness, z_o, as presented in references 29 and 31. In both cases the variability of z_o, based on many hundreds of velocity profiles measured near the water surface below z = 10 m is several orders of magnitude, varying between 10^{-3} mm and 100 mm. Krügermeyer et al. [14] showed that the mean wind profile is distorded by the waves to heights equivalent to three wave heights. Under strong wind conditions U > 15 m/s, the significant wave height may be as much as 5 m.

8.3 Conclusions for the Turbulence Statistics

Near the water surface the turbulence statistics such as variances and covariances are dependent on the thermal stability of the atmosphere and on the sea state which itself is closely related to the prevailing wind speed and the origin of the generated wave field. The significant conclusions based on the reference survey and the data analyzed in this report can be summarized as follows.

8.3.1 Turbulence Ratios σ_α/U^*

1. Turbulence ratios σ_α/U^* in the surface layer over water ($z \leq 20$ m) deviate from the average observations over land, provided the phase velocity C of the energy containing waves is at least 40 times the friction velocity U^* [13].
2. Under the above conditions increases in the turbulence ratios σ_α/U^* are due to an increase in σ_α and a decrease in U^* [15].
3. For the data sets used in this report, values of C/U^* are generally not available. However, based on the Davidson results [13], it seems appropriate to assume that for fully developed waves, which generally occur over the open ocean, the ratio C/U^* is generally larger than 40. Therefore larger values of σ_α/U^* can be expected in the surface layer over water than over land. (Figs. 21, 22 and 23).
4. The turbulence ratios σ_α/U^* are generally independent with wind speed (Fig. 39).
5. The stability dependence of the turbulence ratios σ_α/U^* is different in the surface layer ($z \leq 20$ m) than at higher elevations ($z > 20$ m) (Figs. 43, 44 and 45).

6. Both σ_u/U^* and σ_v/U^* increase appreciably with decreasing stability (Figs. 40, 41 and 42).
7. In the surface layer ($z \leq 20$ m) the linear regressions $\sigma_u/U^* = 2.64 - 1.02\ z/L$ and $\sigma_v/U^* = 2.22 - 3.09\ z/L$ are the best fit to the available data (Figs. 46 and 47).
8. In the surface layer ($z \leq 20$ m) the turbulence ratio σ_w/U^* is relatively independent with stability (Figs. 40, 41, 42 and 48).
9. In the surface layer ($z \leq 20$ m) and for near-neutral stability conditions average values for σ_α/U^* are 2.67, 2.20 and 1.38 for α = u, v and w respectively. Average over-land values are 2.39, 1.92 and 1.25 (Table 11).

8.3.2 Velocity Ratios σ_α/U and U^*/U

1. The velocity ratios σ_α/U and U^*/U vary with height (Figs. 18, 19 and 20), with wind speed (Figs. 24 through 31 and 38), and with thermal stability (Figs. 32 through 37).
2. The standard deviations of the turbulence, σ_α, and the friction velocity, $U^* = \sqrt{-\overline{uw}}$ vary with mean wind speed in different ways depending whether the mean wind speed is below or above some critical value (Table 8).
3. This change in mean wind-speed dependence is probably the result of increased roughness which occurs under strong wind conditions.
4. The critical value for U varies with height but is approximately 10 m/s at z = 10 m.
5. For wind speeds below the critical value, σ_α and U^* vary linearly with U. The line of best fit generally passes the origin closely (Table 8).

6. For wind speeds in excess of the critical wind speed, τ_s and U^* still vary linearly with U. However, the slope of the linear regression is increased and definitely does not pass through the origin (Figs. 24 through 31).
7. For mean velocities below the critical wind speed and for near-neutral thermal stability conditions, values for the turbulence intensities, σ_α/U, can be otained from Figures 18, 19 and 20. Average values under these conditions at z = 10 m are σ_u/U = 8%, σ_v/U = 6% and σ_w/U = 4.2% while U^*/U = 0.034.
8. For near-neutral conditions and for wind speeds in excess of the critical wind speeds, values for the turbulence intensities σ_α/U vary with height and wind speeds (Table 9).
9. Averaged turbulence intensities at z = 13.5 m for four specific values of mean wind speeds (U = 10, 13, 16 and 19 m/s) in excess of the critical wind speed and for three stability conditions (z/L = -0.2, 0.0, +0.2) are prsented in Table 10.
10. At z = 13.5 m, depending on stability and mean wind speed, σ_u/U varies between 6.6 and 12.8%, σ_v/U between 4.2 and 10.9%, and σ_w/U between 4.2 and 5.8%.

8.3.3 Integral Scales and Spectra

1. Integral scales obtained from auto or space correlation coefficients are very sensitive to the presence of low-frequency or large-scale velocity fluctuations, and consequently vary greatly in magnitude (Table 12).
2. Integral scales obtained from the wavelength corresponding to the peak of the logarithmic velocity spectra compare rasonably well with those obtained from correlation coefficients.

3. Over water the measured integral scales are generally several times larger than those observed over uniform land terrain.
4. The shape of the velocity spectra depends primarily on stability and in the case of aircraft data on the flight direction (along wind or across wind) [67].
5. Independent of stability, more low-frequency energy ($f < 0.1$) is observed in the along-wind measured u and w spectra while in the high-frequency range $f > 0.1$ more energy is present in the across-wind measured spectra [67].
6. The shape of spectra measured in the along-wind direction agrees well with the shape of velocity spectra measured over land [67].

8.4 Final Remarks

The meteorological data which were analyzed in this report were primarily acquired for vertical flux studies of momentum, heat and water vapor, and were not acquired for the purpose of providing design input and operation criteria for low-flying aircraft. Despite this and the limited amount of data available, a reasonable description of the mean and turbulent flow in the surface layer over the ocean has been presented in this report. Notwithstanding the fact that the presented results do not provide a complete picture of the flow, it is believed they are adequate as an input to the design and operation of remotely piloted aircraft flying at low-Reynolds numbers just above the ocean.

References

1. Lissaman, P. B. S., 1983, Low-Reynolds-Number Airfoils, Annual Review of Fluid Mechanics, Annual Reviews Inc., 15, 223-239.

2. Houbolt, J. C., 1973, Survey on Effect of Surface Winds on Aircraft Design and Operation and Recommendations for Needed Wind Research, NASA-CR-2360.

3. Frost, W. and Lin, M. C., 1983, Statistical Analysis of Turbulence Data from the NASA Marshall Space Flight Center Atmospheric Boundary Layer Tower Array Facility, NASA-CR-3737.

4. Arya, S. P., 1982, Atmospheric Boundary Layers Over Homogeneous Terrain, Engineering Meteorology, Elsevier, New York, 233-267.

5. Lumley, J. L. and Panofsky, H. A., 1964, The Structure of Atmospheric Turbulence, Interscience, New York, 239 pp.

6. Tennekes, H. and Lumley, J. L., 1972, A First Course in Turbulence, The MIT Press, Cambridge, Mass., 300 pp.

7. Tennekes, H., 1973, Similarity Laws and Scale Relations in Planetary Boundary Layers, Workshop on Micrometeorology, American Meteorological Society, Boston, Mass., 177-216.

8. Monin, A. S. and Obukhov, A. M., 1954, Basic Regularity in Turbulent Mixing in the Surface Layer of the Atmosphere, Trudy Geophys. Inst. ANSSSR, No. 24, 163-187.

9. Jensen, N. O. and Busch, N.E., 1982, Atmospheric Turbulence, Engineering Meteorology, Elsevier, New York, 179-231.

10. Haugen, D. A. Ed., 1973, Workshop on Micrometeorology, American Meteorological Society, Boston, Mass.

11. Panofsky, H. A. and Dutton, J. A., 1984, Atmospheric Turbulence, Wiley-Interscience, New York.

12. Kondo, J. et al., 1972, Wave-Induced Wind Fluctuation Over the Sea, Journal Fluid Mechanics, 51, 751-771.

13. Davidson, K. L., 1974, Observational Results on the Influence of Stability and Wind-Wave Coupling on Momentum Transfer and Turbulent Fluctuations Over Ocean Waves, Boundary-Layer Meteorology, 6, 305-331.

14. Krügermeyer, L. et al., 1978, The Influence of Sea Waves on the Wind Profile, Boundary-Layer Meteorology, 14, 403-414.

15. Antonia, R. A. and Chambers, A. J., 1980, The Wind-Wave-Induced Disturbances in the Marine Surface Layer, Journal of Physical Oceanography, 10, 611-622.

16. Miyake, M., et al., 1971, Comparison of Acoustic Instruments in an Atmospheric Turbulent Flow Over Water, Boundary Layer Meteorology, 2, 228-245.

17. Smith, S. D. et al., 1976, A Comparison of the Air-Sea Interaction Flux Measurement Systems of the Bedford Institute of Oceanography and the Institute of Oceanography, University of British Columbia, Report Series, BI-R-76-17, Bedford Institute of Oceanography, Dartmouth, Nova Scotia, Canada.

18. Blanc, T. V., 1983, A Practical Approach to Flux Measurements of Long Duration in the Marine Atmospheric Surface Layer, Journal of Climate and Applied Meteorology, 22, 1093-1110.

19. Paulson, C. A., 1970, The Mathematical Representation of Wind Speed and Temperature Profiles in the Atmospheric Surface Layer, Journal Applied Meteorology, 9, 857-861.

20. Blanc, T. V., 1983, An Error Analysis of Profile Flux, Stability and Roughness Length Measurements Made in the Marine Atmospheric Surface Layer, Boundary-Layer Meteorology, 26, 243-267.

21. Wieringa, J., 1974, Comparison of Three Methods for Determining Strong Wind Stress Over Lake Flevo, Boundary Layer Meteorology, 7, 3-19.

22. Schmitt, K. F., et al., 1978, Sea Surface Stress Measurements, Boundary-Layer Meteorolgoy, 15, 215-228.

23. LeMone, M. A. and Pennell, W. T., 1976, The Relationship of Trade Wind Cumulus Distribution to Subcloud Layer Fluxes and Structure, Monthly Weather Review, 104, 524-539.

24. Charnock, H., et al., 1956, An Investigation of Wind Structure in the Trades: Anegada 1953, Philosophical Transactions of the Royal Society of London, A249, 179-234.

25. Nicholls, S. and Readings, C. J., 1979, Aircraft Observations of the Structure of the Lower Boundary Layer Over the Sea, Quarterly Journal of the Royal Meteorological Society, 105, 785-802.

26. SethuRaman, S., 1980, A Case of Persistent Breaking of Internal Gravity Waves in the Atmospheric Surface Layer Over the Ocean, Boundary-Layer Meteorology, 19, 67-80.

27. Tieleman, H. W. and Mullins, S. E., 1980, The Structure of Moderately Strong Winds at a Mid-Atlantic Coastal Site (Below 75m), Wind Engineering, Vol. 1, 145-159, Pergamon Press.

28. Pennell, W. T. and LeMone, M. A., 1974, An Experimental Study of Turbulence Structure in the Fair-Weather Trade Wind Boundary Layer, Journal of the Atmospheric Sciences, 31, 1308-1323.

29. Brocks, K. and Krügermeyer, L., 1972, The Hydrodynamic Roughness of the Sea Surface, Studies in Physical Oceanography 1, Paper #5, Gordon and Breach, New York.

30. Wieringa, J. and Rijkoort, P. J., 1983, Wind Klimaat van Nederland, (Wind Climate of the Netherlands) Staatsuitgeverij, The Hague, The Netherlands.

31. Ruggles, K. W., 1970, The Vertical Mean Wind Profile Over the Ocean for Light to Moderate Winds, Journal Applied Meteorology, 9, 389-395.

32. Fujita, T., 1983, Vertical Profile of Wind Speed Over the Open Sea, Journal of the Meteorological Society of Japan, 61, 100-109.

33. LeMone, M. A., 1978, The Marine Boundary Layer, Workshop on the Planetary Boundary Layer, American Meteorological Society, Boston, 182-231.

34. SethuRaman, S., 1977, The Observed Generation and Breaking of Atmospheric Internal Gravity Waves Over the Ocean, Boundary-Layer Meteorology, 12, 331-349.

35. Nicholls, S. and LeMone, M. A., 1980, The Fair Weather Boundary Layer in GATE: The Relationship of Subcloud Fluxes and Structure to the Distribution and Enhancement of Cumulus Clouds, Journal of the Atmospheric Sciences, 37, 2051-2067.

36. Nicholls, S., 1978, Measurement of Turbulence by an Instrumented Aircraft in a Convective Atmospheric Boundary Layer Over the Sea, Quarterly Journal of the Royal Meteorological Society, 104, 653-676.

37. Naito, G., and Kondo, J., 1974, Spatial Structure of Fluctuating Components of the Horizontal Wind Speed Above the Ocean, Journal of the Meteorological Society of Japan, 52, 391-399.

38. Zubkovskii, S. L., and Kravchenko, T. K., 1967, Direct Measurements of Some Characteristics of Atmospheric Turbulence in the Near-Water Layer, Atmospheric and Oceanic Physics (English Translation) 3, 73-77.

39. Miyake, M., et al., 1970, Comparison of Turbulent Fluxes Over Water Determined by Profile and Eddy Correlation Techniques, Quarterly Journal of the Royal Meteorological Society, 96, 132-137.

40. Miyake, M., et al., 1970, Spectra and Cospectra of Turbulence Over Water, Quarterly Journal of the Royal Meteorological Society, 96, 138-143.

41. Smith, S. D., 1967, Thrust-Anemometer Measurements of Wind-Velocity Spectra and of Reynolds Stress Over a Coastal Inlet, Journal of Marine Research, 25, 239-262.

42. Antonia, R. A., et al., 1978, Measurements of Turbulent Fluxes in Bass Strait, Journal of Physical Oceanography, 8, 28-37.

43. Smith, S. D., 1974, Eddy Flux Measurements Over Lake Ontario, Boundary-Layer Meteorology, 6, 235-255.

44. Pond, S., et al., 1971, Measurements of the Turbulent Fluxes of Momentum, Moisture and Sensible Heat Over the Ocean, Journal of Atmospheric Sciences, 28, 901-917.

45. Leavitt, E. and Paulson, C. A., 1975, Statistics of Surface Layer Turbulence Over the Tropical Ocean, Journal of Physical Oceanography, 5, 143-156.

46. SethuRaman, S. and Raynor, G. S., 1980, Comparison of Mean Wind Speeds and Turbulence at a Coastal Site and an Offshore Location, Journal of Applied Meteorology, 19, 15-21.

47. Wieringa, J., 1973, Applications of Turbulence Measurements Over Lake Flevo, Ph.D. Thesis University of Utrecht, The Netherlands.

48. Smith, S. D. and Banke, E. G., 1975, Variation of the Sea Surface Drag Coefficient With Wind Speed, Quarterly Journal of the Royal Meterological Society, 101, 665-673.

49. SethuRaman, S., 1979, Structure of Turbulence Over Water During High Winds, Journal of Applied Meteorology, 18, 324-328.

50. Smith, S. D., 1970, Thrust-Anemometer Measurements of Wind Turbulence, Reynolds Stress and Drag Coefficient Over the Sea, Journal of Geophysical Research, 75, 6758-6770.

51. Large, W. G., 1979, The Turbulent Fluxes of Momentum and Sensible Heat Over the Open Sea During Moderate to Strong Winds, Ph.D. Thesis, University of British Columbia.

52. Large, W. G. and Pond, S., 1981, Open Ocean Momentum Flux Measurements in Moderate to Strong Winds, Journal of Physical Oceanography, 11, 324-336.

53. Smith, S. D., 1980, Wind Stress and Heat Flux Over the Ocean in Gale Force Winds, Journal of Physical Oceanography, 10, 709-726.

54. Rayner, G. S., et al., 1975, Studies of Atmospheric Diffusion from a Nearshore Oceanic Site, Journal of Applied Meteorology, 14, 1080-1094.

55. SethuRaman, S. et al., 1978, A Comparison of a Eulerian and Lagrangian Time Scale for Over-Water Atmospheric Flows During Stable Conditions, Boundary-Layer Meteorology, 14, 557-565.

56. Mitsuta, Y. and Fujitani, T., 1974, Direct Measurement of Turbulent Fluxes on a Cruising Ship, Boundary-Layer Meteorology, 6, 203-217.

57. Donelan, M. and Miyake, M., 1973, Spectra Fluxes in the Boundary Layer of the Trade-Wind Zone, Journal of the Atmospheric Sciences, 30, 444-464.

58. Miyake, M. et al., 1970, Airborne Measurement of Turbulent Fluxes, Journal of Geophysical Research, 75, 4506-4518.

59. Schmitt, K. F. et al., 1979, Structure of Marine Surface Layer Turbulence, Journal of the Atmospheric Sciences, 36, 602-618.

60. Tieleman, H. W., 1980, Planetary Boundary Layer Wind Model Evaluation at a Mid-Atlantic Coastal Site, Department of Energy Report, DOE/ET/23007-80/1.

61. Panofsky, H. A. et al., 1977, The Characteristics of Turbulent Velocity Components in the Surface Layer Under Convective Conditons, Boundary-Layer Meteorology, 11, 355-361.

62. Naito, G., 1983, Spatial Structure of Surface Wind over the Ocean, Journal of Wind Engineering and Industrial Aerodynamics, 13, 67-76.

63. DeLeonibus, P. S., 1971, Momentum Flux and Wave Spectra Observations from an Ocean Tower, Journal of Geophysical Research, 76, No. 27, 6506-6527.

64. Shiotani, M., Iwatani, Y., 1976, Horizontal Space Correlations of Velocity Fluctuations During Strong Winds, Journal of the Meteorological Society of Japan, 54, 1, 59-66.

65. Shiotani, M., et al., 1978, Magnitudes and Horizontal Correlations of Vertical Velocities in High Winds, Journal of the Meteorological Society of Japan, 56, 1, 35-42.

66. Kaimal, J. C., 1973, Turbulence Spectra, Length Scales and Structure Parameters in the Stable Surface Layer, Boundary-Layer Meteorology, 4, 289-309.

67. Nicholls, S. and Readings, C. J ., 1981, Spectral Characteristics of Surface Layer Turbulence Over the Sea, Quarterly Journal of the Royal Meteorological Society, 107, 591-614.

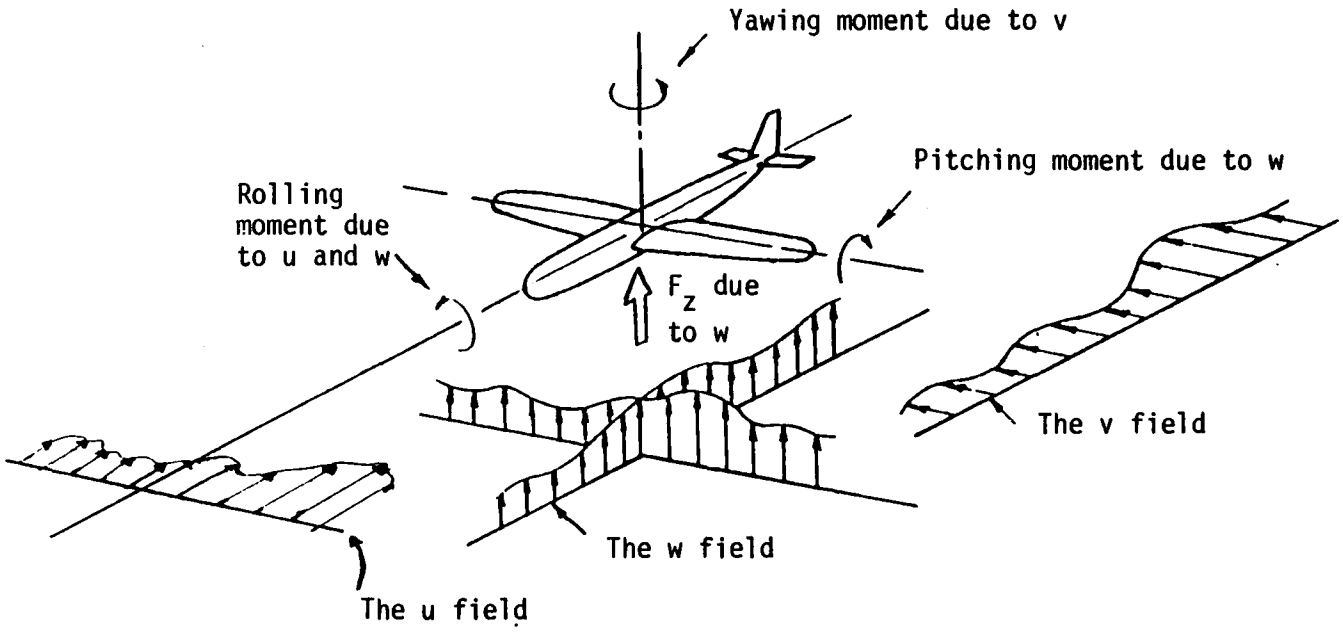

FIGURE 1 Predominant Force and Moments that Act on an Airplane in Turbulence (Taken from Reference 2).

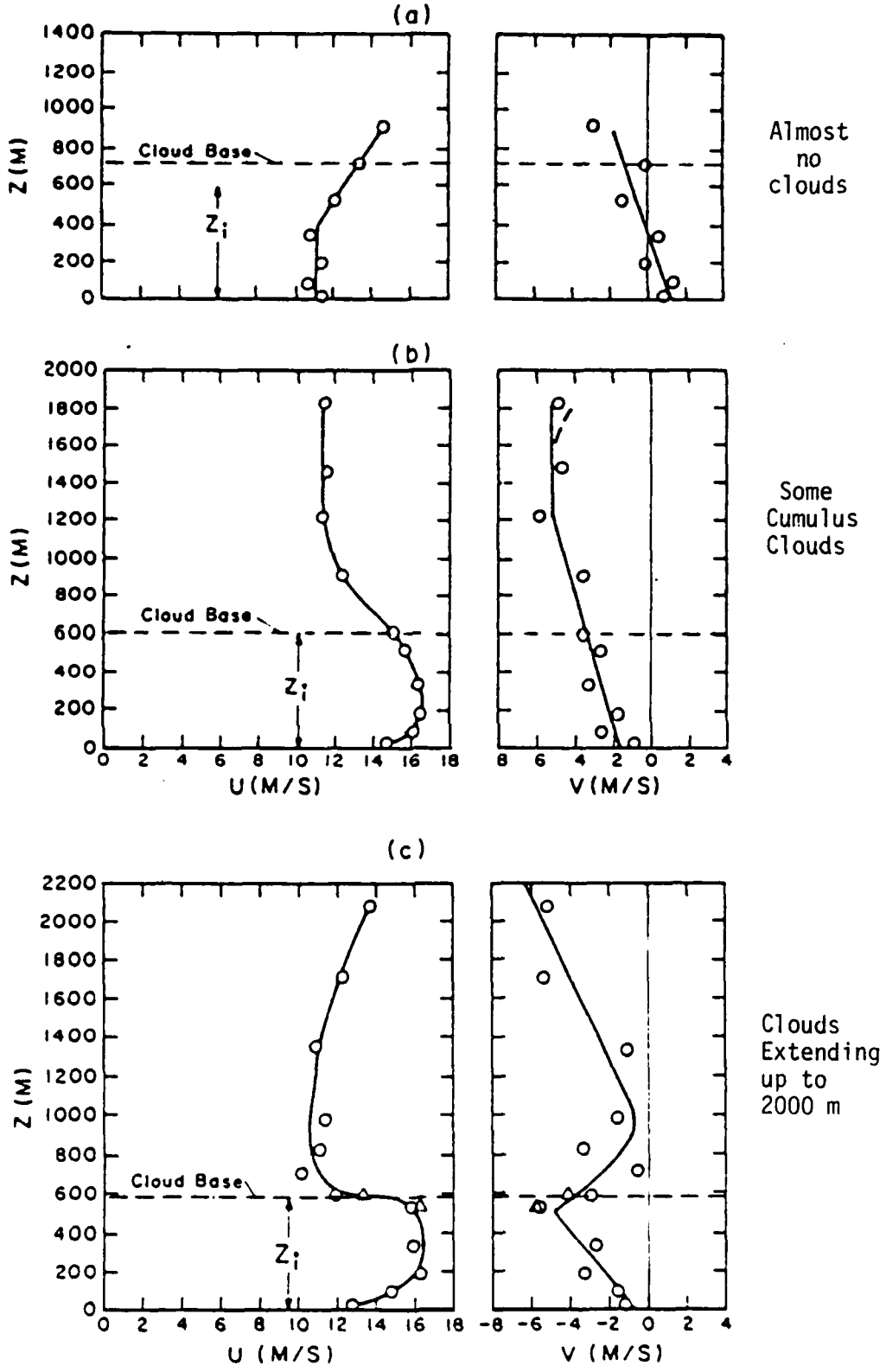

FIGURE 2 Mean Velocity profiles in the trade-wind boundary layer (a) near neutral conditions, (b) intermediate convection, (c) stronger convection. U-west component, V-south component. Surface wind predominantly from east (Reference 23).

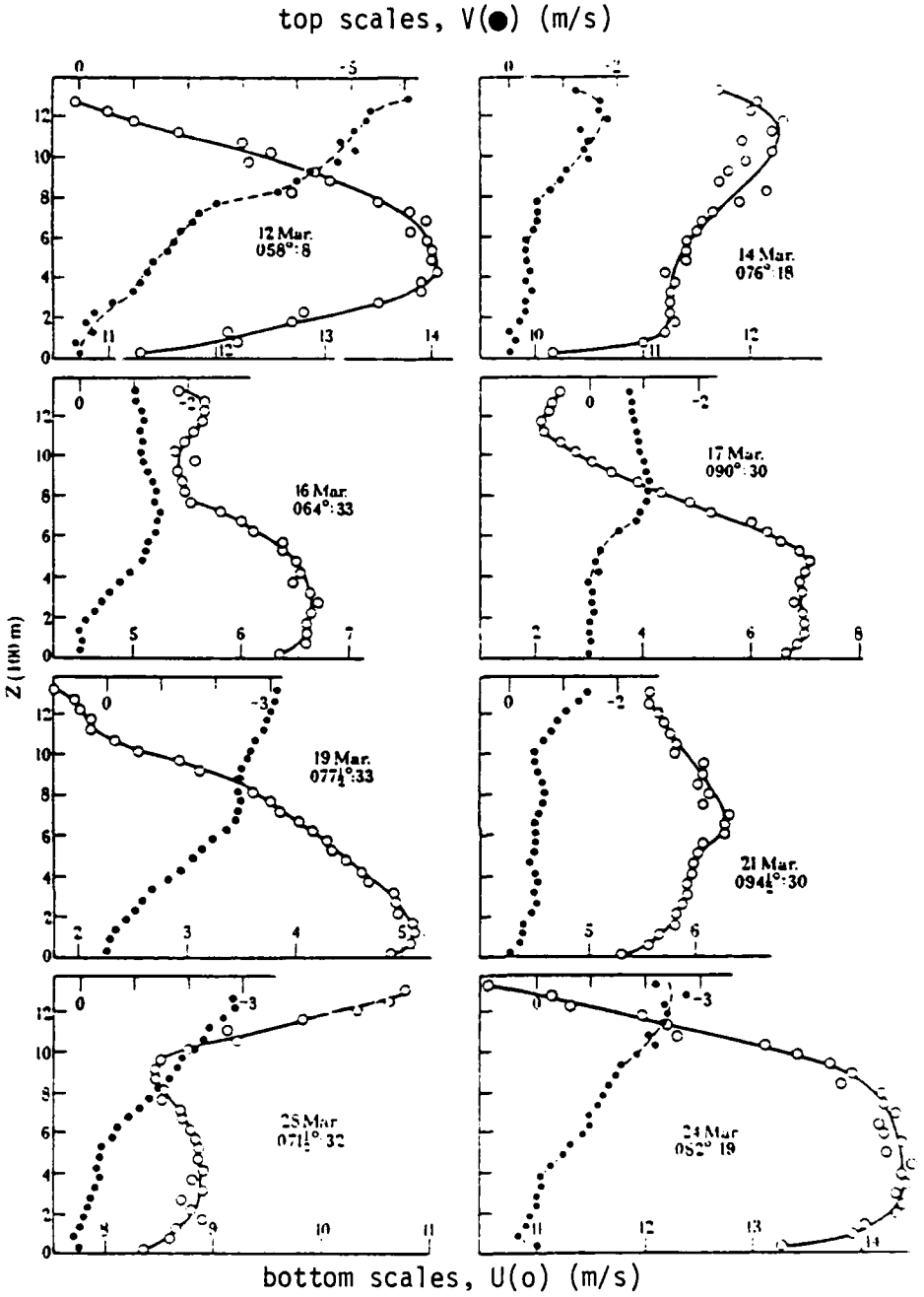

FIGURE 3a Averaged mean velocity profiles taken at the small island of Anegada north-east of Puerto Rico (Reference 24).

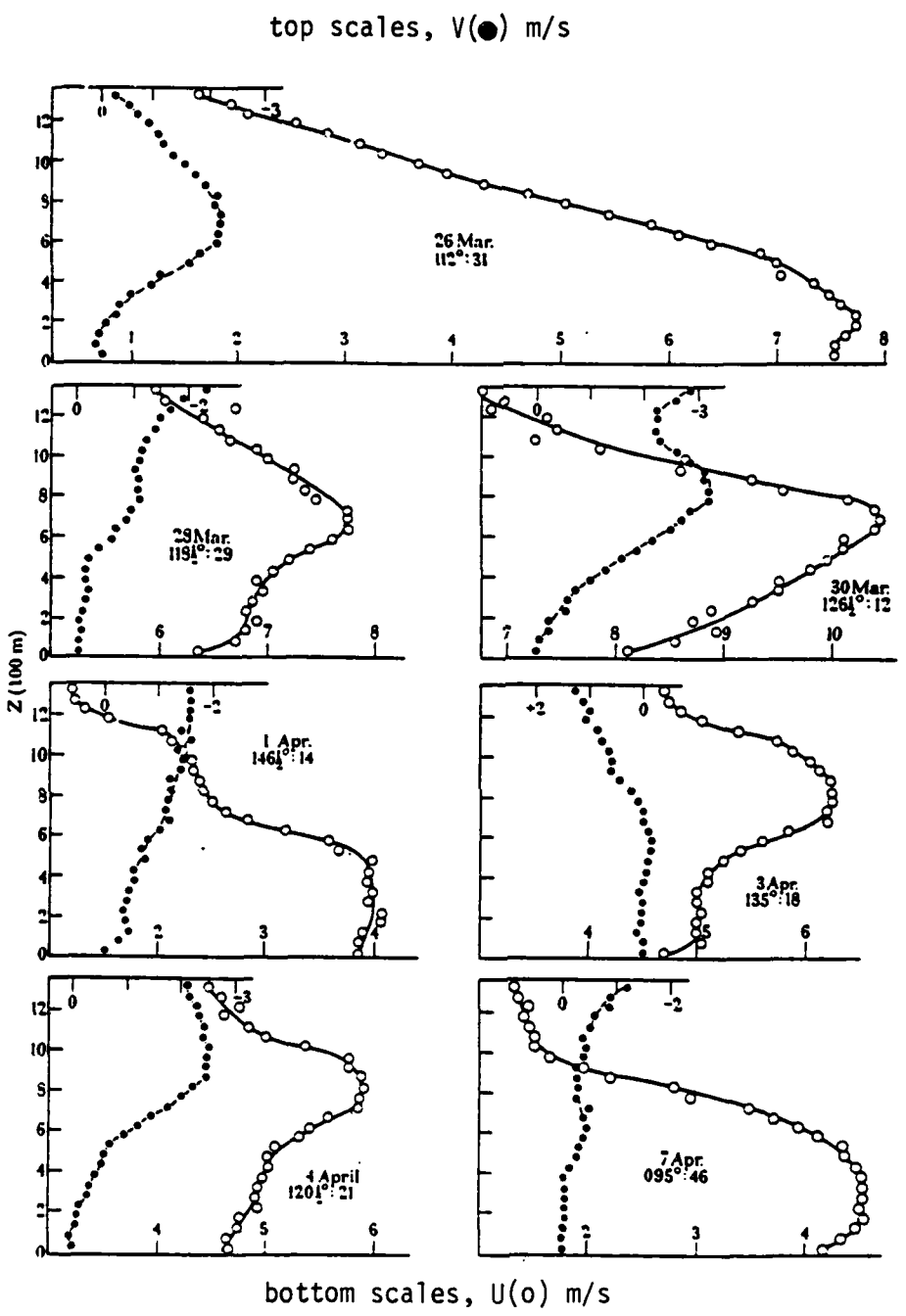

FIGURE 3b Averaged mean velocity profiles taken at the small island of Anegada northeast of Puerto Rico (Reference 24).

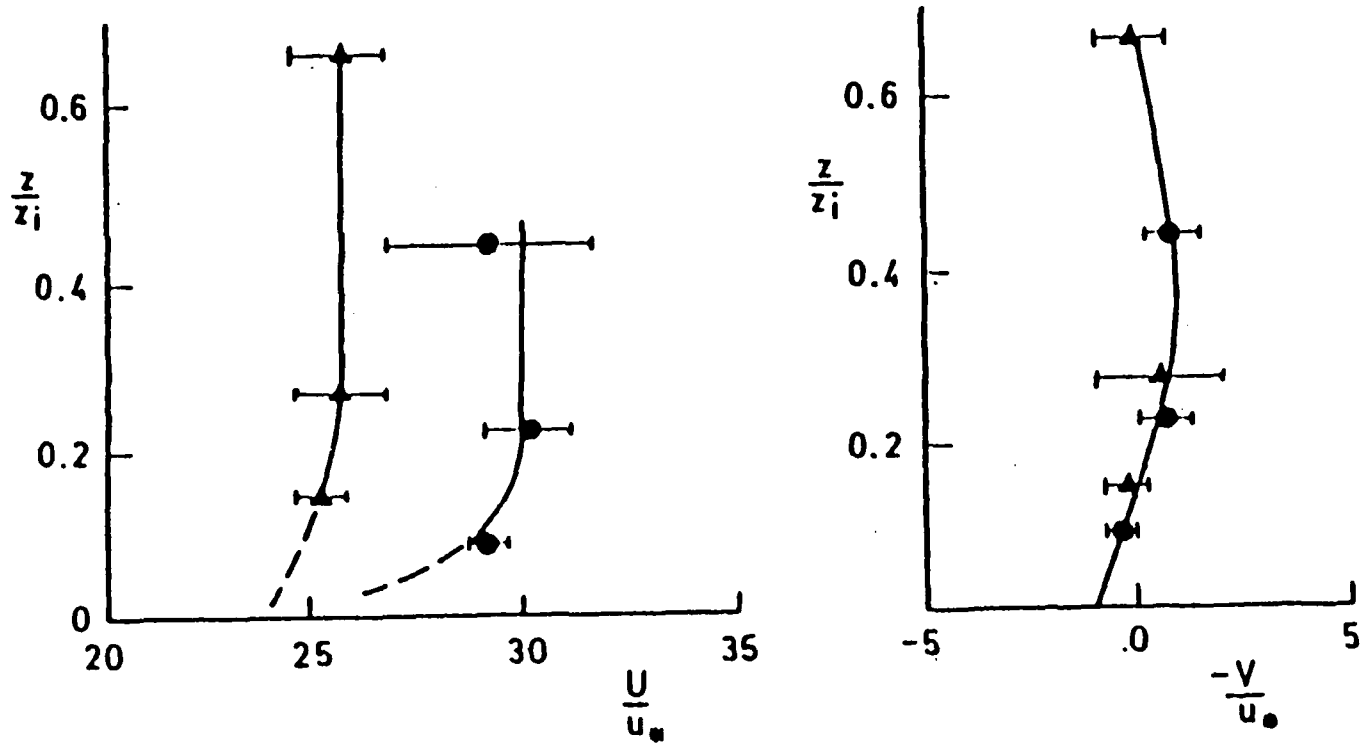

FIGURE 4 Average mean velocity profiles over the sea around Great Britain ▲) $(z_i/L)_{avg}$ = -3.9 (more unstable category) ●) $(z_i/L)_{avg}$ = -0.9 (less unstable) (Reference 25)

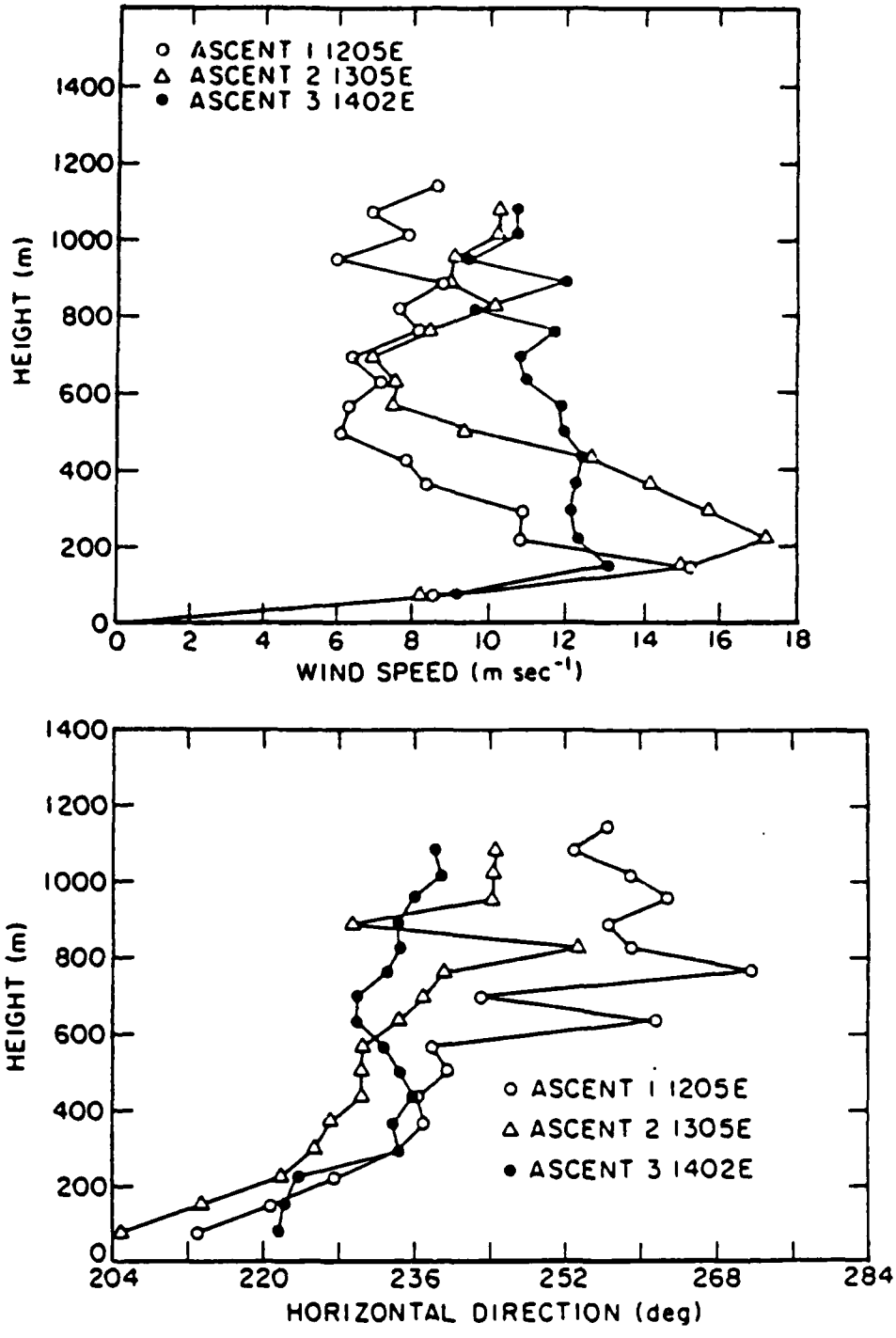

FIGURE 5 Wind speed and direction profiles at Long Island Beach obtained by pilot-balloon soundings (Reference 26). Thermally stable conditions.

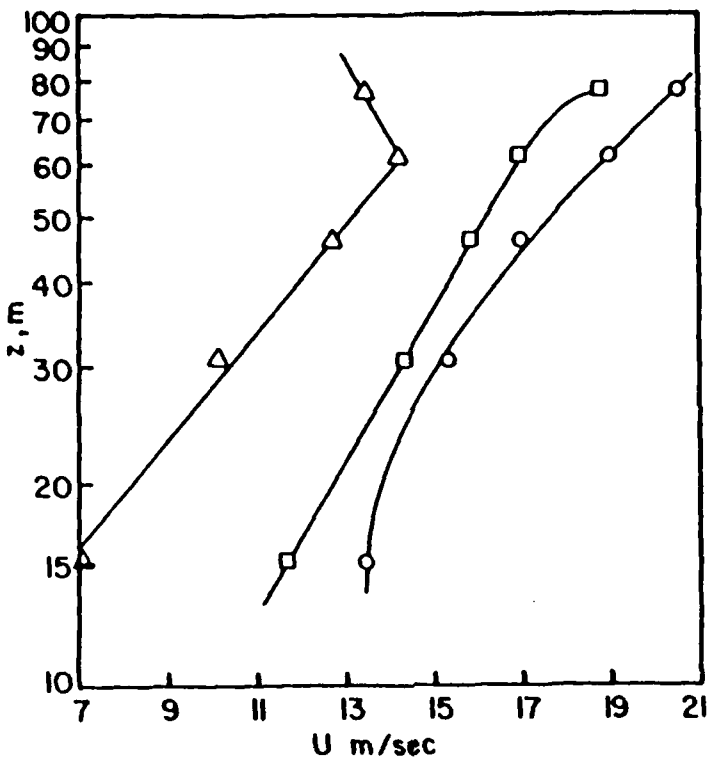

FIGURE 6 Mean velocity profiles at Wallops Island from tower mounted instrumentation (Reference 27).

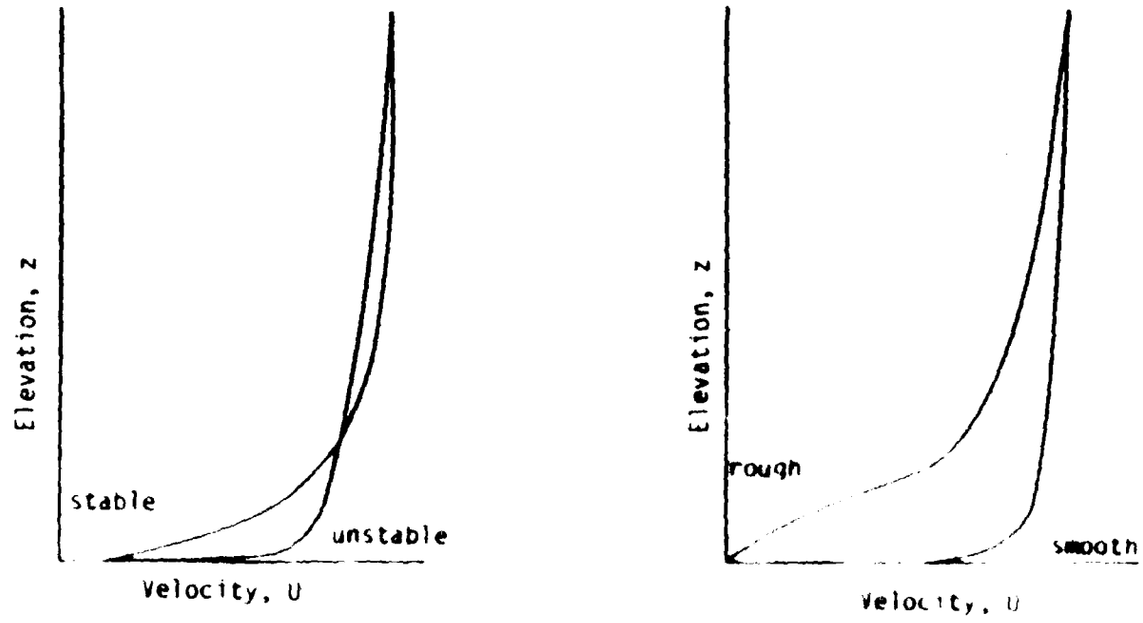

FIGURE 7 Schematic diagram of the influence of thermal stability and surface roughness on the wind profile (Reference 30).

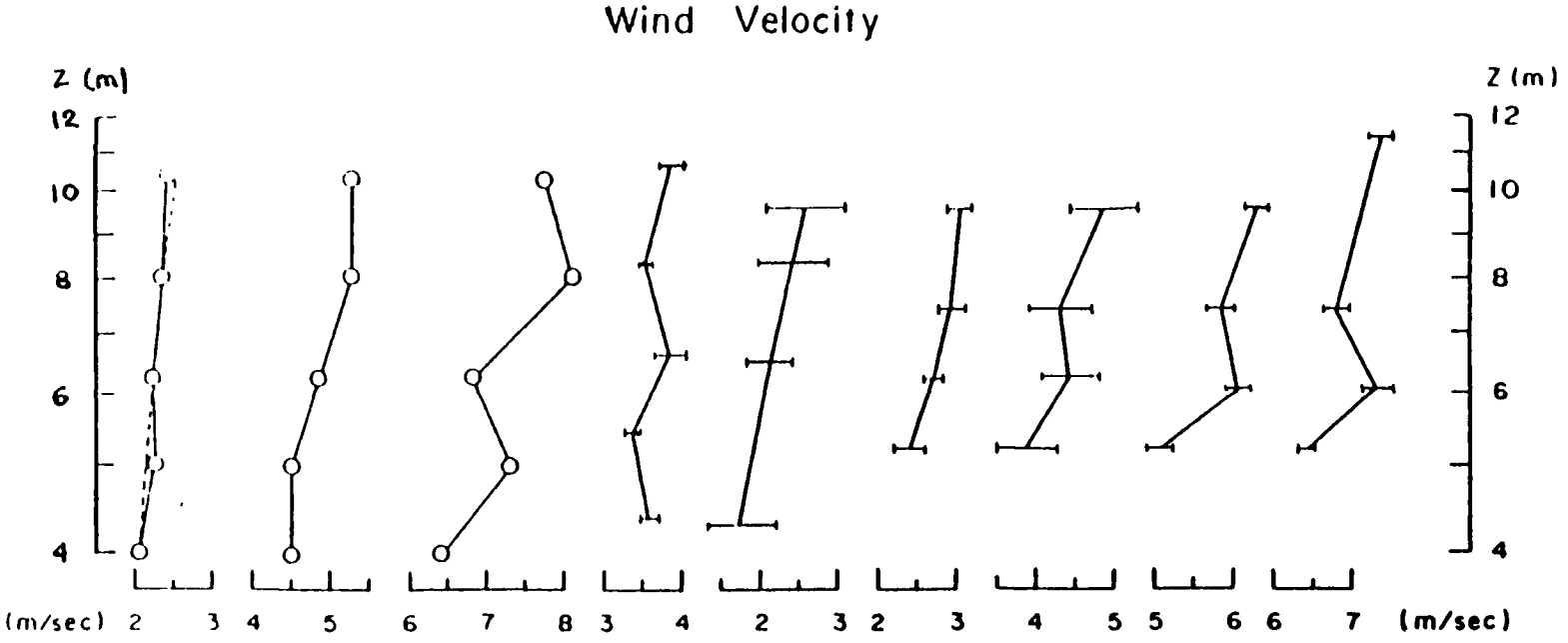

FIGURE 8 Mean velocity profiles measured near the ocean surface (Reference 32).

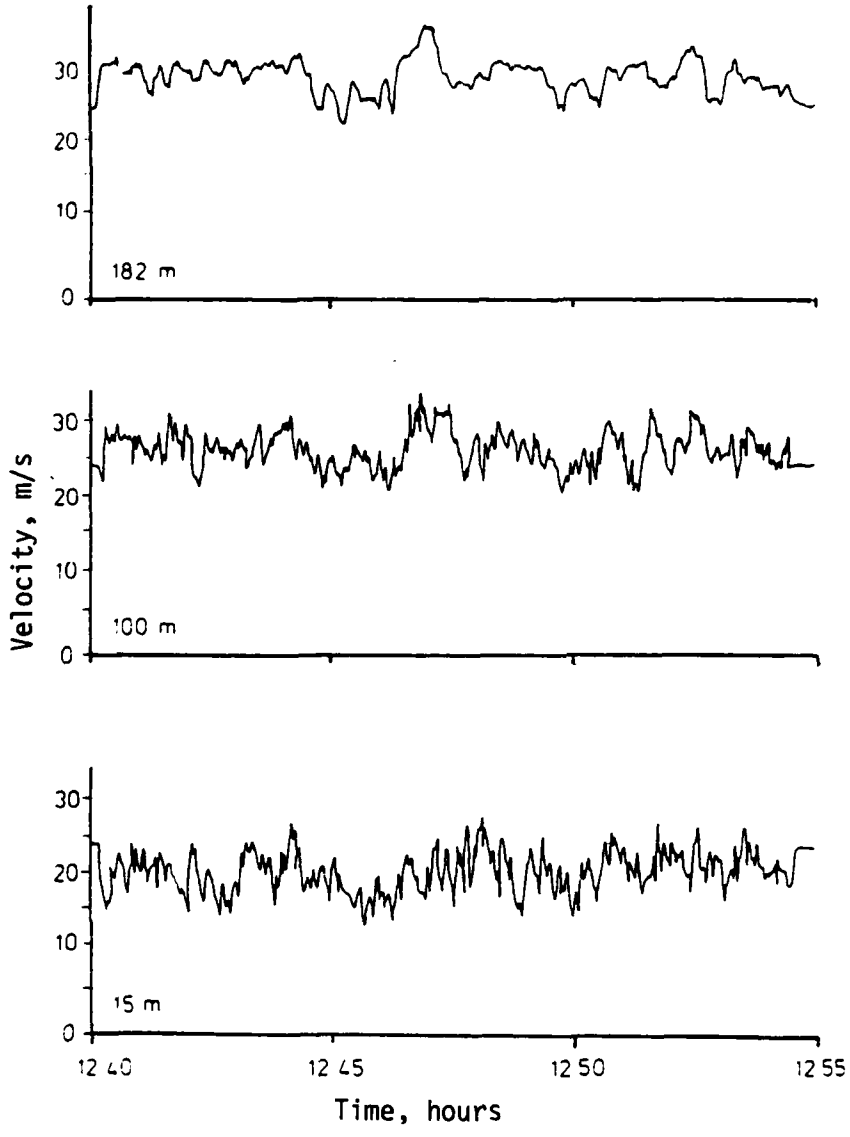

FIGURE 9 Times series of the turbulence at several heights sampled simultaneous (Reference 30).

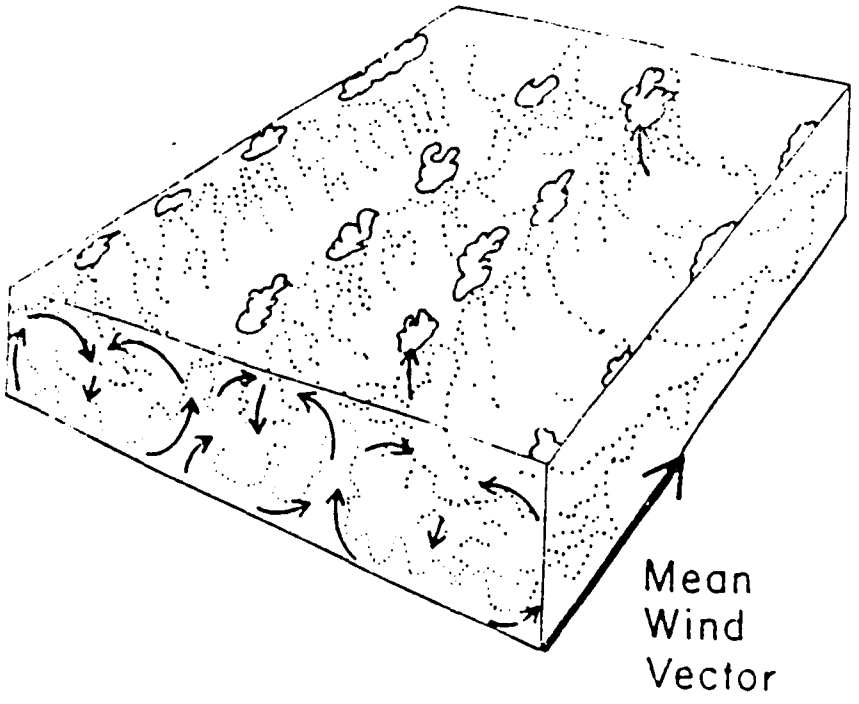

FIGURE 10 Schematic diagram showing the circulation associated with longitudinal roll vortices, and their association with cloud streets. Buoyant eddies (stippled) drawn into the circulation are helped to the condensation level, where they can form clouds (Reference 33).

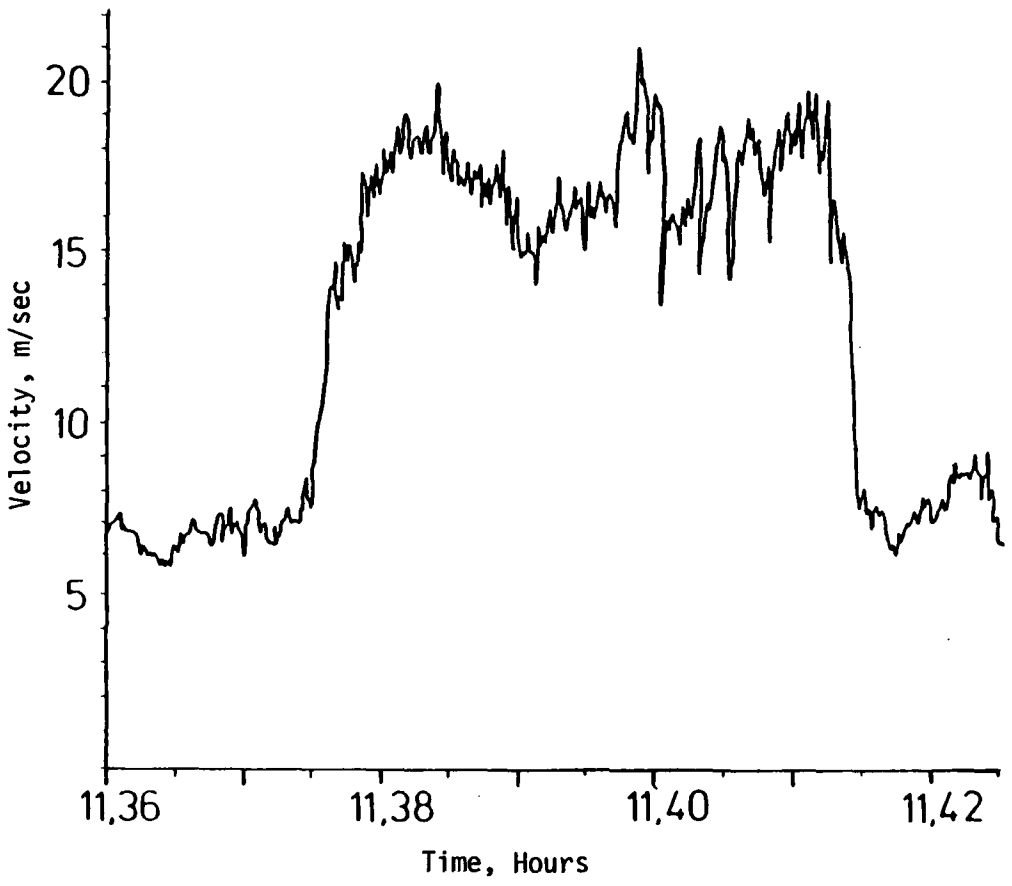

FIGURE 11 Time Series of the wind velocity sampled during the passage of a thunder storm over Lake Flevo, Netherlands (Reference 30).

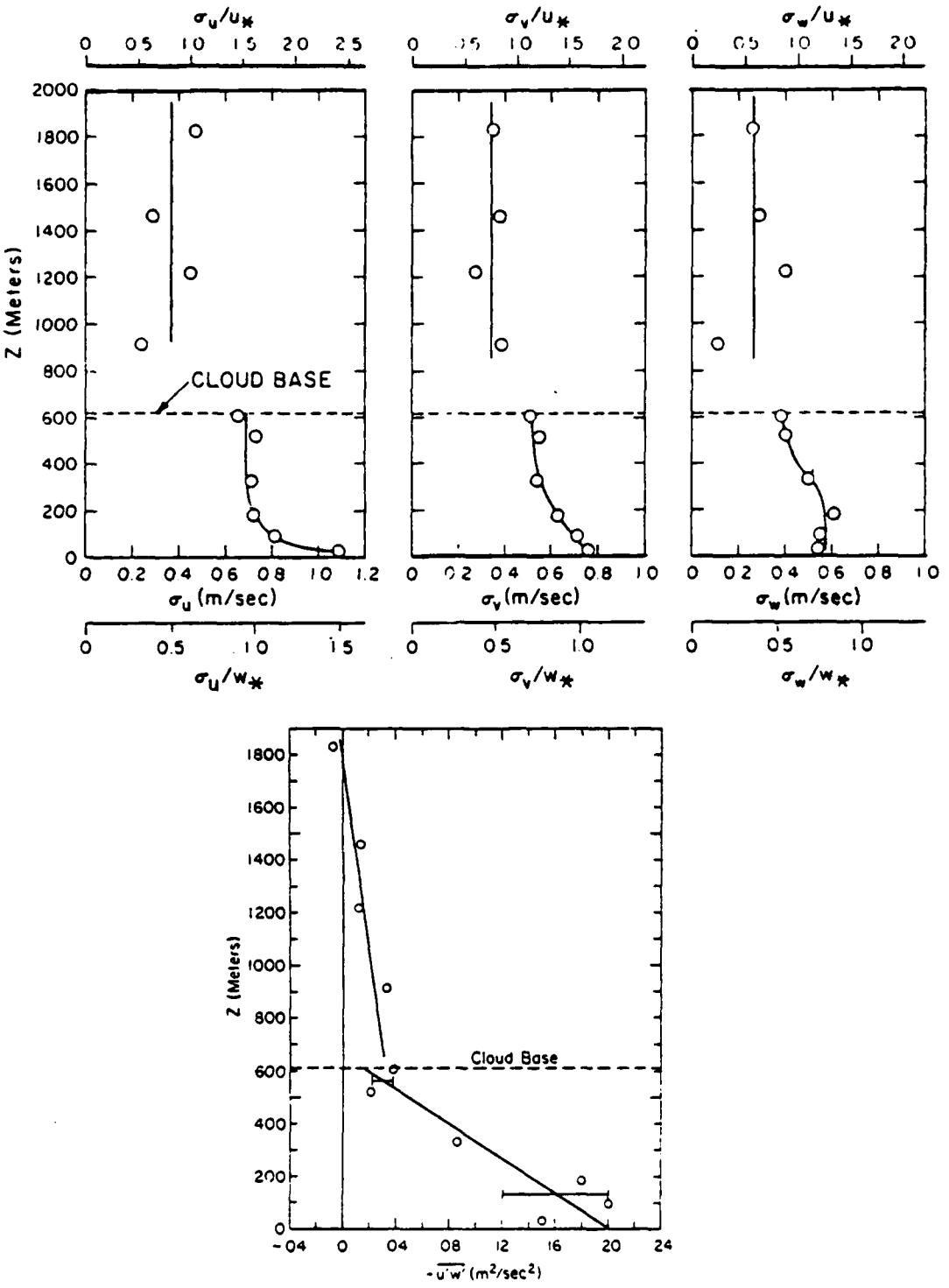

FIGURE 12 Standard deviations σ_α (α = u, v and w) and $-\overline{uw}$ versus elevation in the trade wind boundary layer northeast of Puerto Rico. ($U^* = 0.45$ m/s, $W^* = 0.73$ m/s, $z/L = -0.07$ and $z_i/L = -1.4$ from Reference 28).

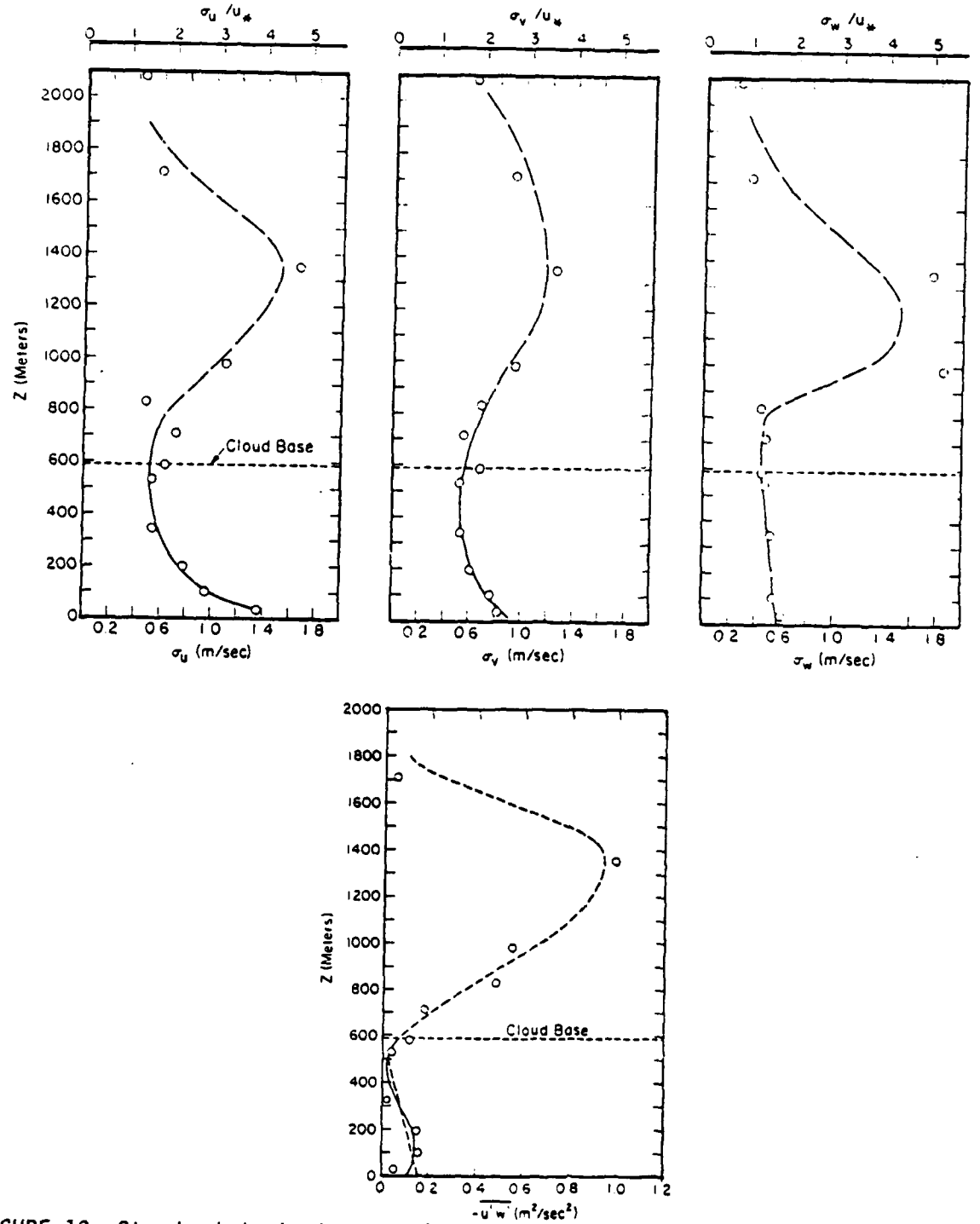

FIGURE 13 Standard deviations σ_α (α = u, v and w) and $-\overline{uw}$ versus elevation in the trade wind boundary layer northeast of Puerto Rico (U^* = 0.35 m/s, z/L = -0.2 and z_i/L = -3.0 from Reference 28).

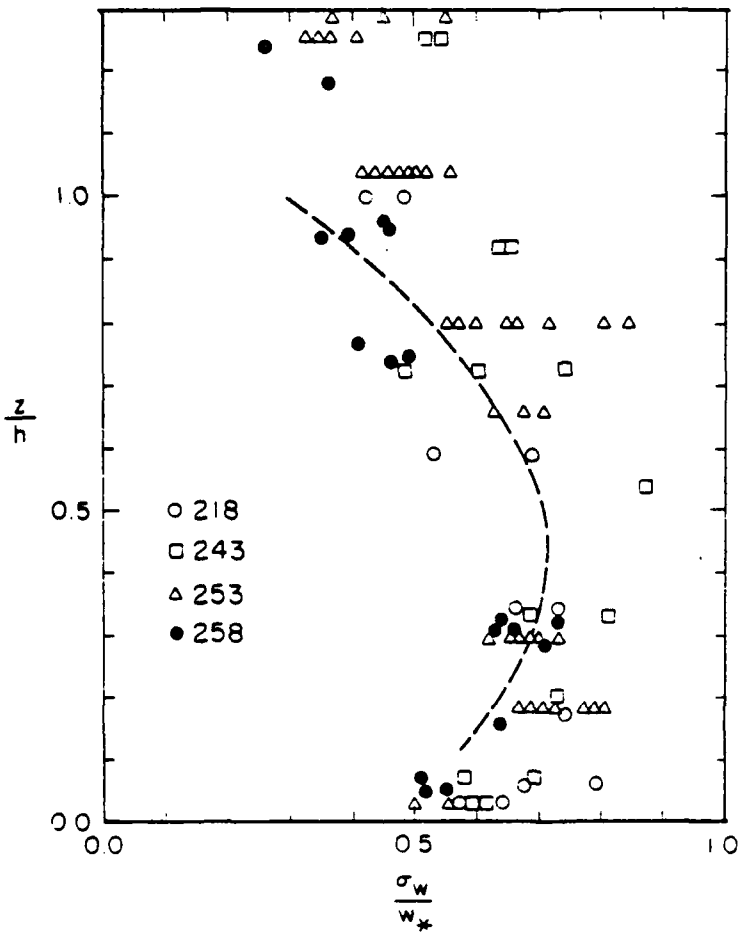

FIGURE 14 Distribution of σ_w/W^* in the ABL under rather unstable conditions, $z_i/L < -10$ (Reference 35).

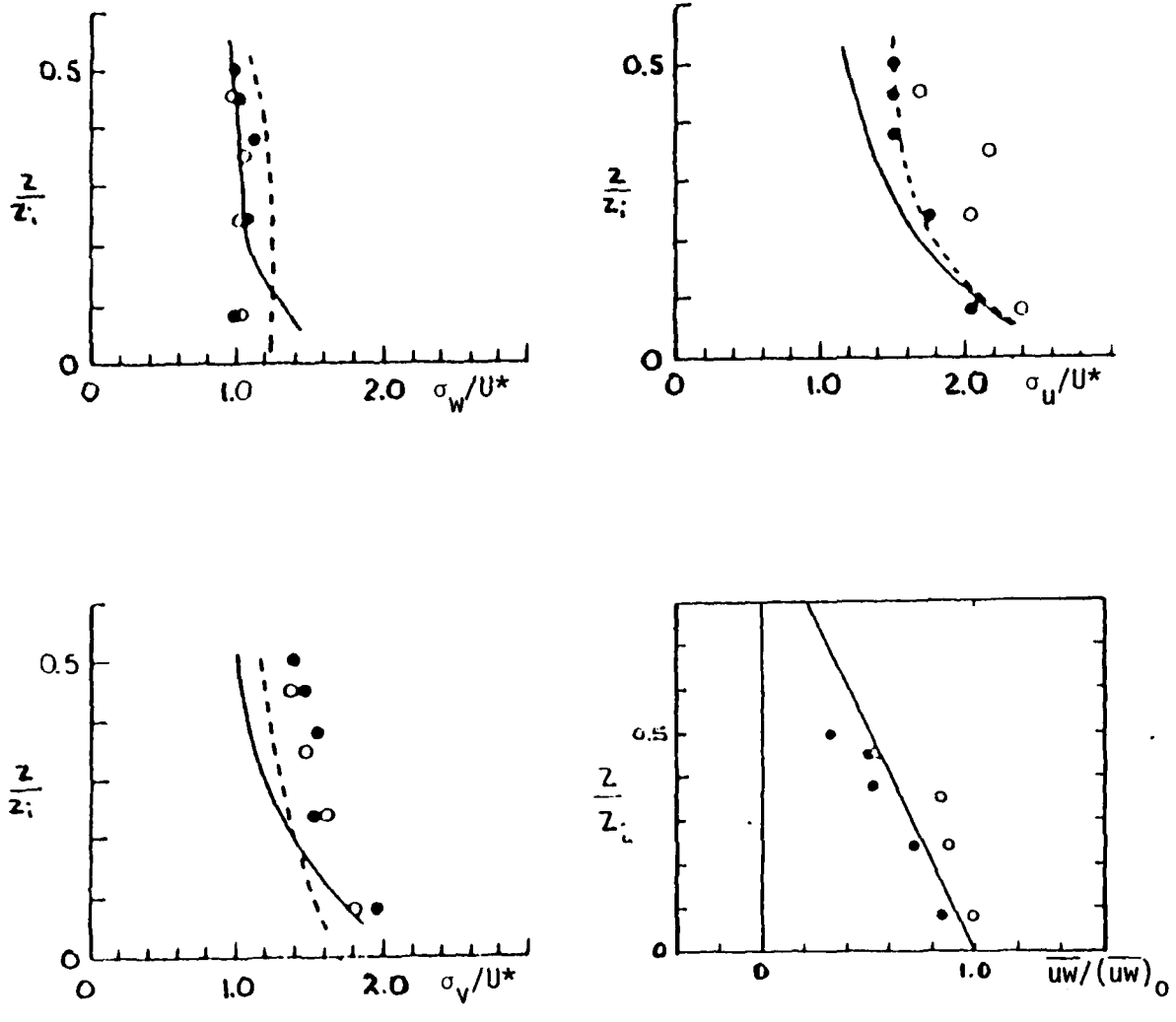

FIGURE 15 Distribution of σ_α/U^* and the momentum flux over the North Sea. o Across wind observations ● Along wind observations (Ref. 36). Dashed curves are the average results of Reference 28. Solid curves numerical prediction.

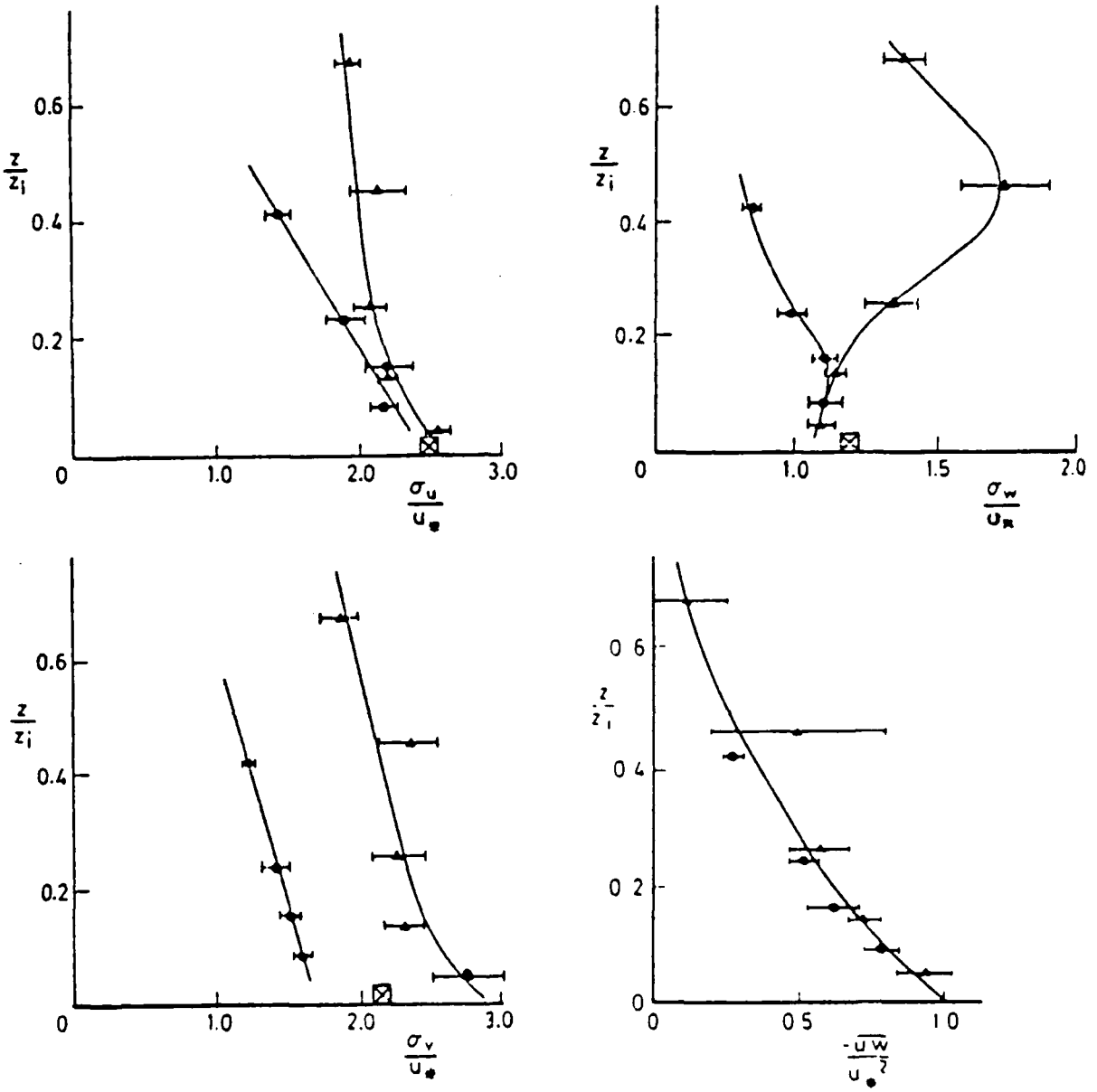

FIGURE 16 Distributions of $(\sigma_\alpha/U^*)_{avg}$ and $(-\overline{uw}/U^{*2})_{avg}$ in the ABL for ▲ Class A ● Class B (see text). Horizontal line through the data points indicate a measure of the standard deviation of the average values. The crosses at $z/z_i = 0$ denote average values observed over water (Reference 25).

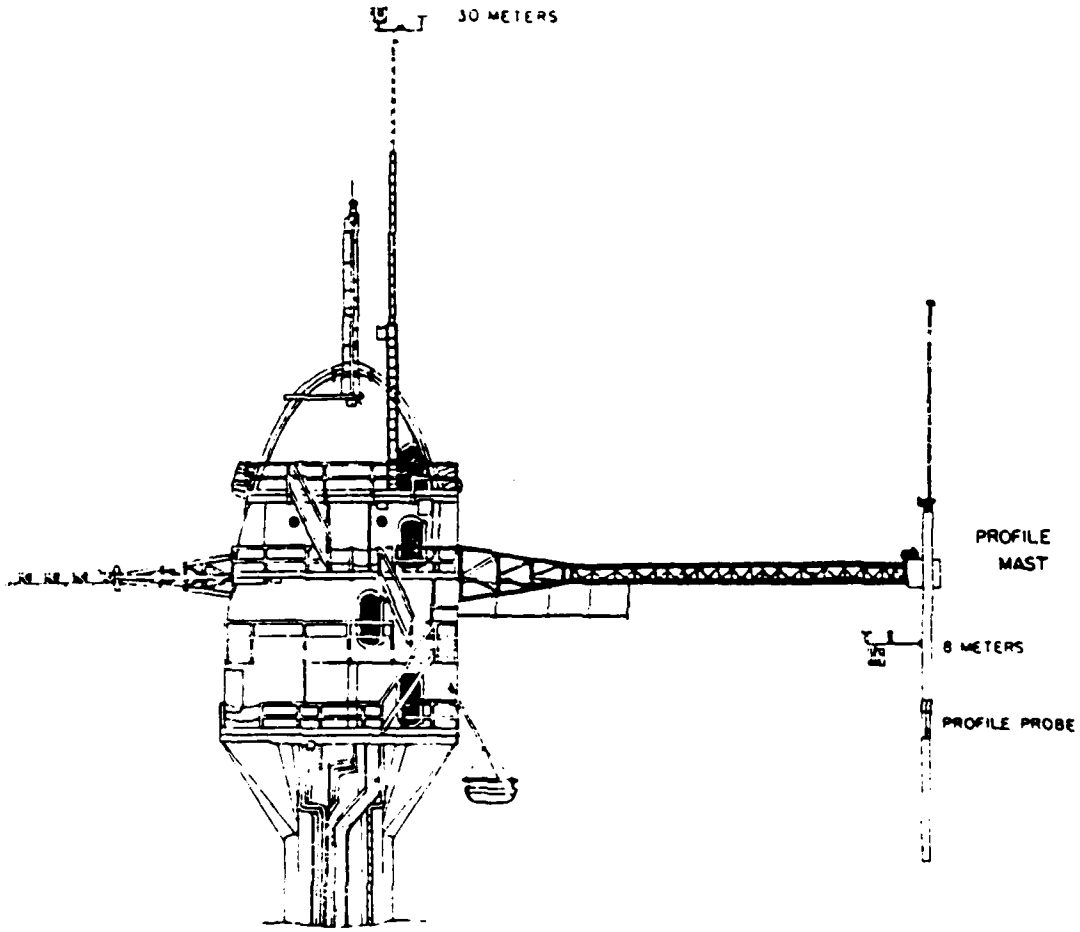

FIGURE 17 Diagram of FLIP (Floating Instrument Platform) showing the experimental arrangement. Integrated accelerometer spectra and the recorded ship's heading were used to correct the measured velocity components.

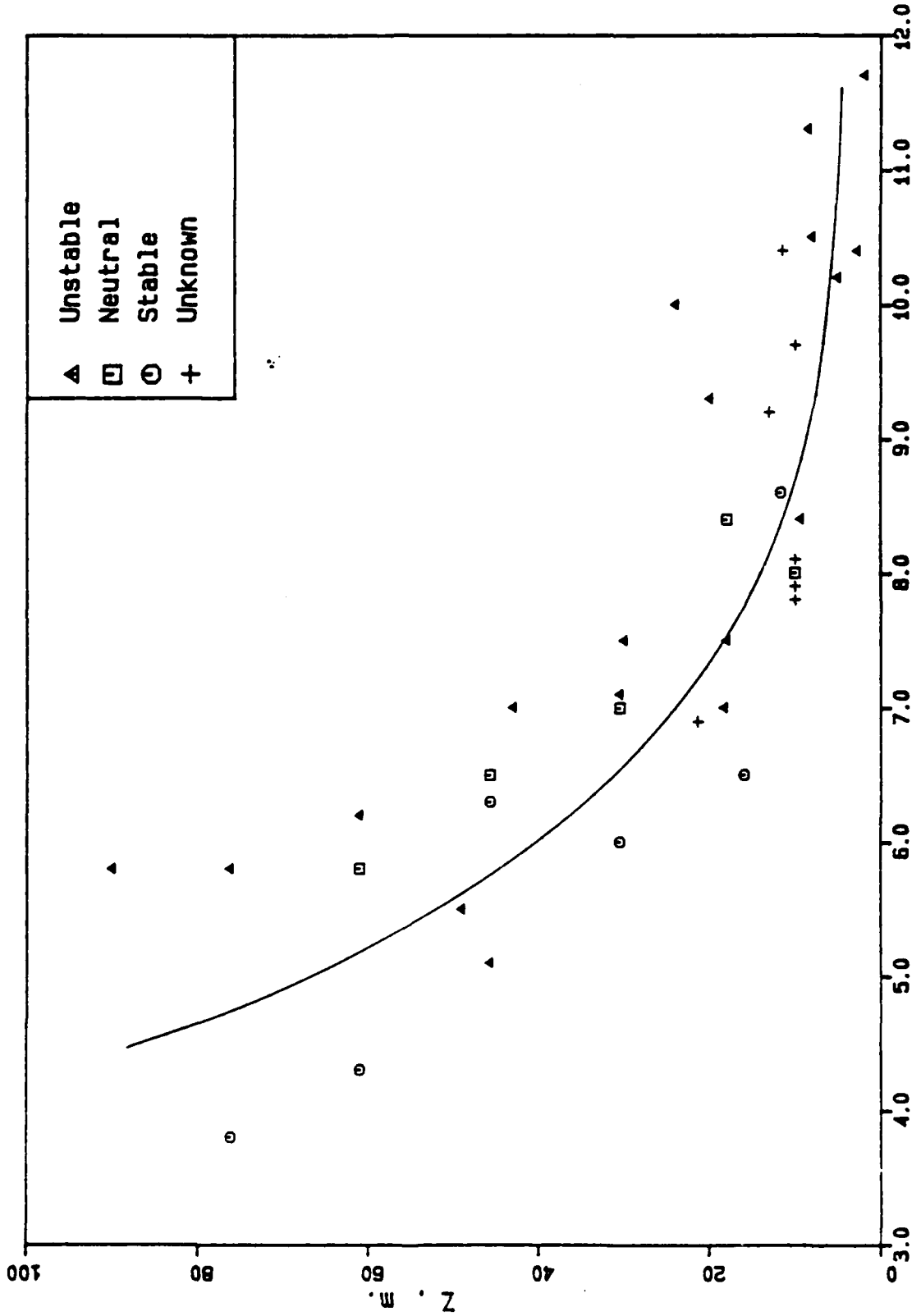

FIGURE 18 Average values of σ_u/U (%) versus height for three stability categories (solid line drawn by eye).

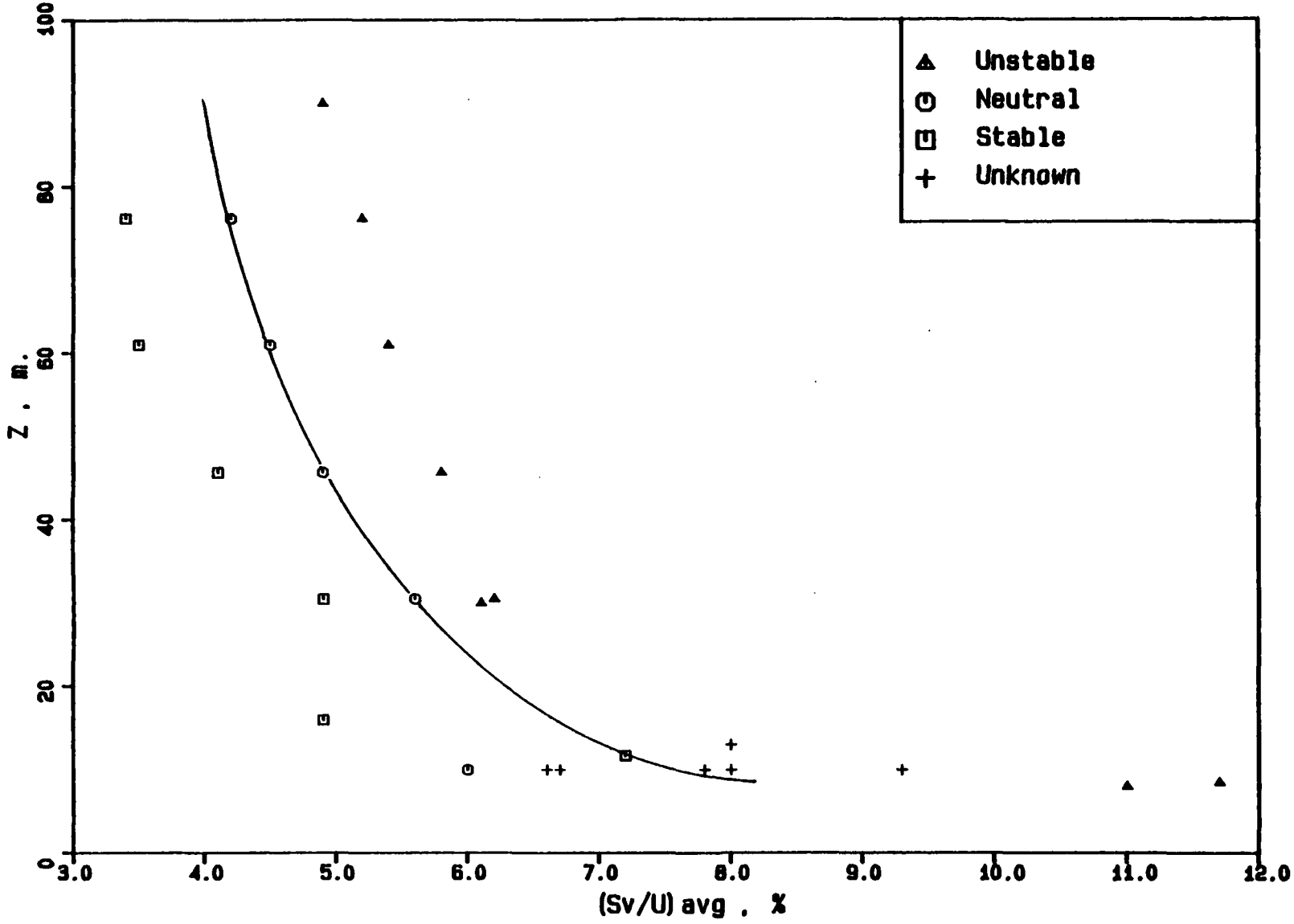

FIGURE 19 Average values of σ_v/U (%) versus height for three stability categories. (Solid line drawn by eye).

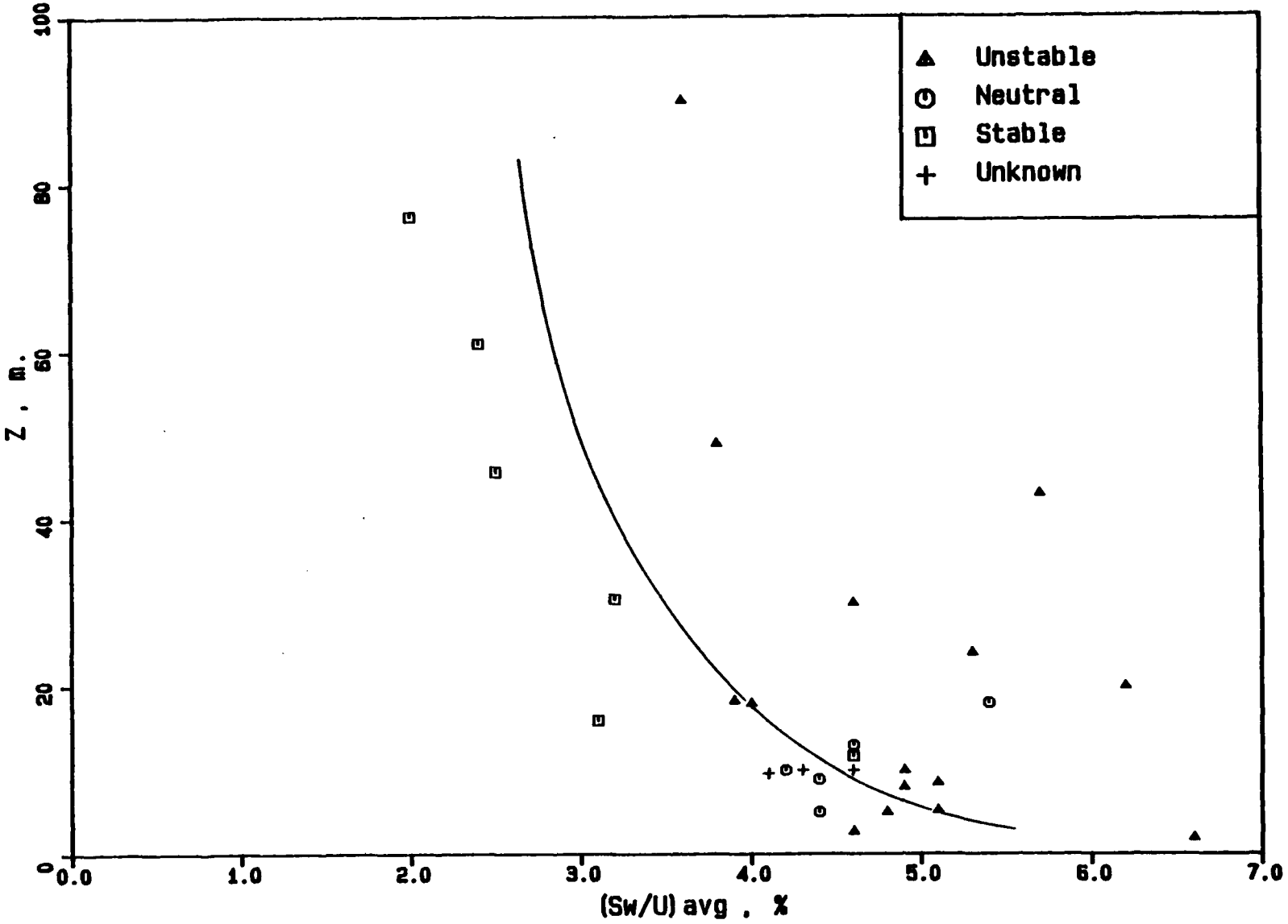

FIGURE 20 Average values of σ_w/U (%) versus height for three stability categories. (Solid line drawn by eye).

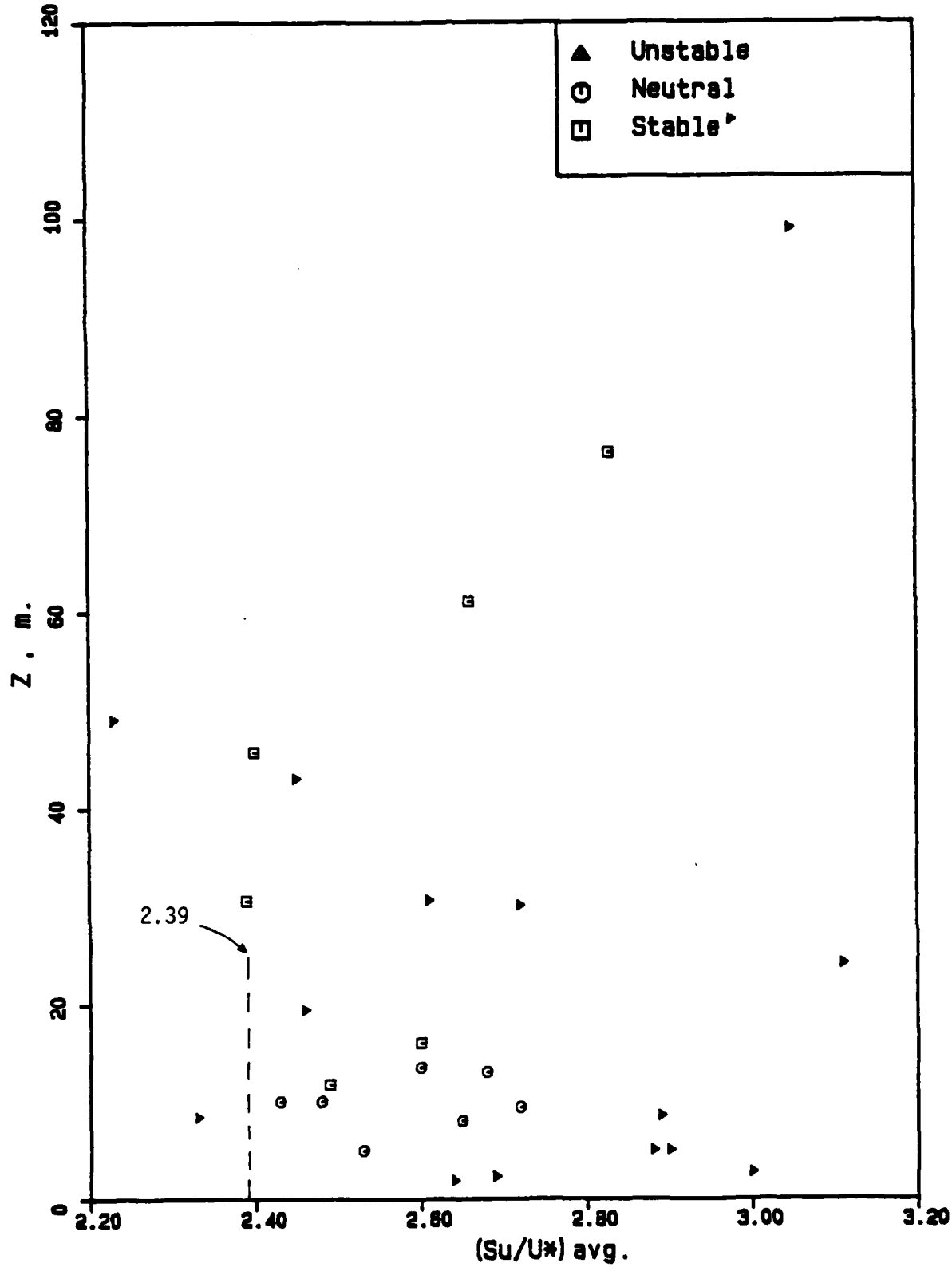

FIGURE 21 Average values of σ_v/U^* versus height for three stability categories. Average land value 2.39 [11].

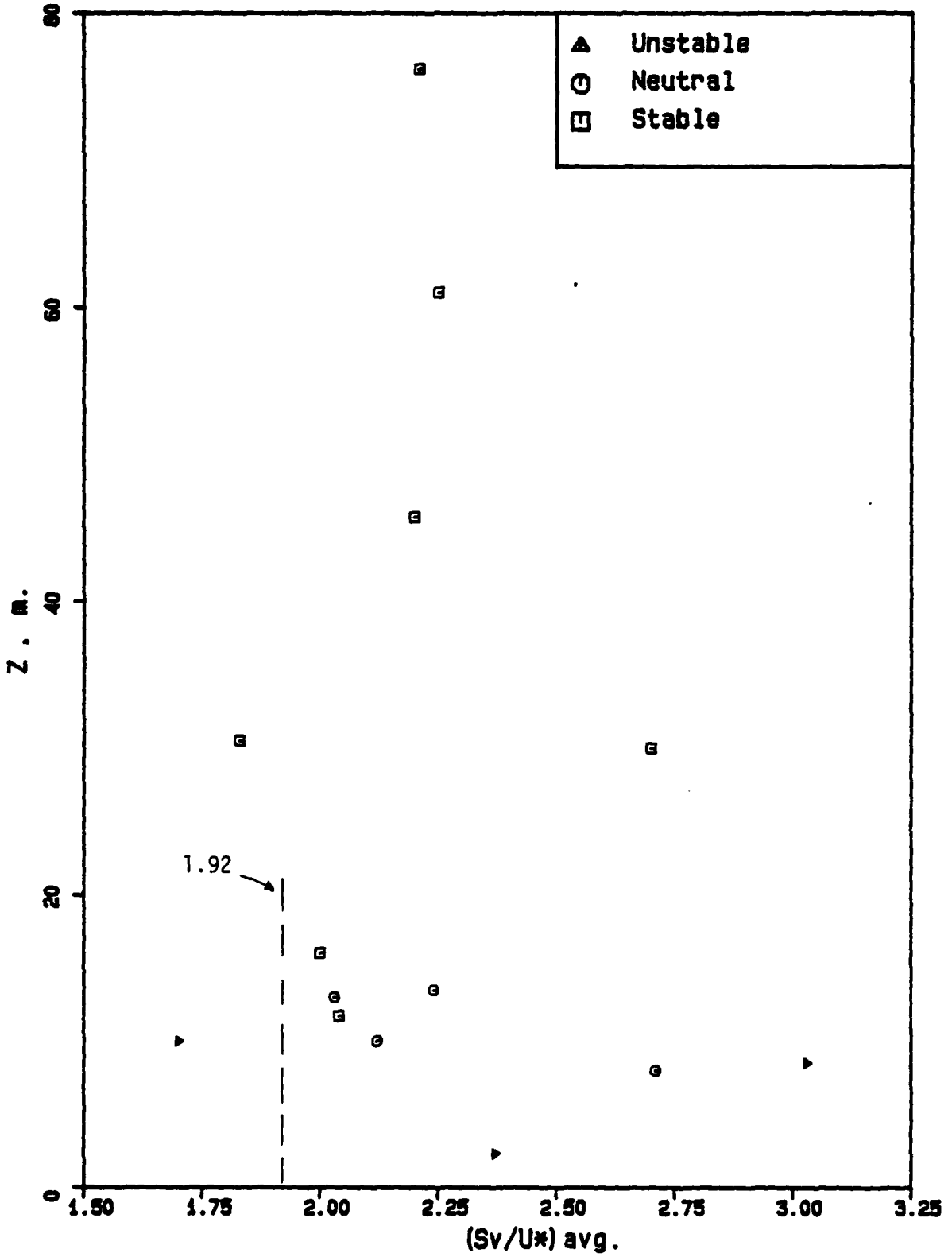

FIGURE 22 Average value of σ_v/U^* versus height for three stability categories. Average land value 1.92 [11].

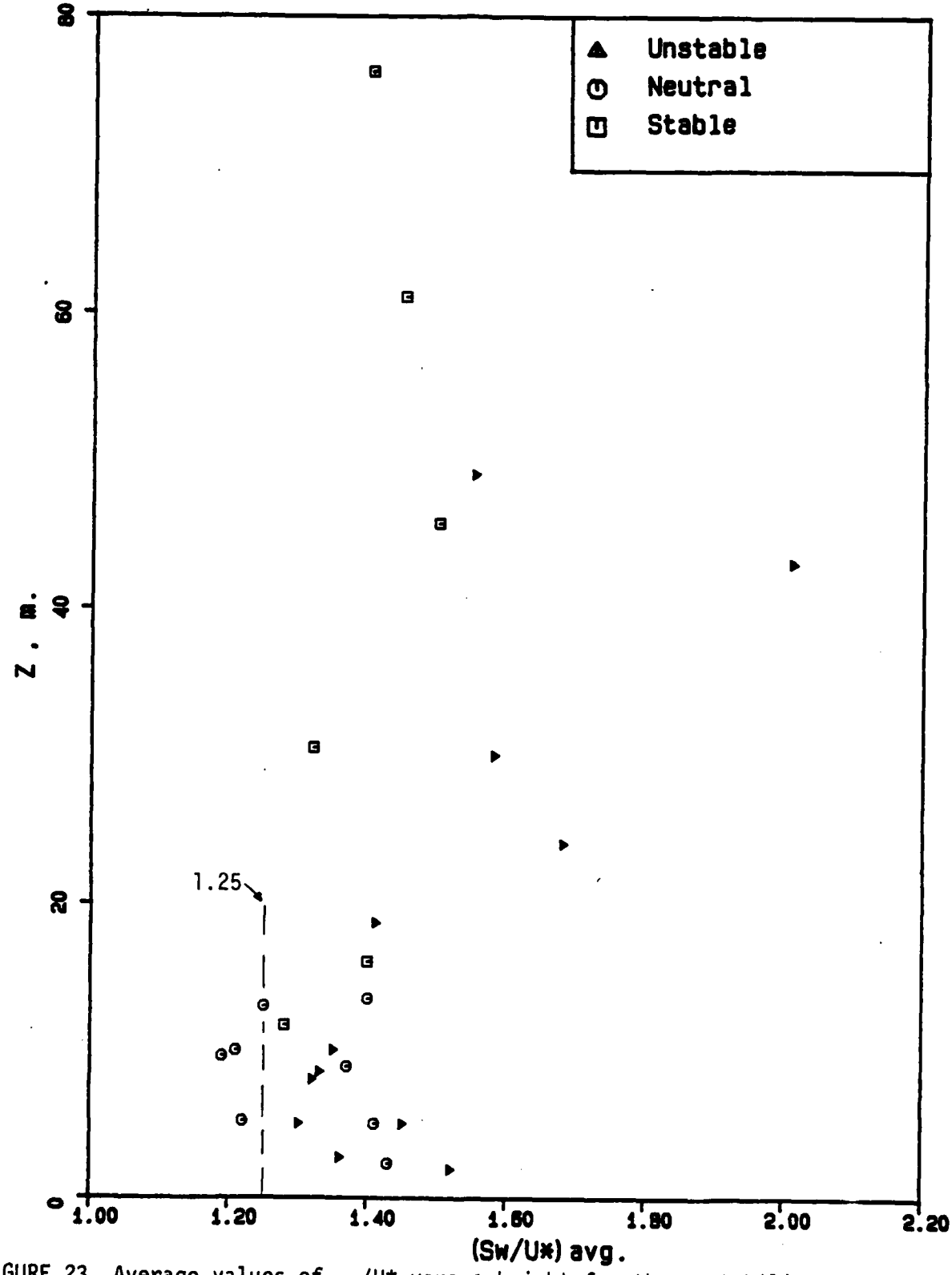

FIGURE 23 Average values of σ_w/U^* versus height for three stability categories. The large value of σ_w/U^* at Z = 43 m represents only a single data point. Average land value 1.25 [11].

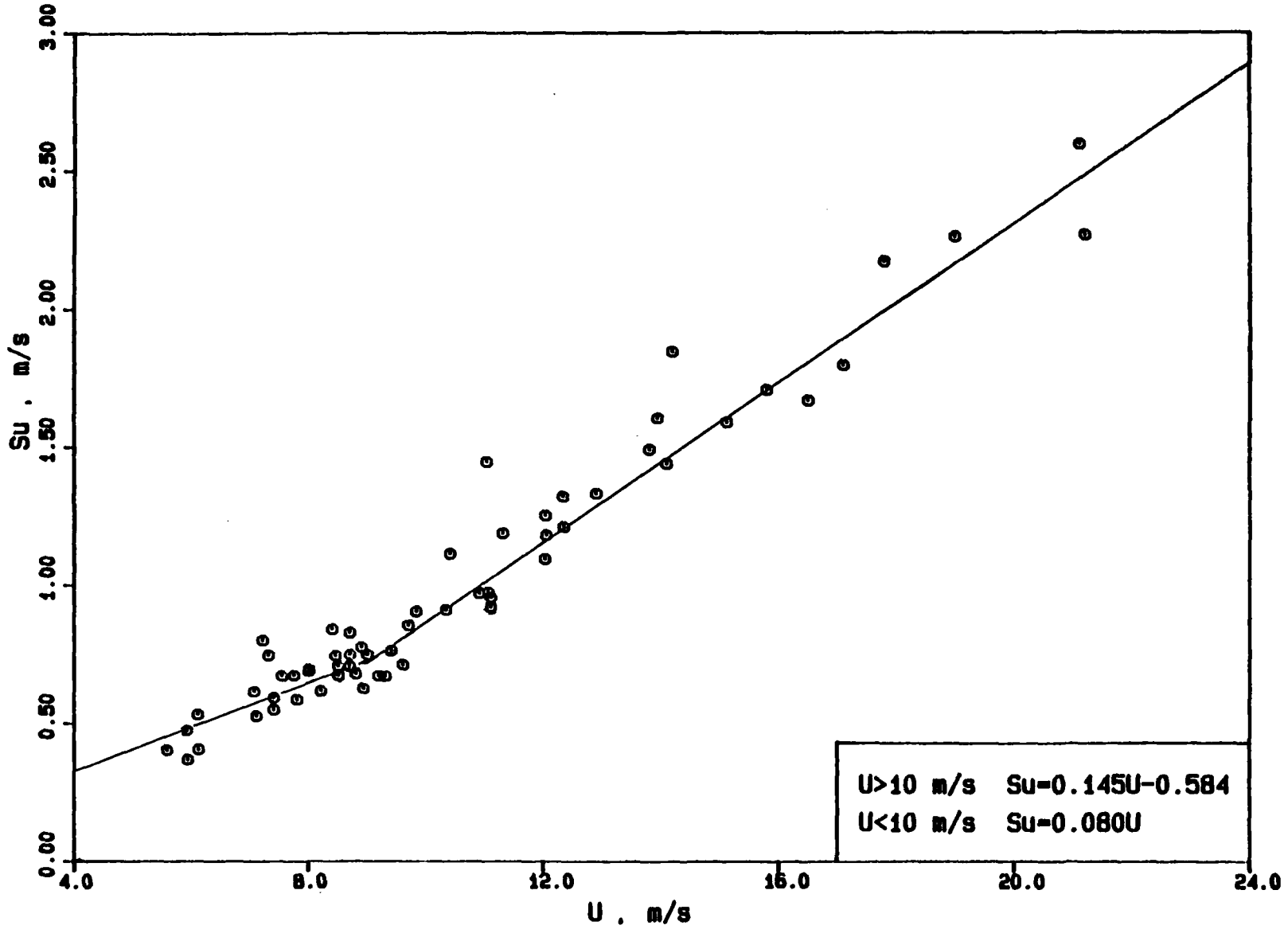

FIGURE 24 Standard deviation σ_u versus mean velocity, for data $|z/L| < 0.15$ from References 17 and 48, z = 10 m.

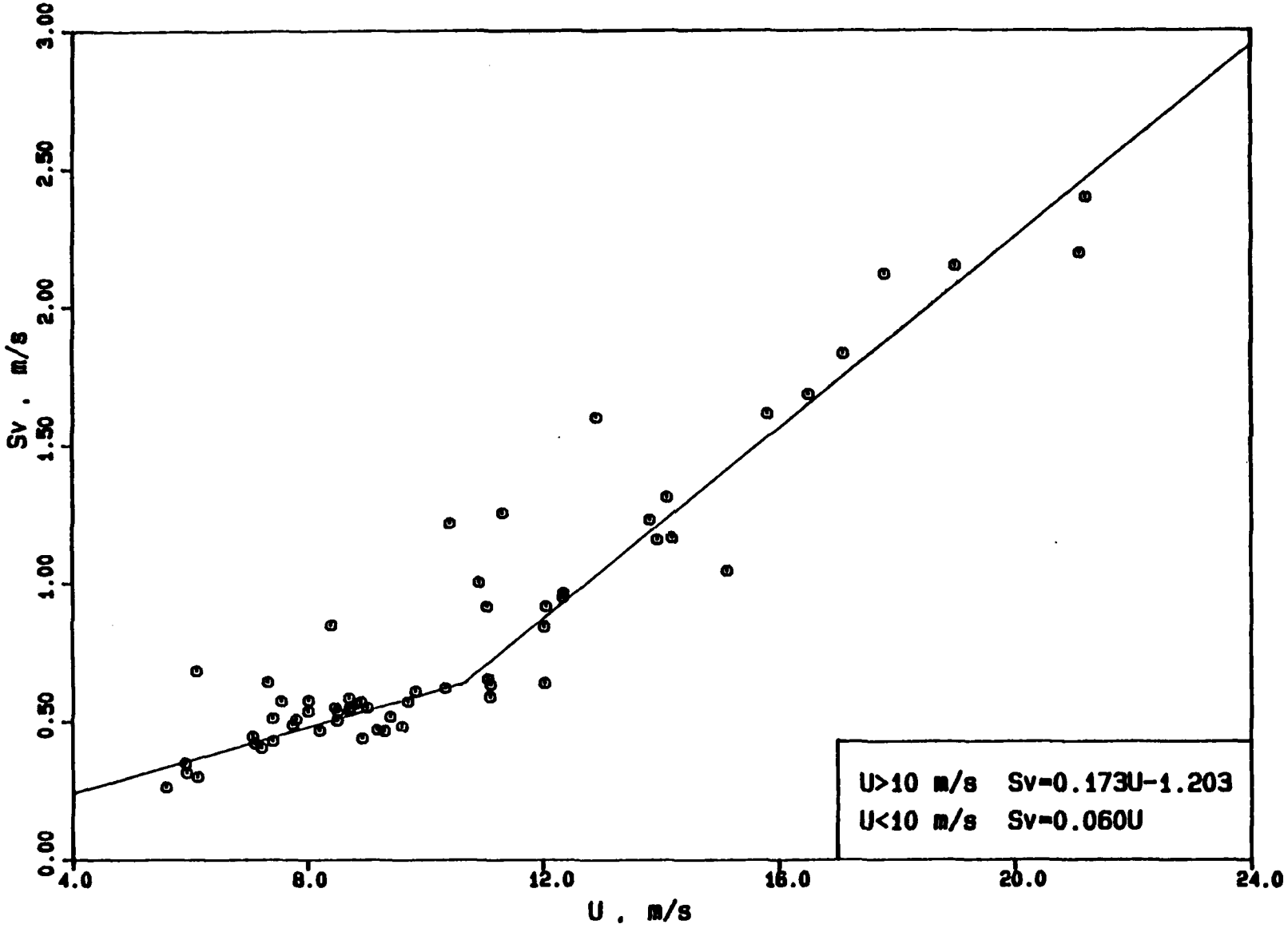

FIGURE 25 Standard deviation σ_v versus mean velocity, for data with $|z/L| < 0.15$ from References 17 and 48, z = 10 m.

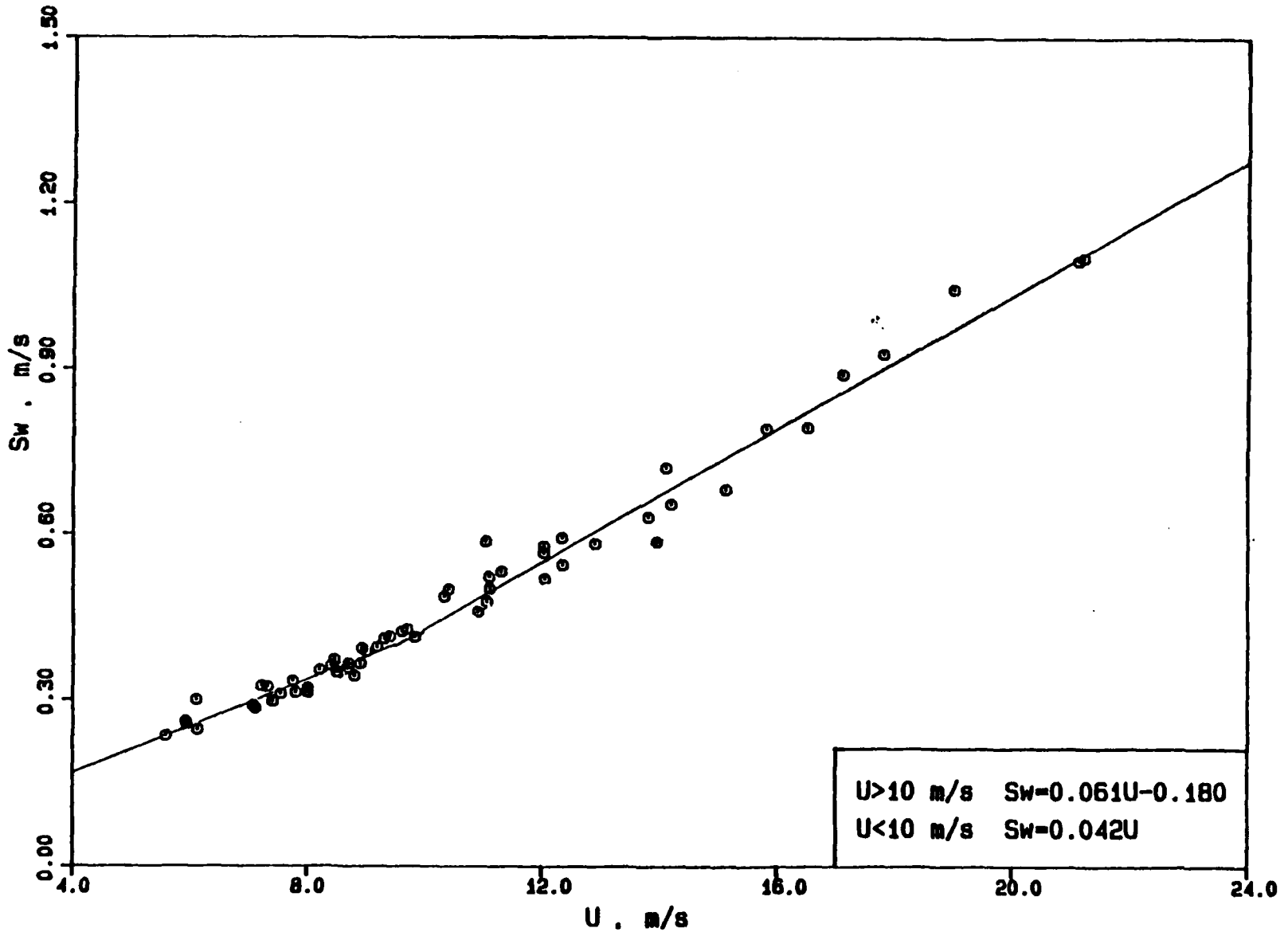

FIGURE 26 Standard deviation σ_w versus mean velocity, for data with $|z/L| < 0.15$ from References 17 and 48, z = 10 m.

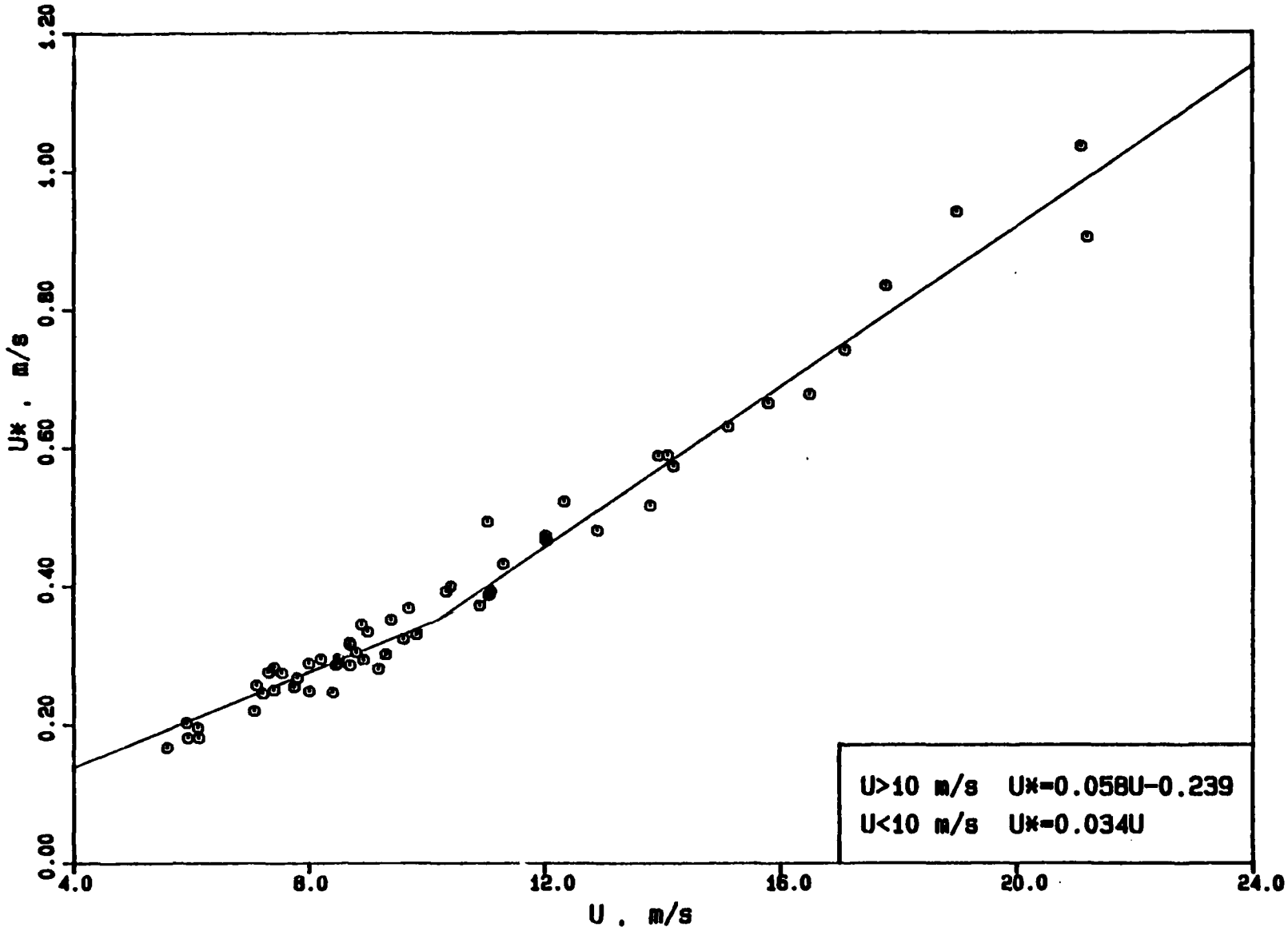

FIGURE 27 Friction velocity, U*, versus mean velocity, for data with |z/L| < 0.15 from References 17 and 48, z = 10 m.

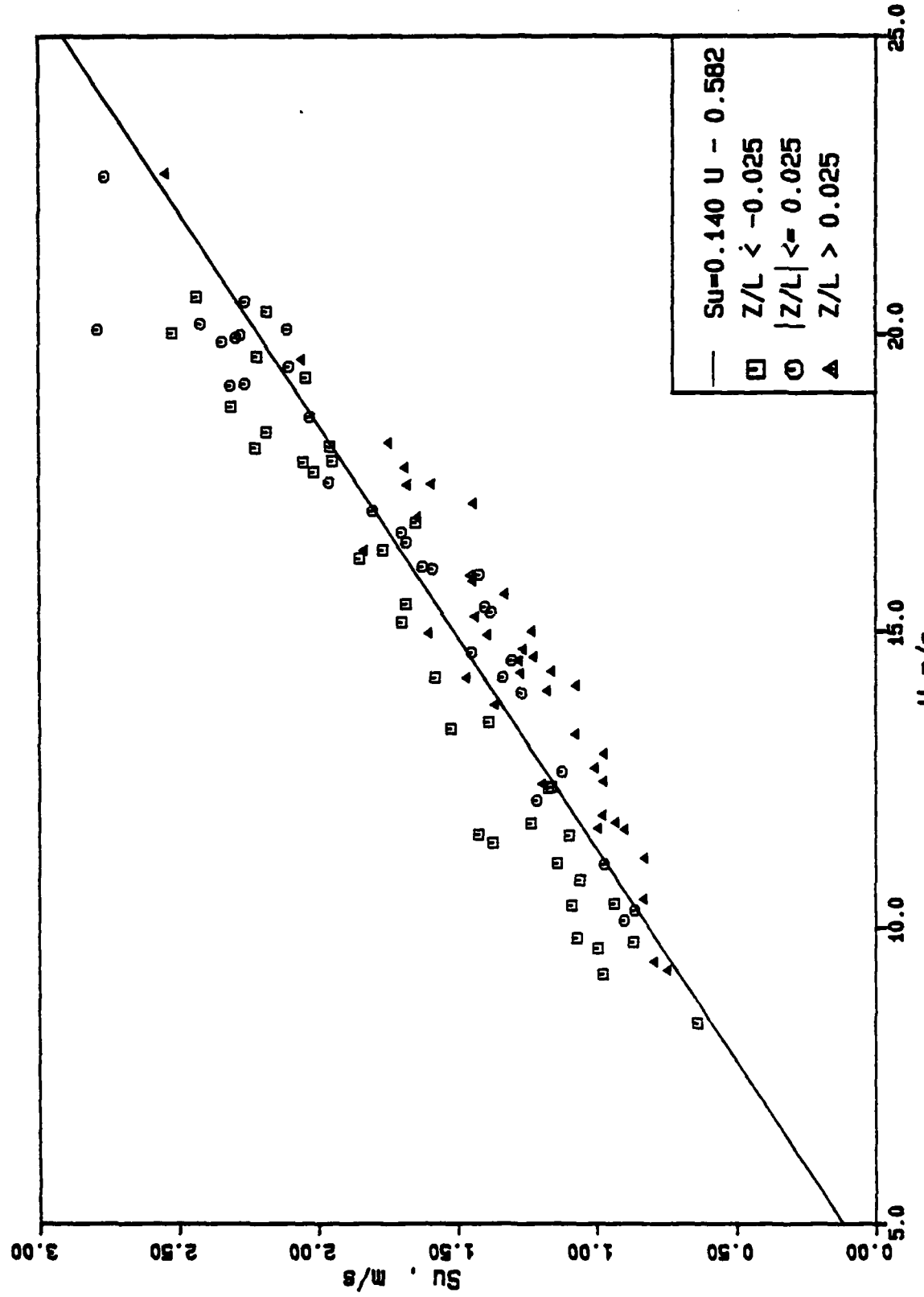

FIGURE 28 Standard deviation, σ_u, versus mean velocity for all observations of Reference 53, z = 13.5 m.

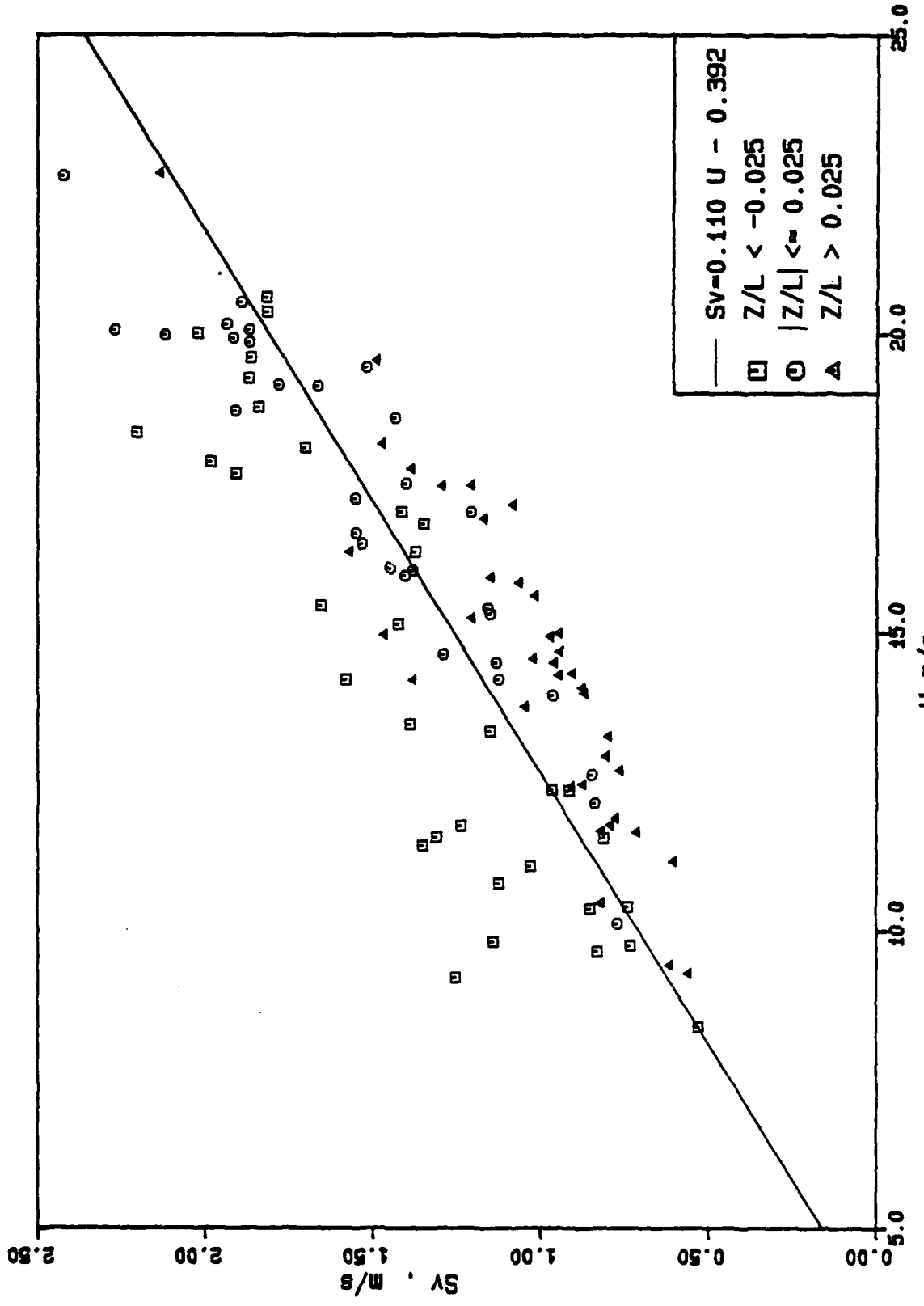

FIGURE 29 Standard deviation, σ_v, versus mean velocity for all observations of Reference 53, z = 13.5 m.

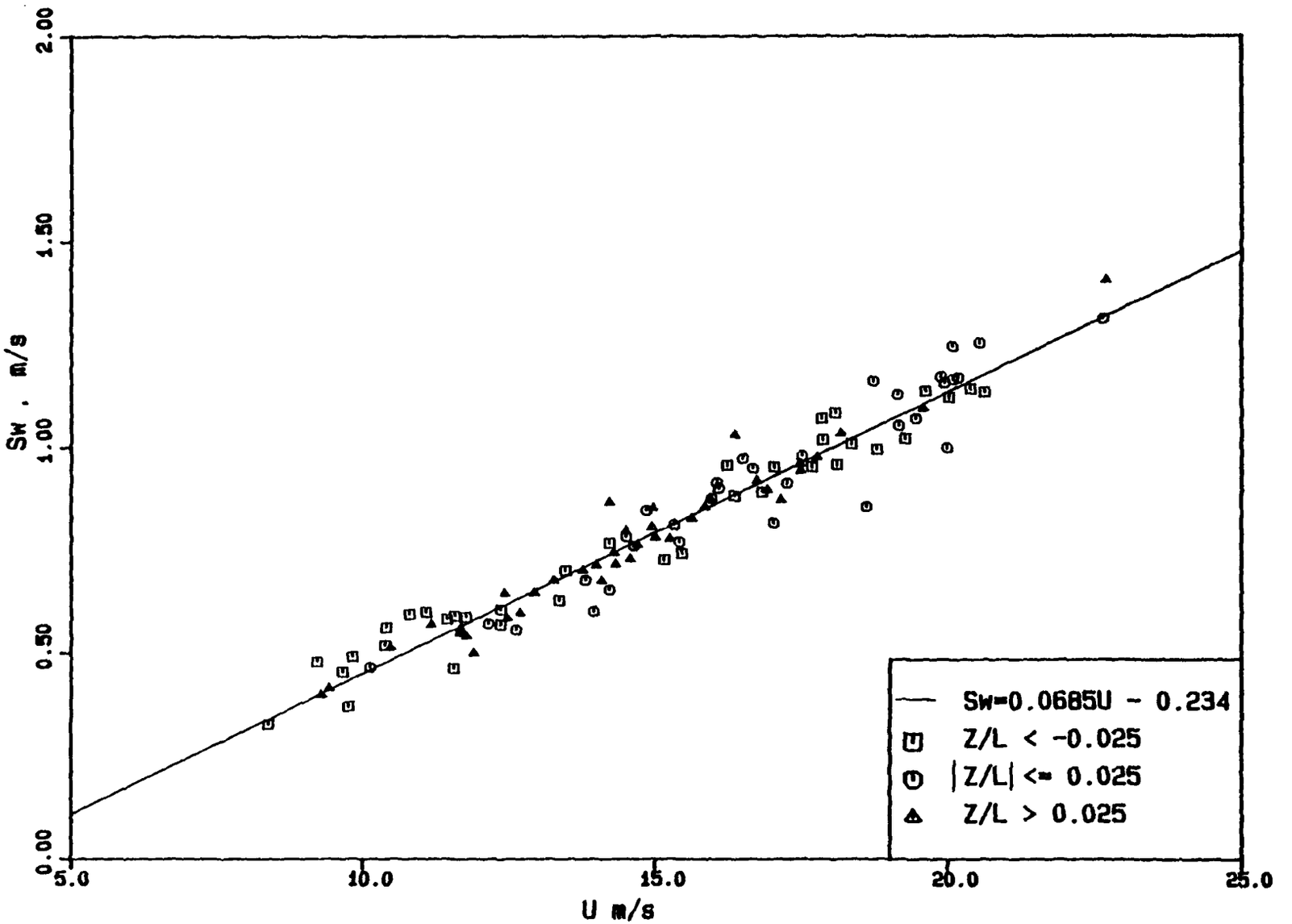

FIGURE 30 Standard deviation, σ_w, versus mean velocity for all observations of Reference 53, z = 13.5 m.

AD-A154 133 A SURVEY OF THE TURBULENCE IN THE MARINE SURFACE LAYER FOR THE OPERATION O..(U) VIRGINIA POLYTECHNIC INST AND STATE UNIV BLACKSBURG DEPT OF E.. H W TIELEMAN MAR 85 VPI-E-85-10 N00014-83-K-0658 F/G 4/2 2/2 NL

UNCLASSIFIED

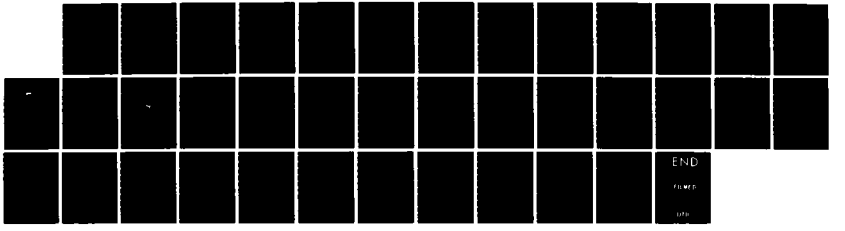

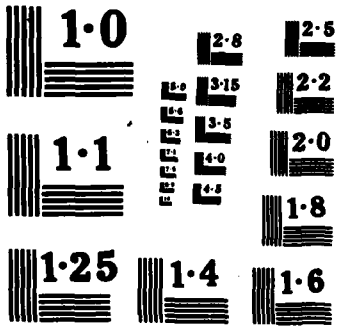
1·0
1·1
1·25
1·4
1·6
1·8
2·0
2·2
2·5
2·8
3·15
3·5
4·0

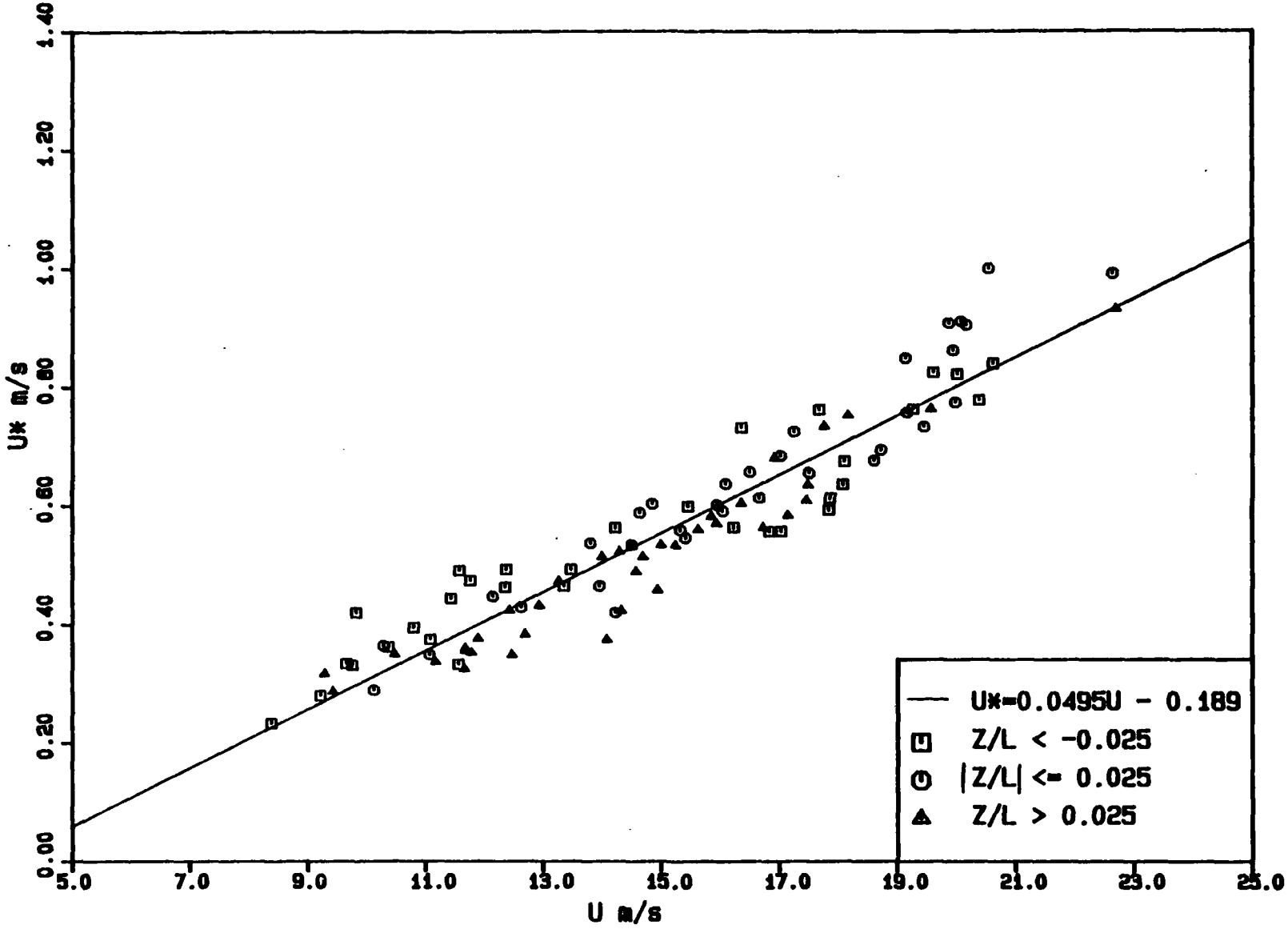

FIGURE 31 Friction velocity U* versus mean velocity for all observations of Reference 53, z = 13.5 m.

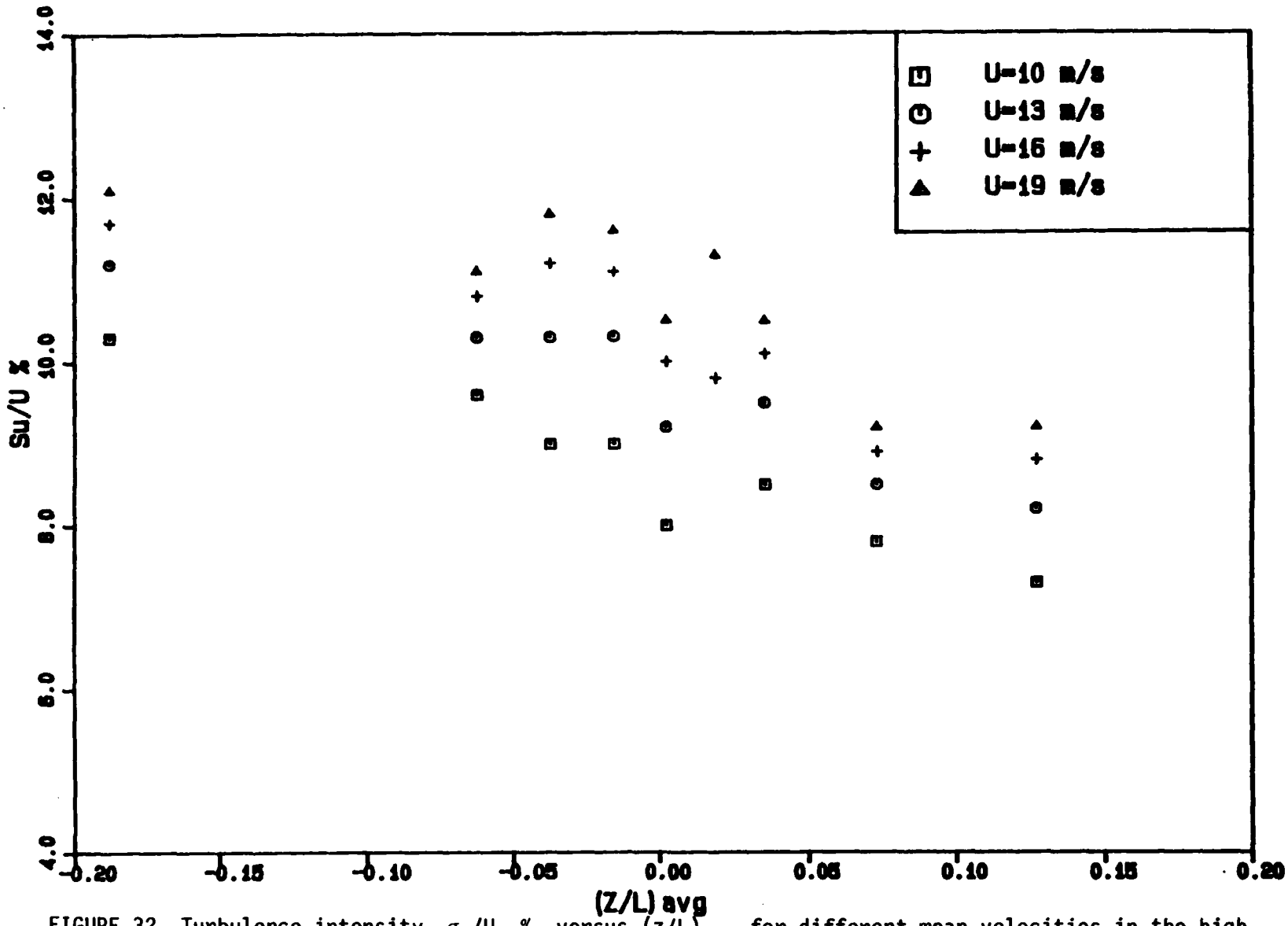

FIGURE 32 Turbulence intensity, σ_u/U, %, versus $(z/L)_{avg}$ for different mean velocities in the high-velocity range and obtained from the lines of best fit through the data in each stability category ($\sigma_u = m\ U + b$). Data from Reference 53, z = 13.5 m.

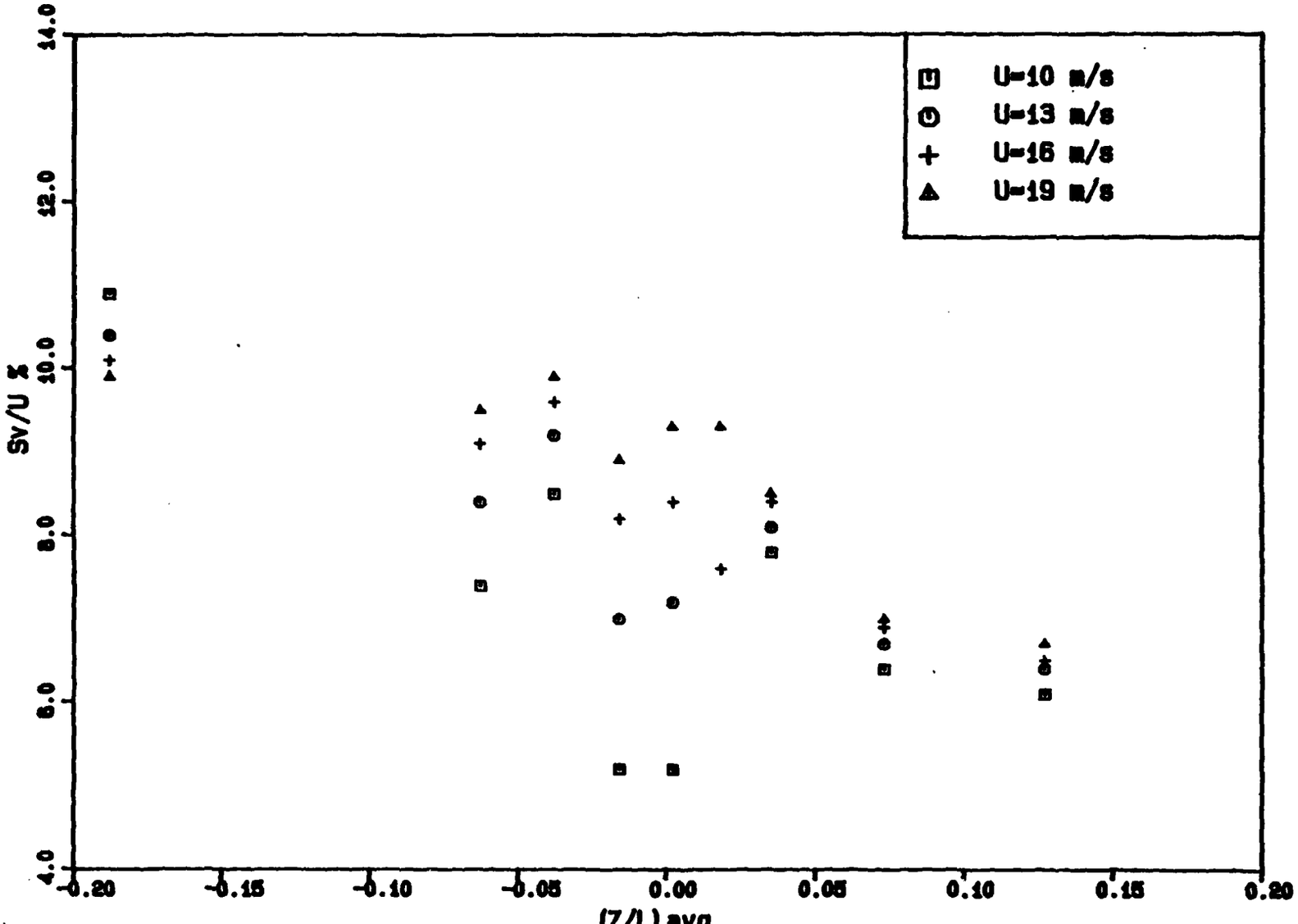

FIGURE 33 The turbulence intensity, σ_v/U, %, versus $(z/L)_{avg}$ for different mean velocities in the high-velocity range and obtained from the lines of best fit through the data in each stability category ($\sigma_v = m\ U + b$). Data from Reference 53, z = 13.5 m.

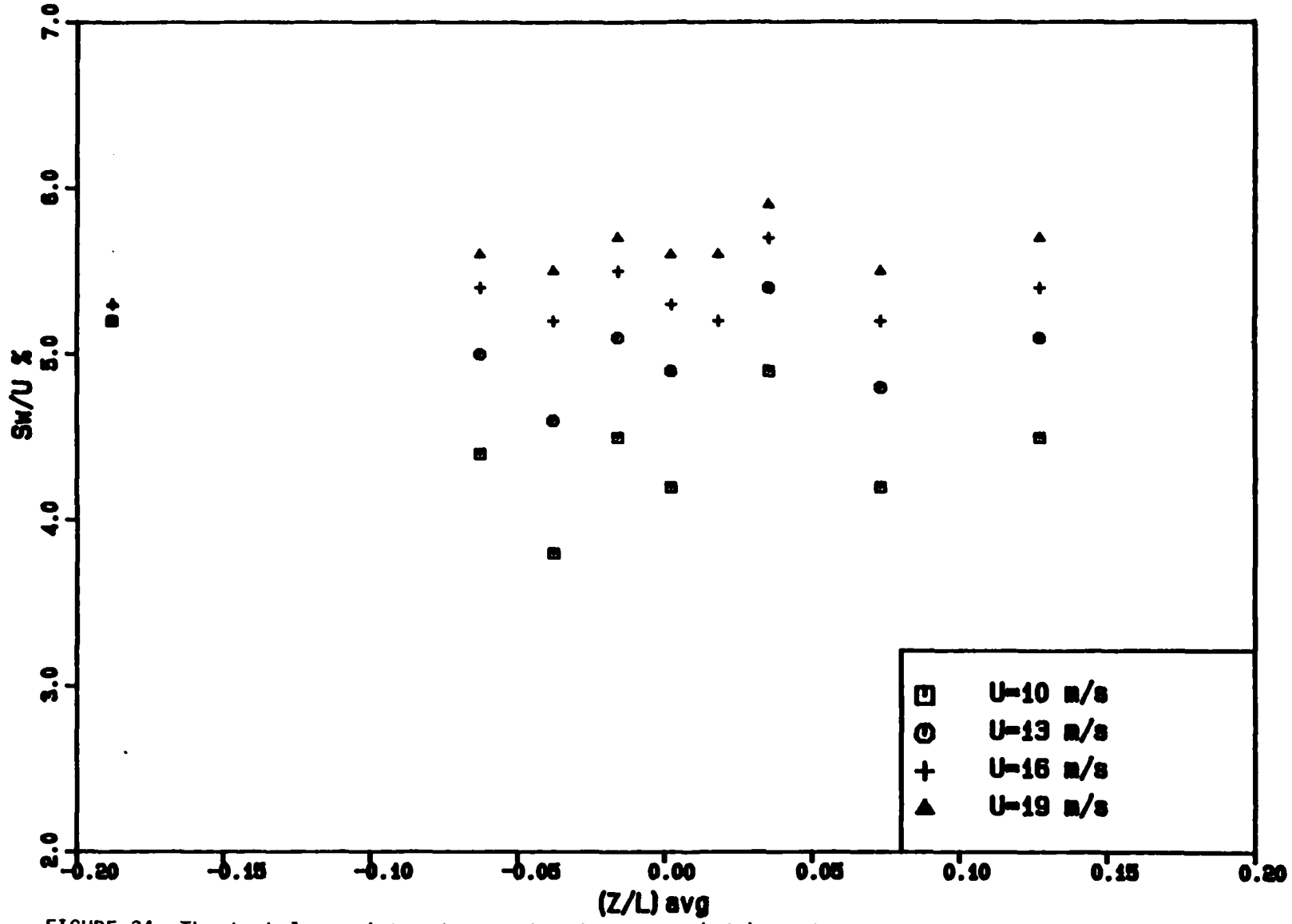

FIGURE 34 The turbulence intensity, σ_w/U, %, versus $(z/L)_{avg}$ for different mean velocities in the high velocity range and obtained from the lines of best fit through the data in each stability category ($\sigma_w = m\ U + b$). Data from Reference 53, z = 13.5 m.

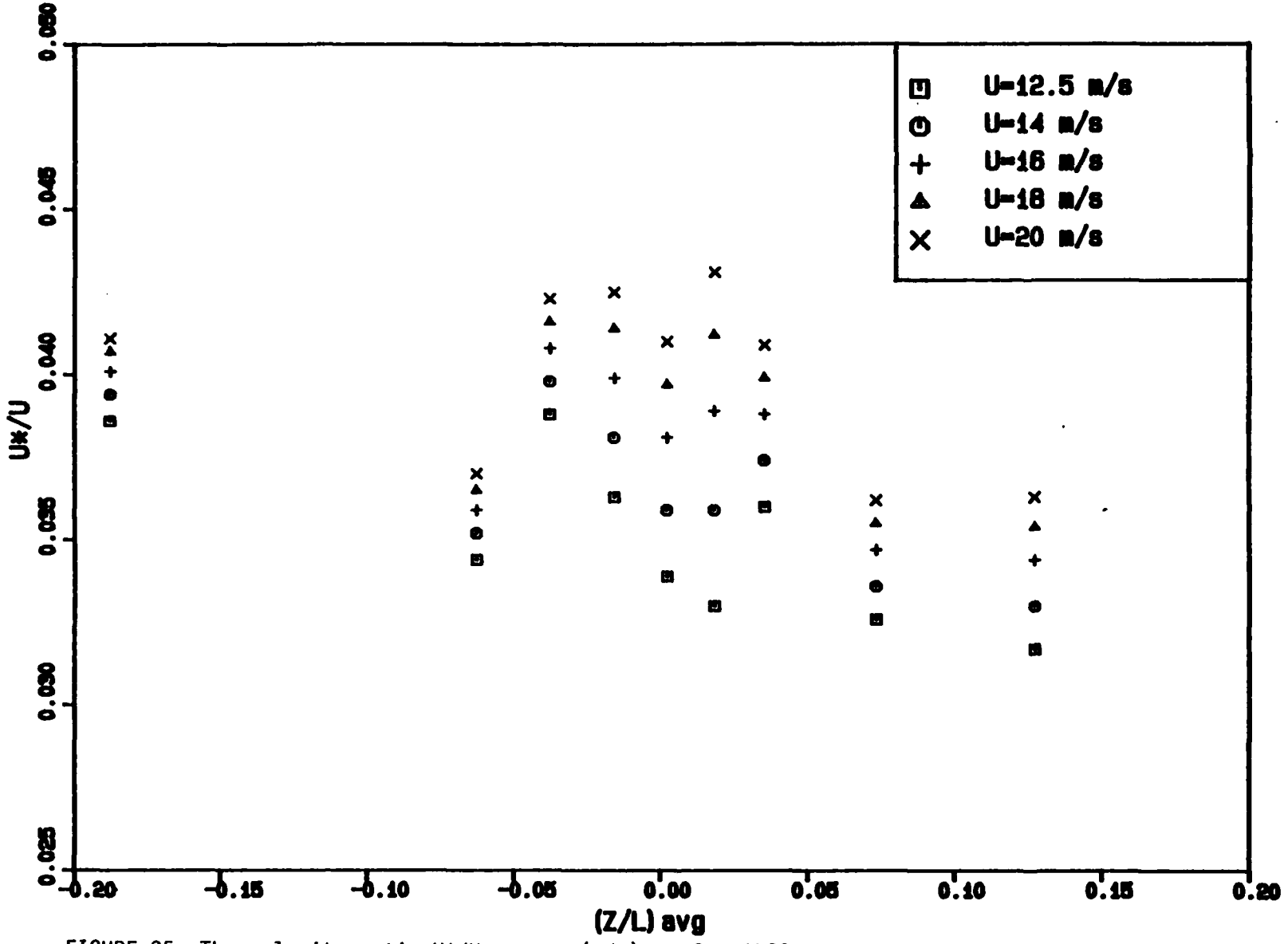

FIGURE 35 The velocity ratio U*/U versus $(z/L)_{avg}$ for different mean velocities in the high-velocity range and obtained from the lines of best fit through the data in each stability category (U* = m U + b). Data from Reference 53, z = 13.5 m.

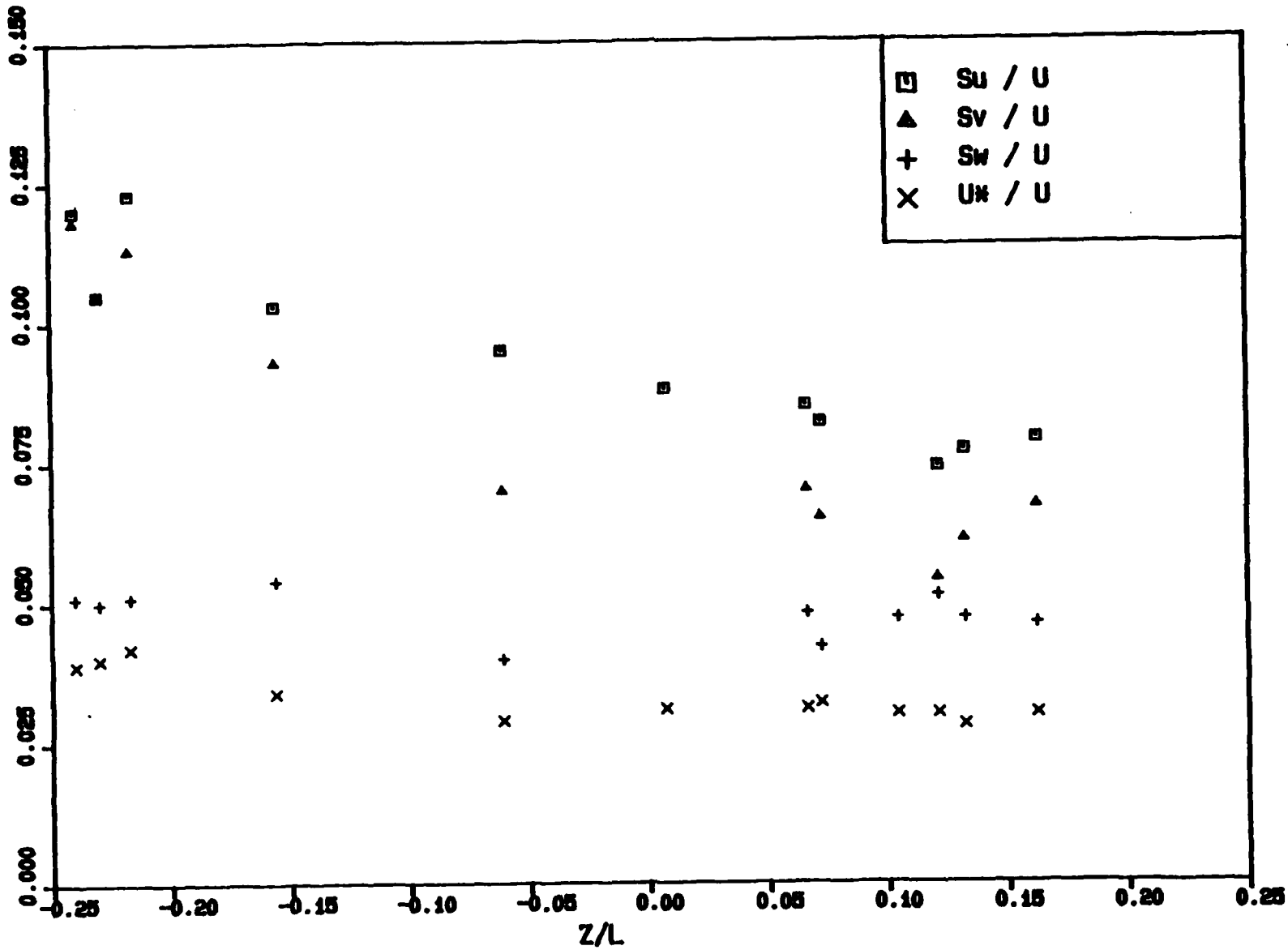

FIGURE 36 Variation of σ_α/U and U^*/U with stability for mean velocities in the range $11.0 \leq U < 12.0$ m/s.

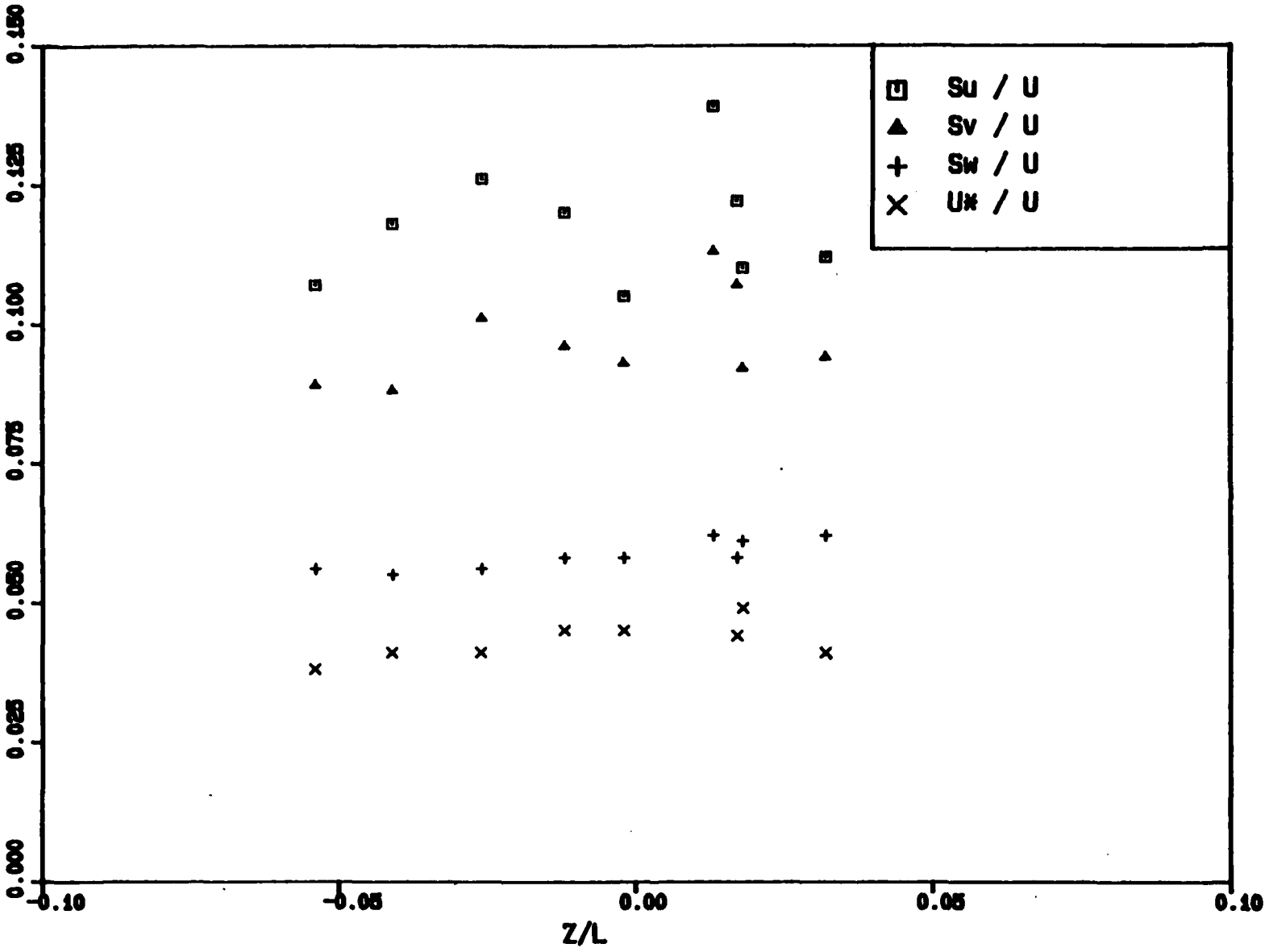

FIGURE 37 Variation of σ_α/U and U*/U with stability for mean velocities in the range U $\geq$ 20 m/s.

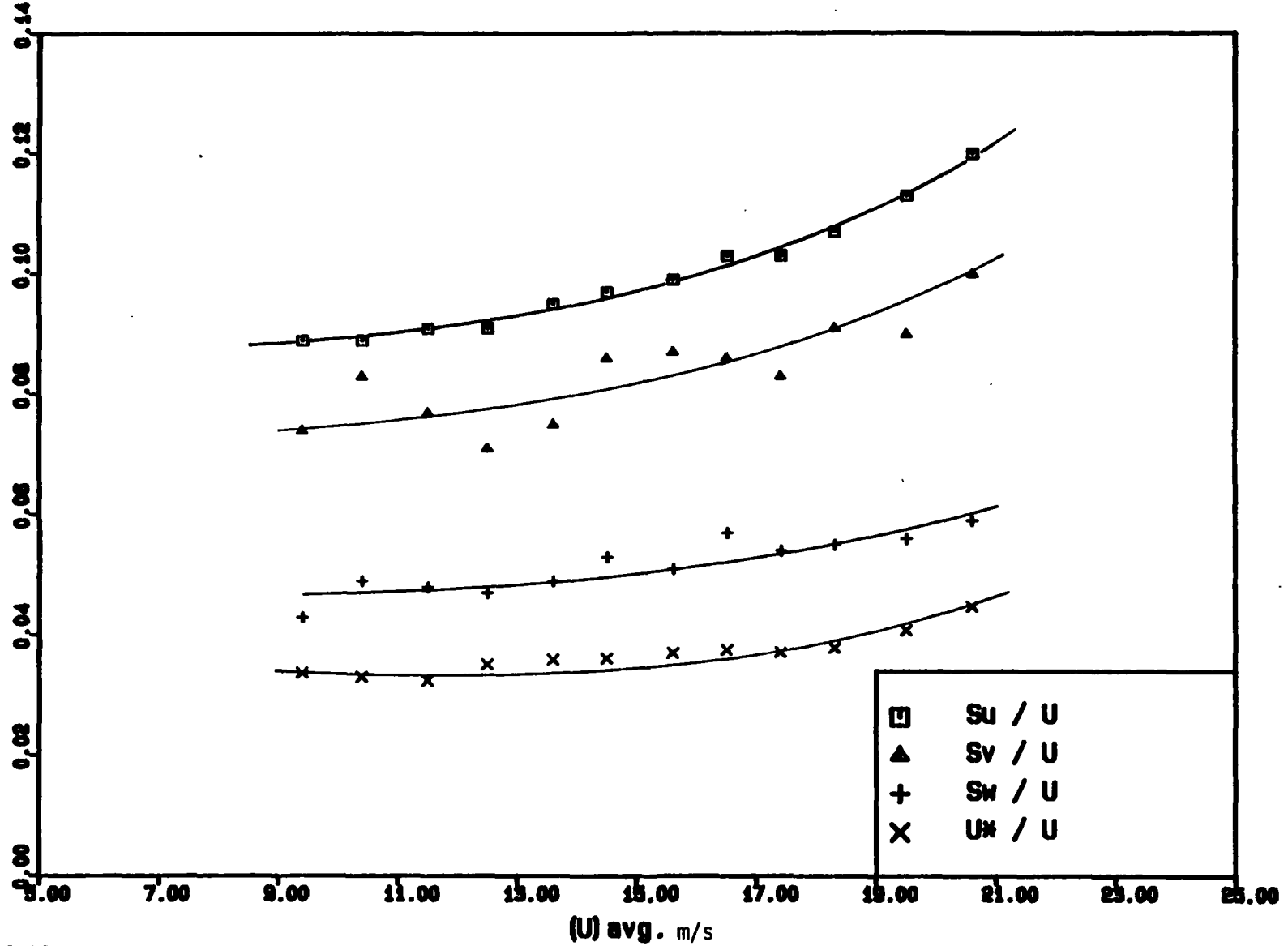

FIGURE 38 Values of σ_α/U and U*/U evaluated at z/L = 0, and obtained from the best fit of $\sigma_\alpha/U = m(z/L) + b)^\alpha$ through the data of mean velocity categories of 1 m/s intervals. Data from Reference 53, z = 13.5 m.

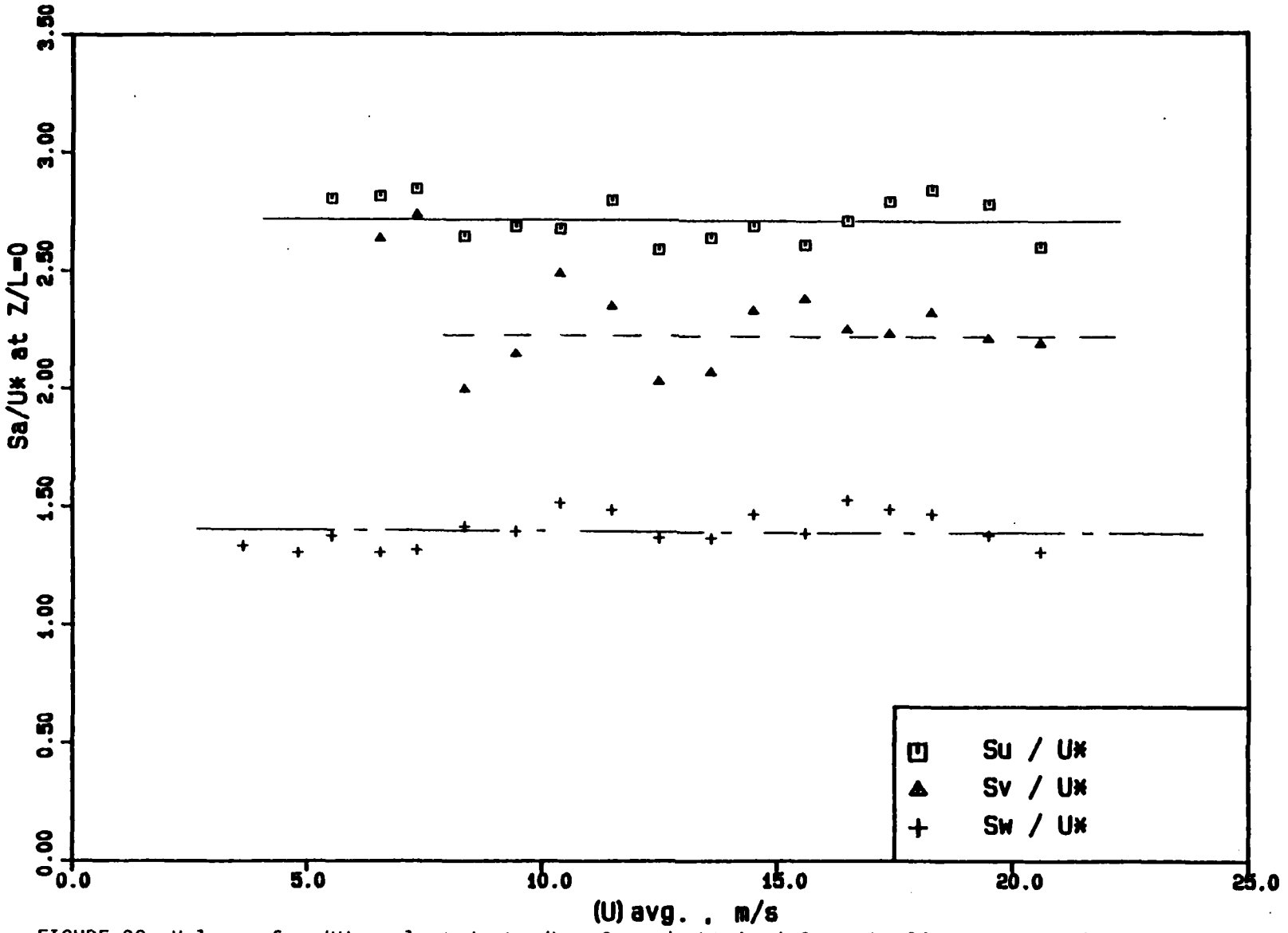

FIGURE 39 Values of σ_α/U^* evaluated at z/L = 0, and obtained from the linear regression of σ_α/U^* on z/L for the data for mean velocity categories of 1 m/s intervals. —— $(\sigma_u/U^*)_{avg} = 2.71$ --- $(\sigma_v/U^*)_{avg} = 2.22$ and — - — $(\sigma_w/U^*)_{avg} = 1.39$.

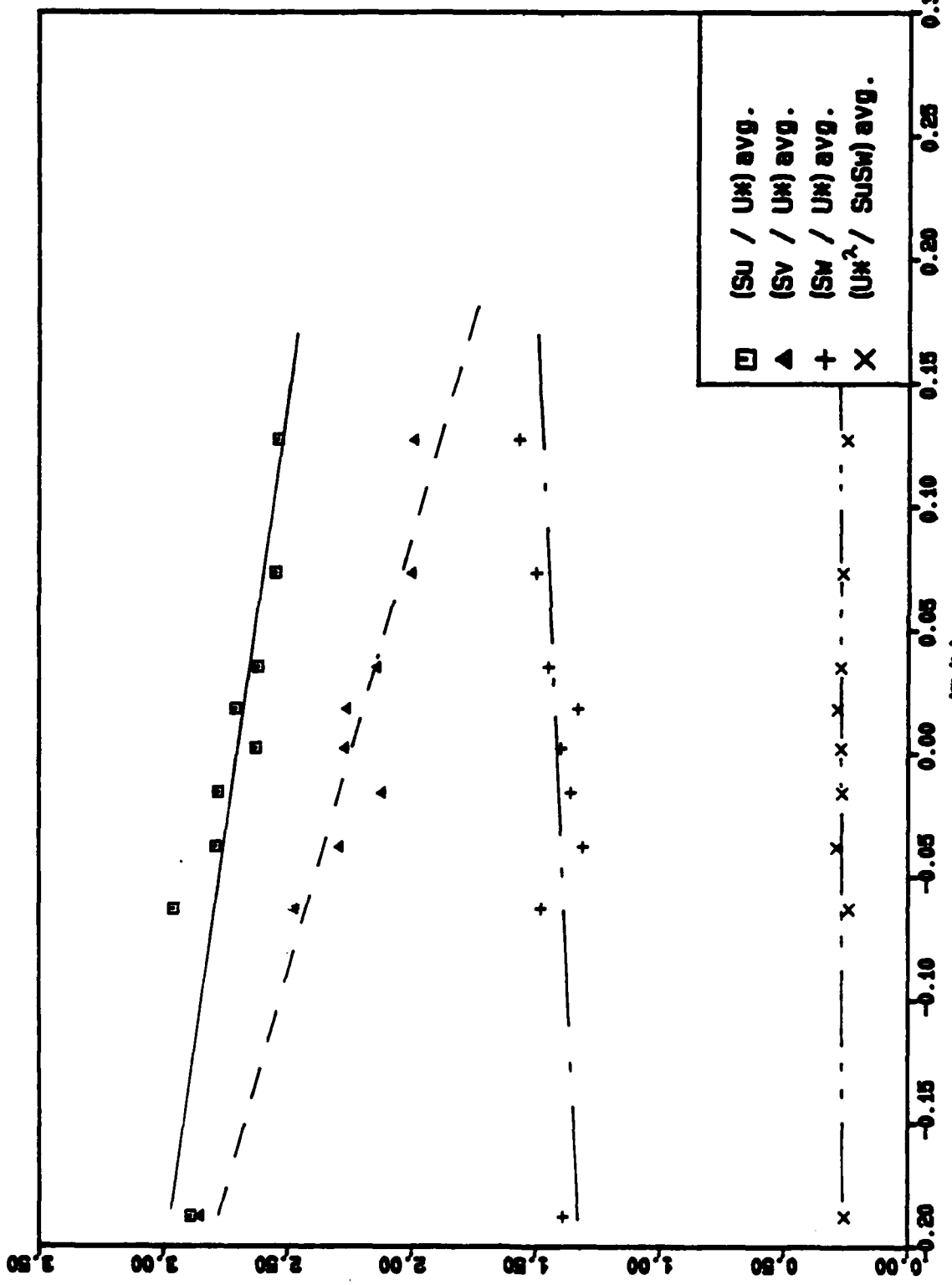

FIGURE 40 Distribution of average turbulence quantities with stability for the data of Reference 53, Z = 13.5 m. ——— $(\sigma_u/U^*)_{avg} = 2.71 - 1.41\ (z/L)_{avg}$ — — — $(\sigma_v/U^*)_{avg} = 2.25 - 2.83(z/L)_{avg}$ — - — $(\sigma_w/U^*)_{avg} = 1.42 + 0.49(z/L)_{avg}$ ——— — — ——— $(U^{*2}/\sigma_u\sigma_w)_{avg} = 0.266 + 0.018(z/L)_{avg}$.

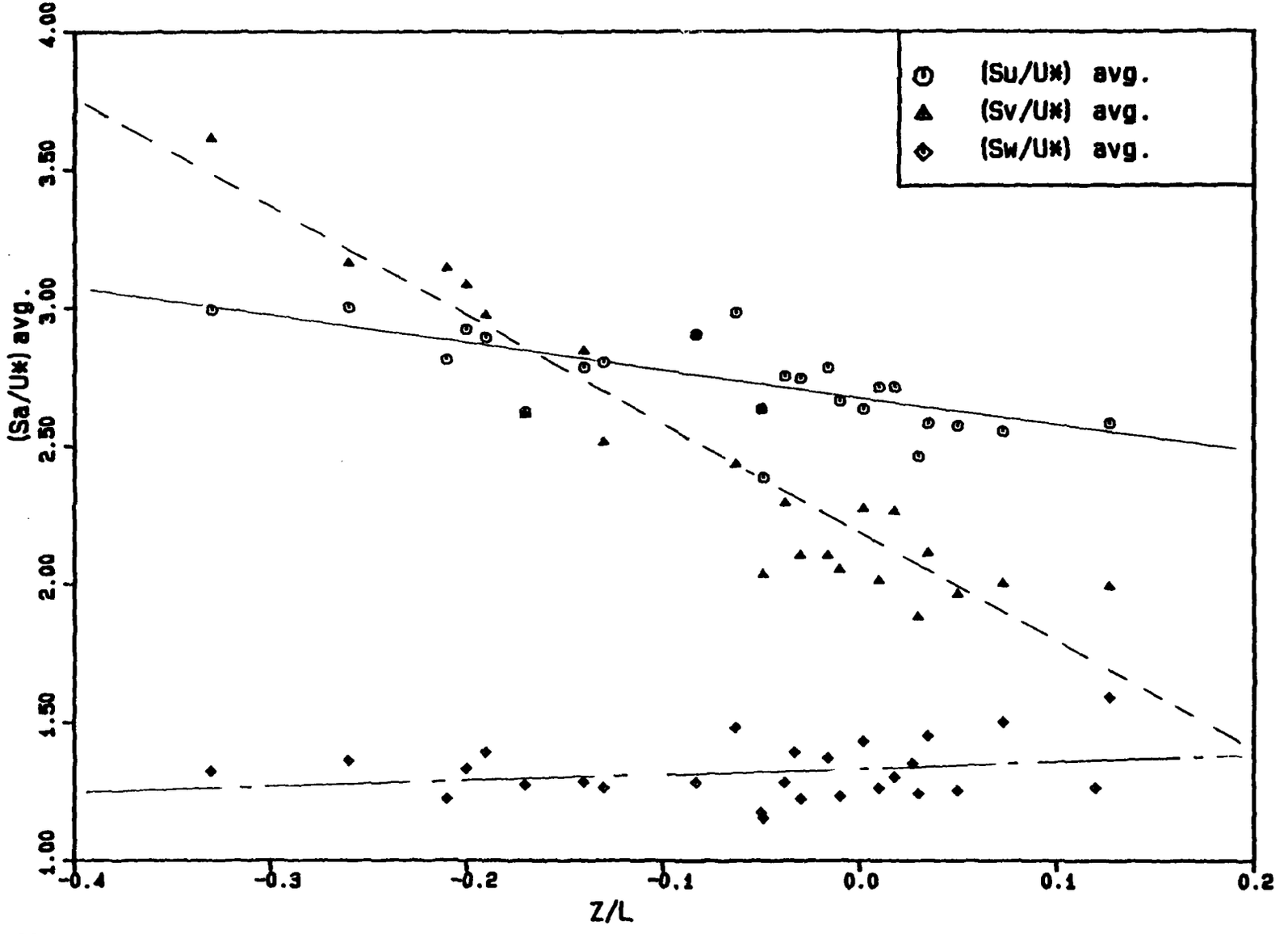

FIGURE 41 Average values of σ_α/U^* versus z/L for observations between z = 8 m and z = 13.5 m

——— $(\sigma_u/U^*)_{avg} = 2.66 - 1.04\ (z/L)_{avg}$

- - - - - - - $(\sigma_v/U^*)_{avg} = 2.19 - 3.93\ (z/L)_{avg}$

— -- — $(\sigma_w/U^*)_{avg} = 1.33 + 0.20\ (z/L)_{avg}$

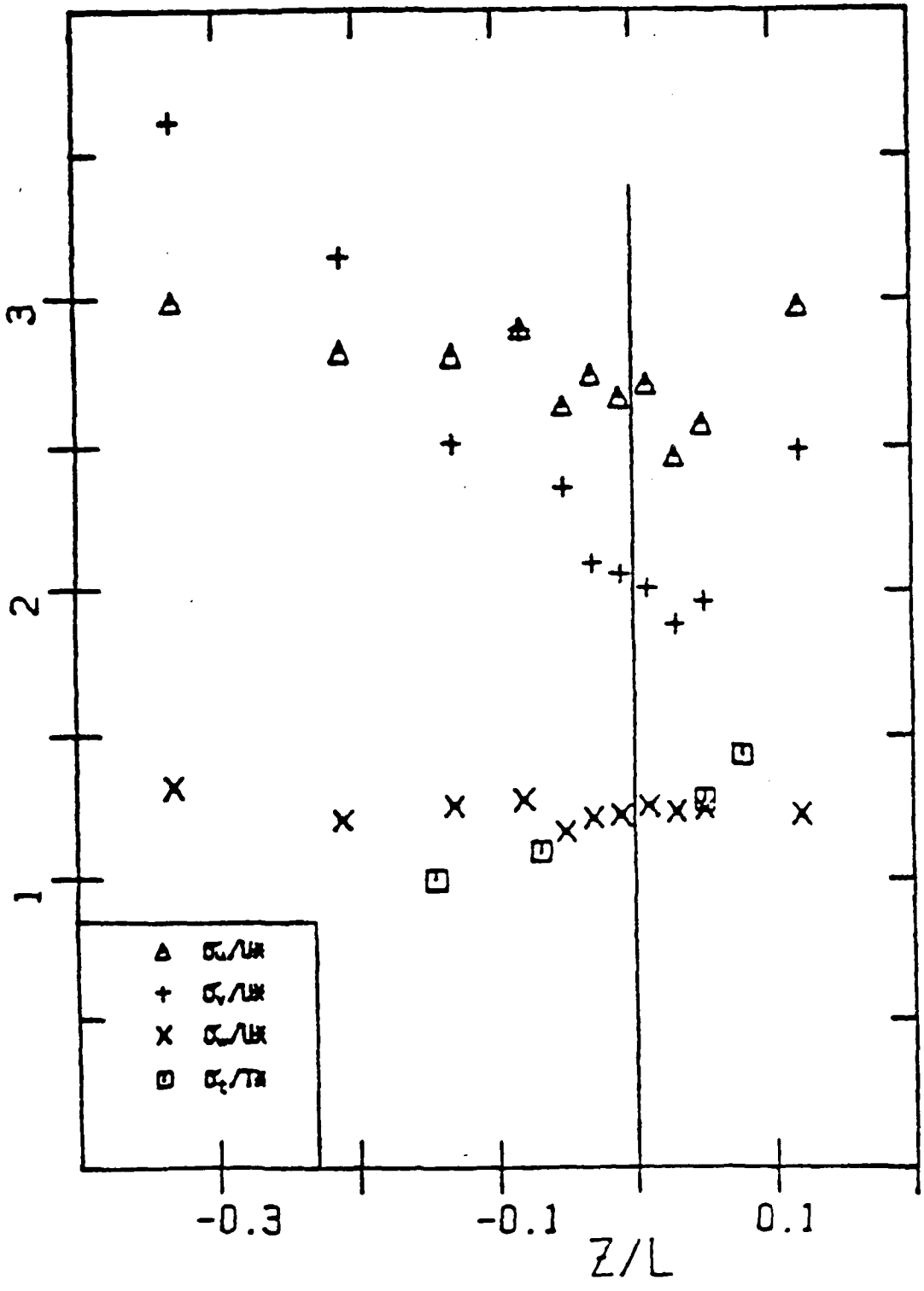

FIGURE 42 Average values of σ_α/U^* versus z/L from Reference 51, Fig. 18. Average values at zero stability are 2.63, 2.19 and 1.25 for α = u, v and w respectively.

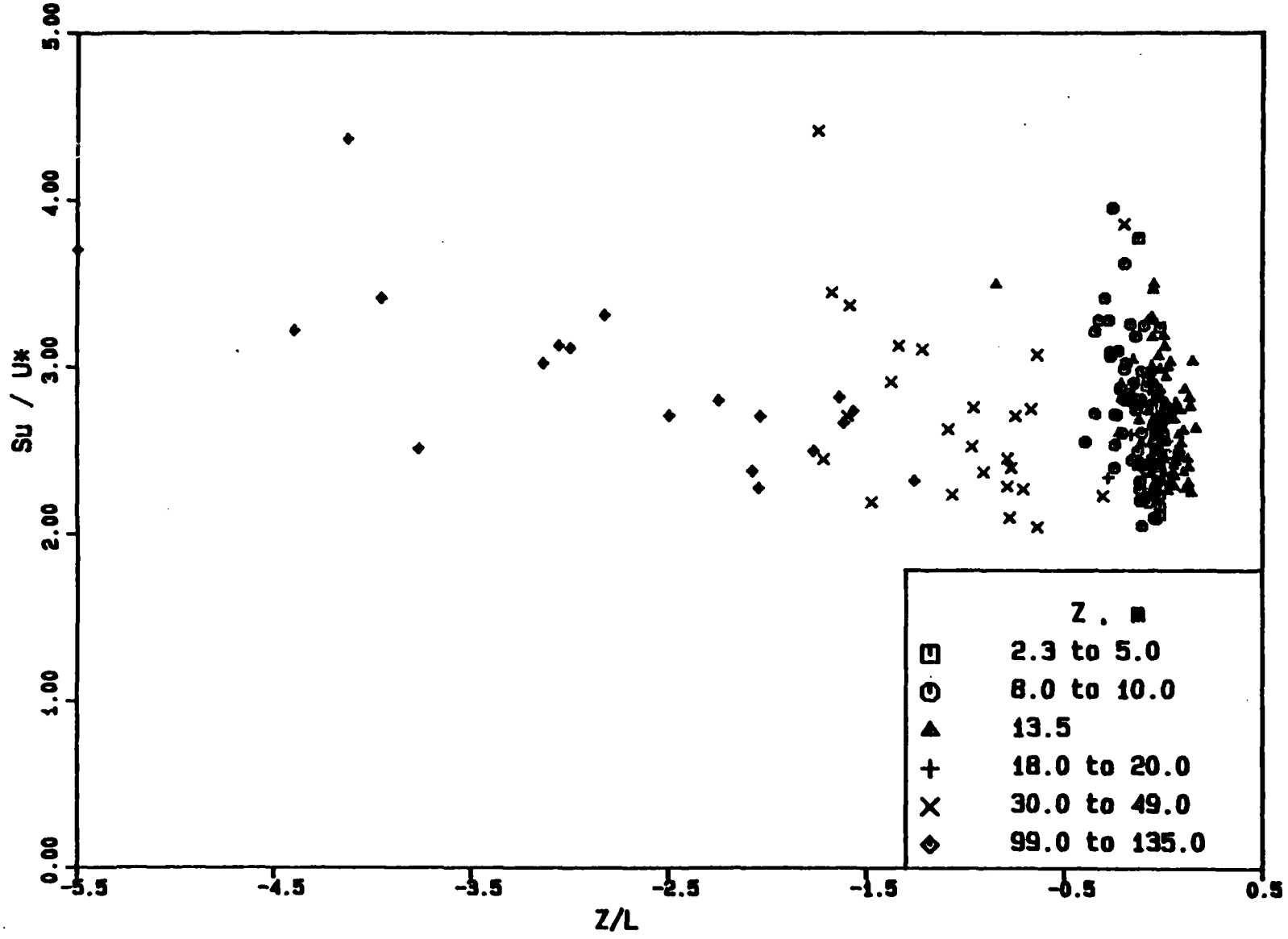

FIGURE 43 Variation of σ_u/U^* versus z/L for all observations below 150 m.

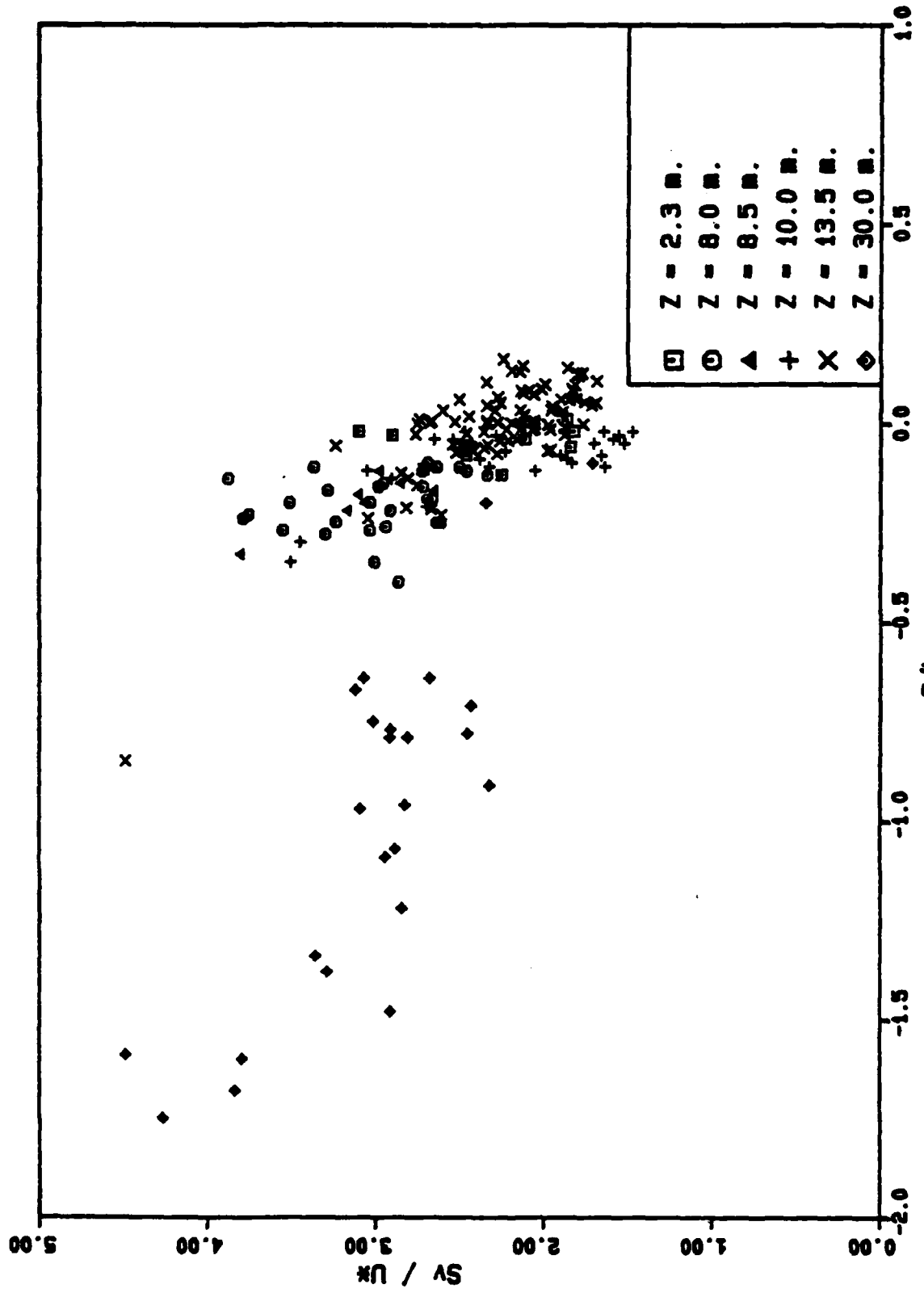

FIGURE 44 Variation of σ_v/U^* versus z/L for all observations below 150 m.

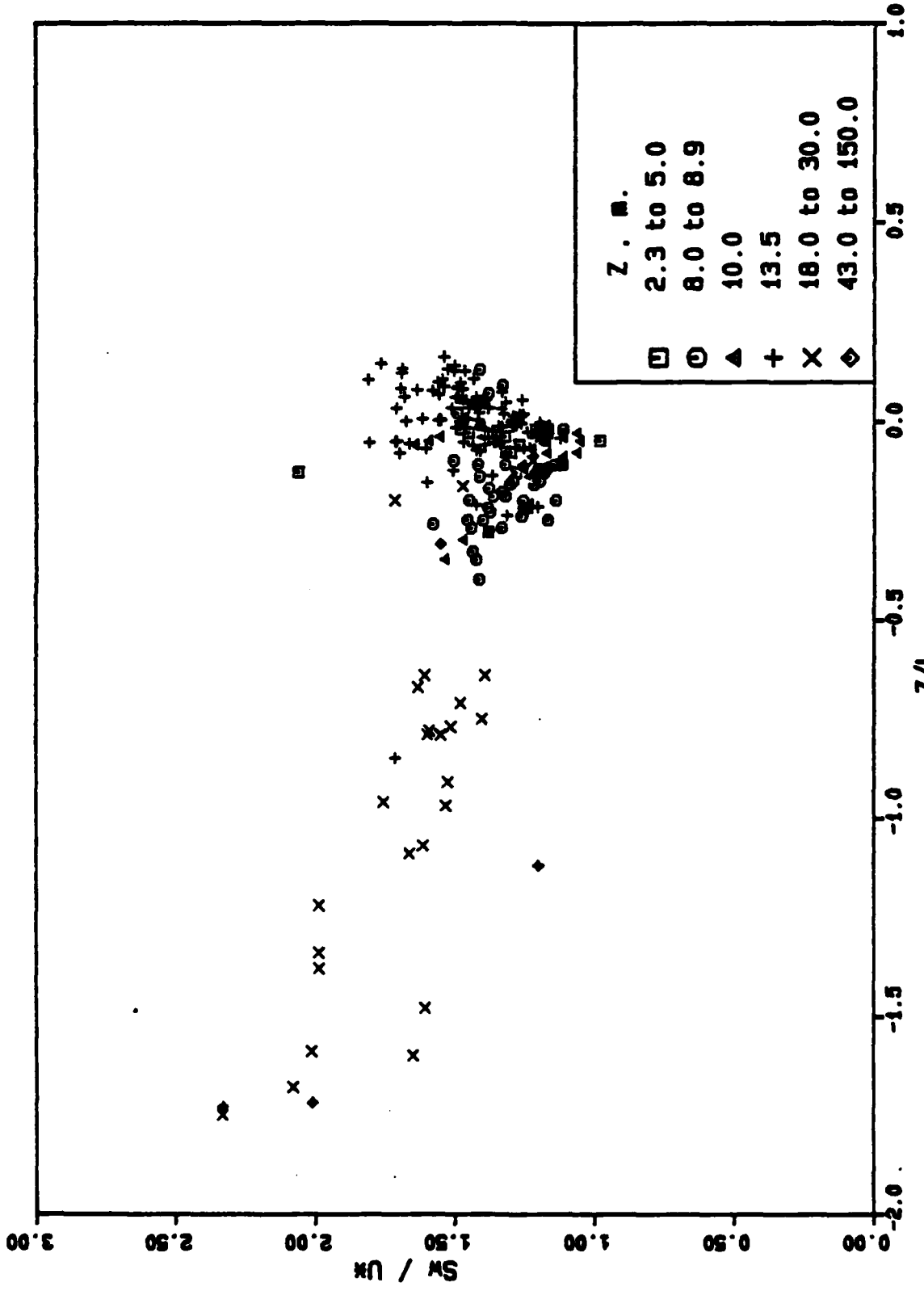

FIGURE 45 Variation of σ_w/U^* versus z/L for all observations below 150 m.

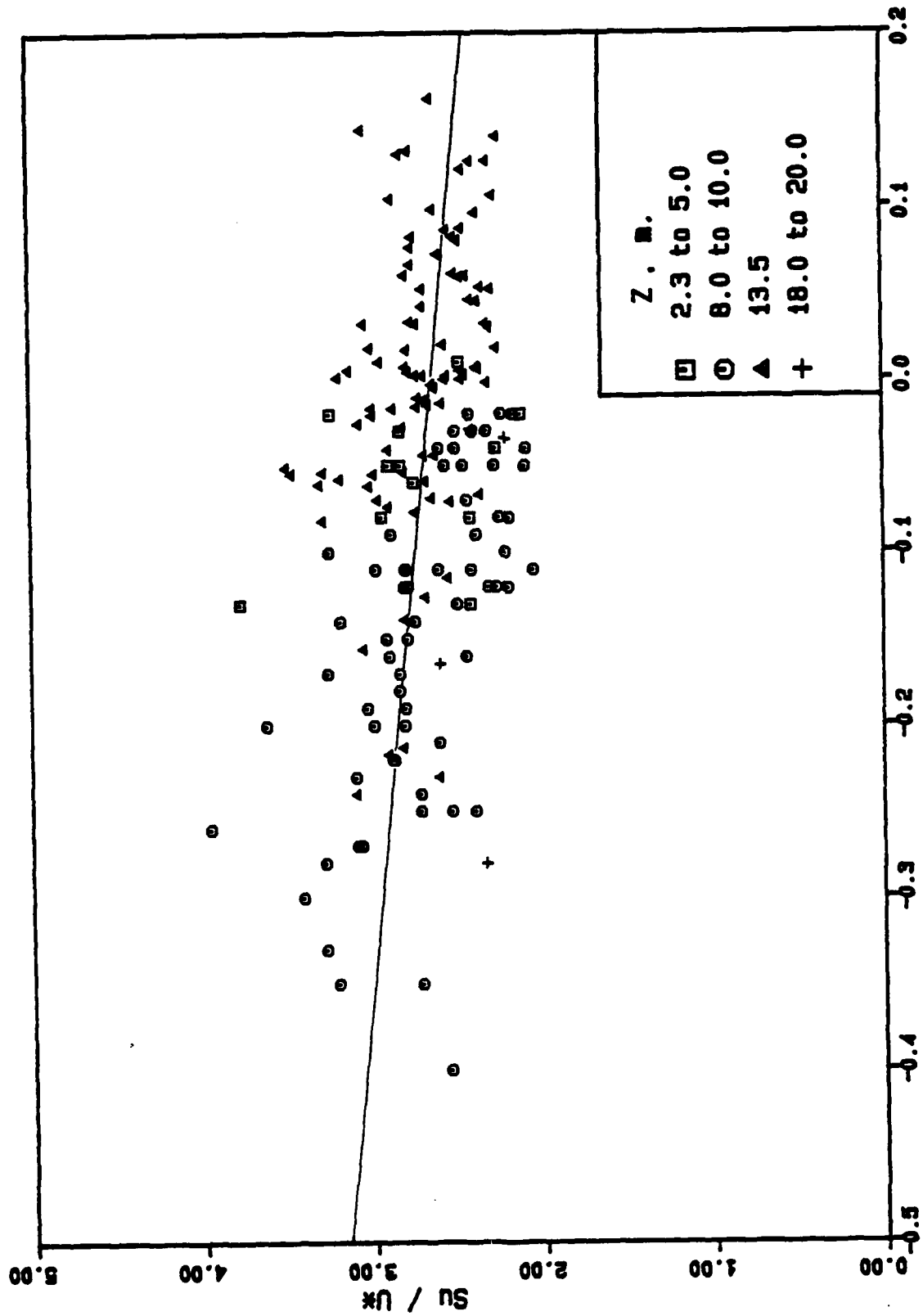

FIGURE 46 Variation of σ_u/U^* versus z/L in the surface layer ($z \leq 20$ m). Linear regression line $\sigma_u/U^* = 2.64 - 1.023$ z/L.

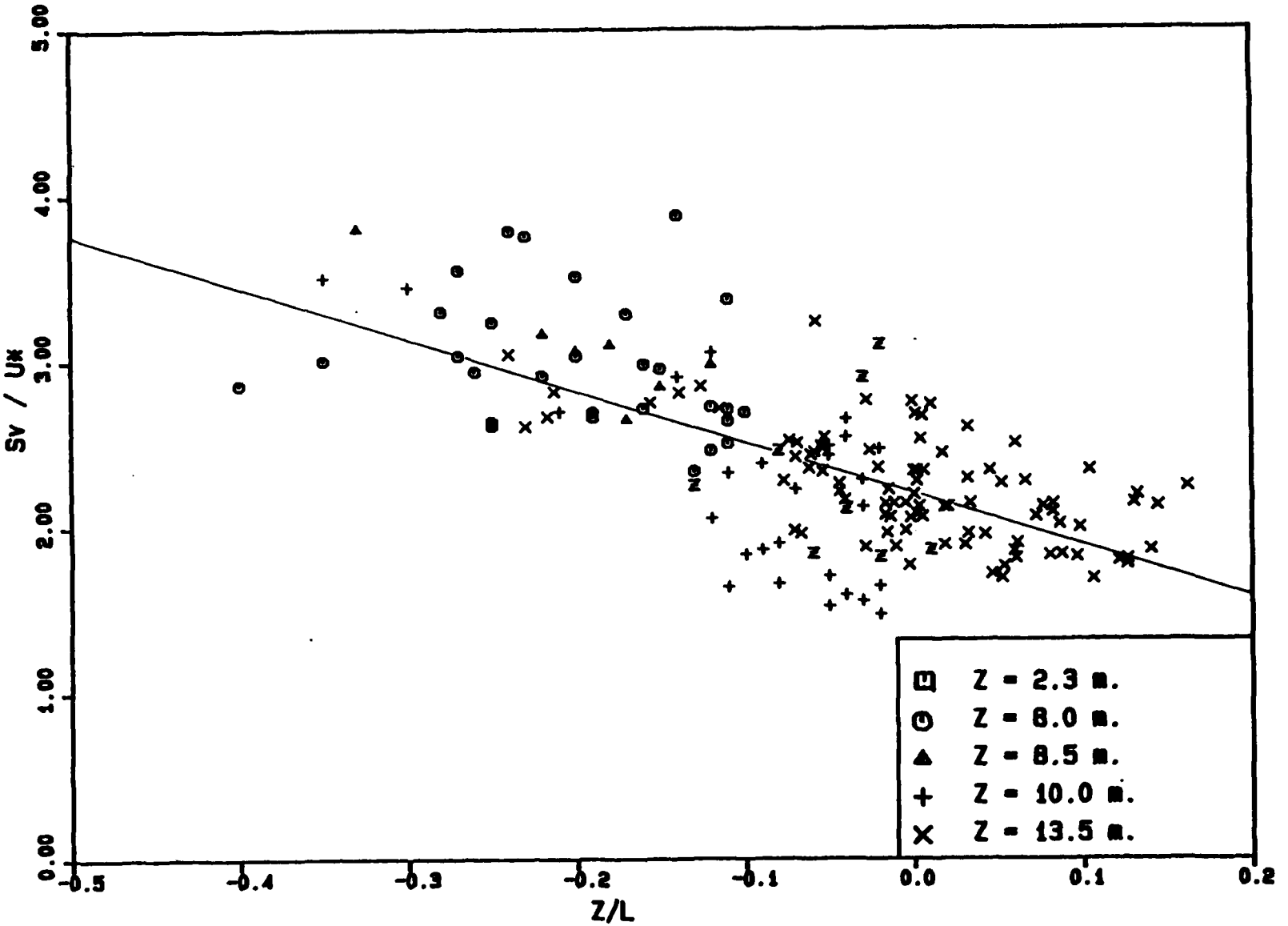

FIGURE 47 Variation of σ_v/U^* versus z/L in the surface layer ($z \leq 13.5$ m). Linear regression line $\sigma_v/U^* = 2.22 - 3.09\ z/L$.

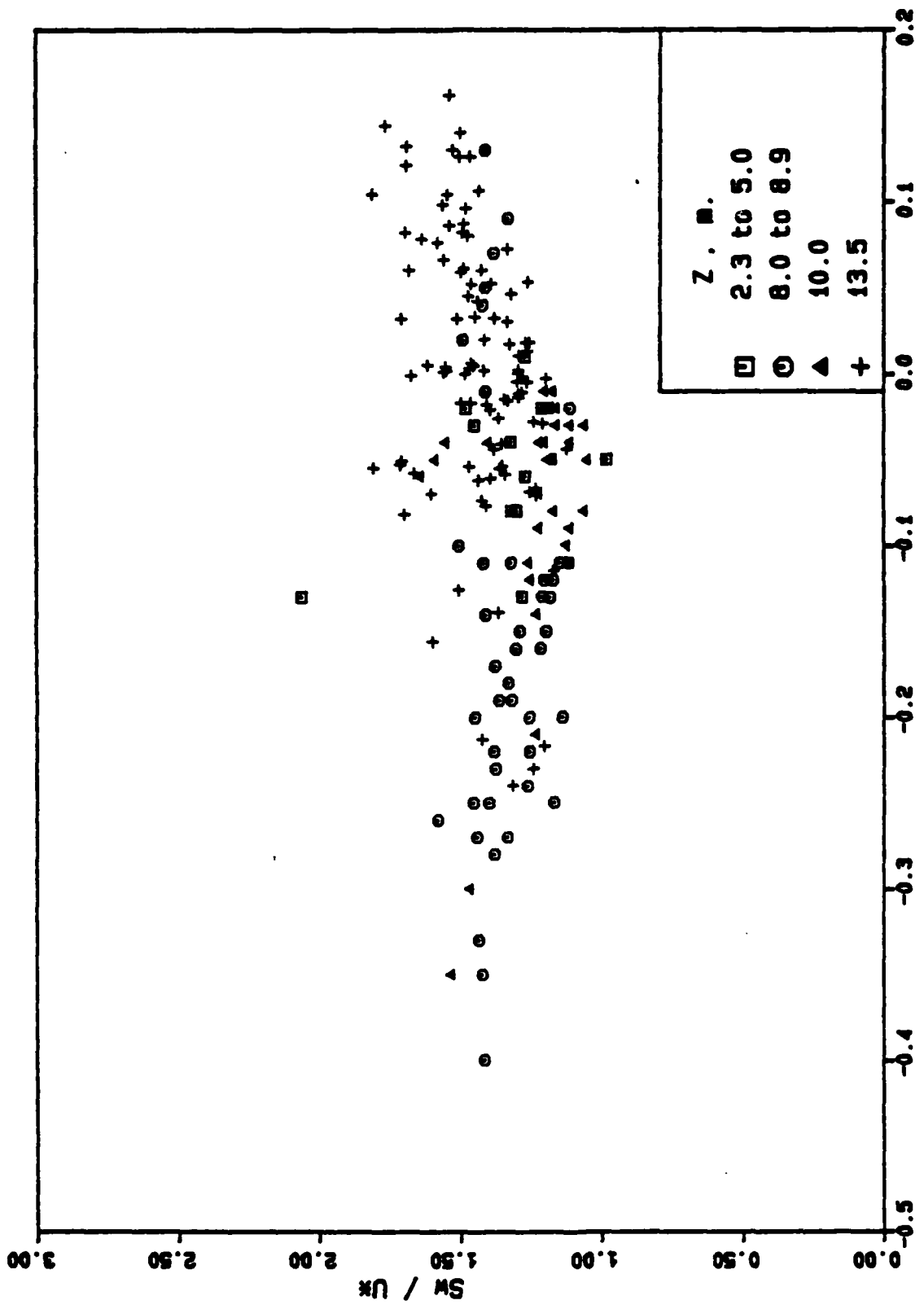

FIGURE 48 Variation of σ_w/U^* versus z/L in the surface layer ($z \leq 13.5$ m).

TABLE 1 Summary of the data sets

Ref.	Location	Country	Instruments	Platform	z/L minimum	z/L maximum	U, m/s max.	U, m/s min.	z,m	Number of Observations Analyzed U	U*	σ_u	σ_v	σ_w	Method for Obtaining U*
37	Sagami Bay	Japan	Cup Anemometer	Fixed Tower	Near Neutral		8.3		1.9	1	1	1	-	-	Velocity Profile
38	Mediterranean	-	Sonic Anemometer	Floating Mast	Near Neutral		8.9	4.0	2.0	19	19	19	-	19	Eddy Correlation
39 40	Tidal Flat	Vancouver Canada	Cup Anemometer & Sonic Anemometer	Fixed Masts	-1.3	+0.01	8.6	3.9	2.3 avg.	8	8	8	8	8	Eddy Correlation & Profile
16	Burrard Inlet	Vancouver, Canada	Sonic Anemometer	Fixed Masts	Slightly Unstable		6.4	3.5	2.7 avg.	5	5	5	-	5	Eddy Correlation & Inertial Dissipation
41	Burrard Inlet	Vancouver, Canada	Thrust Anemometer	Fixed Masts	Near Neutral		12	7	5.0	8	8 Averages taken from Fig. 13 of text	8	-	8	Eddy Correlation
37	Sagami Bay	Japan	Cup Anemometer	Fixed Tower	Near Neutral		9.2		5.0	1	1	1	-	-	Velocity Profile
15	Bass Strait	Victoria Australia	Hot Wire Anemometer	Fixed Drilling Platform	-0.16	-0.04	9.4	5.3	5.0	4	4	4	-	4	Eddy Correlation
42	Bass Strait	Victoria Australia	Hot Wire Anemometer	Fixed Drilling Platform	Slightly Unstable		9	5	5.0	Averages taken from text (12 Hours)					Eddy Correlation
43	Lake Ontario	U.S.	Sonic Anemometer	Fixed Mast	-0.05	+0.01	6.3	3.3	5.2	12	12	12	-	12	Eddy Correlation
44	Atlantic	Barbados	Sonic Anemometer	F.L.I.P.	-0.40	-0.11	7.2	3.9	8.1	12	12	12	12	12	Eddy Correlation & Inertial Dissipation
45	Atlantic	Barbados	Sonic Anemometer	F.L.I.P.	-0.35	-0.10	7.5	5.1	8.0	17	17	17	17	15	Eddy Correlation
22	Pacific	San Diego U.S.	Sonic Anemometer	Fixed Tower	-0.4	-0.05	7.2	5.5	8.0	6	6	-	-	-	Eddy Correlation & Inertial Dissipation
46	Atlantic	Long Island U.S.	Bivane	Fixed Mast	Neutral		-	-	8.0	Average of σ_u/U taken from text					-----
47	Lake Flevo	Netherlands	Trivane	Fixed Mast	-0.09	-0.01	10.3	7.8	8.4	33	30	33	-	-	Eddy Correlation
44	Pacific	San Diego U.S.	Sonid Anemometer	F.L.I.P.	-0.20	-0.12	6.6	4.8	8.5	3	3	3	3	3	Eddy Correlation & Inertial Dissipation
	Atlantic	Barbados	Sonic Anemometer	F.L.I.P.	-0.33	-0.15	6.8	5.0	8.6	4	4	4	4	4	
43	Lake Ontario	U.S.	Sonic Anemometer	Fixed Mast	-0.13	+0.13	9.5	2.9	8.9	13	13	13	-	13	Eddy Correlation

TABLE 1 (Continued)

Ref.	Location	Country	Instruments	Platform	z/L minimum	z/L maximum	U, m/s max.	U, m/s min.	z,m	Number of Observations Analyzed U	U*	σ_u	σ_v	σ_w	Method for Obtaining U*
37	Sagami Bay	Japan	Cup Anemometer	Fixed Tower	Near Neutral		9.4		9.4	1	1	1	-	-	Velocity Profile
43	Lake Ontario	U.S.	Thrust Anemometer	Fixed Mast	Near Neutral		10.0	4.4	9.6	8	8	8	-	8	Eddy Correlation
43	Lake Ontario	U.S.	Sonic Anenometer	Fixed Mast	-0.06	-0.01	7.8	5.3	10.0	7	7	7	-	7	Eddy Correlation
43	Lake Ontario	U.S.	Sonic and Thrust Anemometers	Fixed Mast	Near Neutral		---		10.0	Averages of σ_α/U (α=u,v and w) taken from text					-----
13	Atlantic	Barbados	Hot-Film Anemometer	F.L.I.P.	Near Neutral		---		10.0	Averages of σ_α/U^* (α=u,v and w) taken from text					Eddy Correlation
48	Atlantic	Sable Island Canada	Thrust Anemometer	Mast on Beach	-0.35	-0.02	6.1	21.2	10.0	30	30	27	26	29	Eddy Correlation
17	Atlantic	Sable Island Canada	Sonic Anemometer Thrust Anemometer Gill Anemometer	Mast on Beach	Mixed		15.1	5.6	10.0	28	25	25	24	28	Eddy Correlation
25	North Sea Atlantic	Great Britain	Vane and Pitot Tube	Airplane	-0.12	-0.01	21.0	5.6	10.0	10	10	-	-	-	Eddy Correlation
49	Atlantic	Long Island U.S.	Bivane	Fixed Mast	---		27.0	2.0	10.0	Averages of σ_α/U (α=u,v and w) taken from text					-----
37	Sagami Bay	Japan	Cup Anemometer	Fixed Tower	Slightly Unstable		9.0	4.0	11.5	4	-	4	-	-	-----
50	Atlantic	Halifax, Canada	Thrust Anemometer Anemometer	Stable Platform	Mostly Stable		15.9	6.7	11.7 avg.	19	19	19	18	19	Eddy Correlation
51,52	Atlantic	Halifax Canada	Propeller-Vane Anemometer	Stable Platform	-0.45	+0.18	19.3	6.1	13.0	195	195	-	-	-	Eddy Correlation & Inertial Dissipation
										Averages of σ_α/U and σ_α/U^* (α=u,v and w) taken from text.					
53	Atlantic	Halifax Canada	Thrust Anemometer	Stable Platform	-0.85	+0.16	22.6	6.2	13.5	114	108	107	106	112	Eddy Correlation
50	Atlantic	Halifax, Canada	Thrust Anemometer	Stable Platform	Mixed		10.7	7.5	13.6	12	12	12	12	12	Eddy Correlation
54	Atlantic	Long Island U.S.	Bivane	Mast on Beach	Stable		10.8	2.5	16.0	17	-	17	17	8	-----

TABLE 1 (Continued)

Ref.	Location	Country	Instruments	Platform	z/L minimum	z/L maximum	U, m/s max.	U, m/s min.	z,m	Number of Observations Analyzed U	U*	σ_u	σ_v	σ_w	Method for Obtaining U*
55	Atlantic	Long Island U.S.	Bivane	Mast on Beach	Stable			---	16.0	Averages of σ_α|U (α=u,v and w) taken from text					----- -----
56	East China Sea	---	Sonic Anemometer	Ship	Weakly Unstable		5.0		18.0	1	1	1	-	1	Eddy Correlation
57	Atlantic	Barbados	Hot Wire and Sonic Anemometer	Airplane	-0.034		10.0		18.0	1	1	1	-	1	Eddy Correlation
58	Atlantic	Barbados	Hot Wire and Sonic Anemometer	Airplane	-0.16		8.5		18.3	1	1	1	-	1	Eddy Correlation
37	Sagami Bay	Japan	Cup Anemometer	Fixed Tower	Slightly Unstable		16.8	7.5	20.0	11	-	11	-	-	-----
57	Atlantic	Barbados	Hot Wire and Sonic Anemometer	Airplane	-0.28		5.0		20.0	1	1	1	-	1	Eddy Correlation
37	Sagami Bay	Japan	Cup Anemometer	Fixed Tower	Slightly Unstable		10.2		21.4	1	1	1	-	-	Velocity Profile
56	East China Sea	---	Sonic Anemometer	Ship	Weakly Unstable		9.1	3.9	24.0	4	4	4	-	4	Eddy Correlation
59	North Pacific	---	Sonic Anemometer	F.L.I.P.	-0.71	+0.27	11.8	5.5	29.0	18	18	-	-	-	Eddy Correlation
28	Atlantic	Puerto Rico	Vanes and Pitot Tube	Airplane	-0.2	-0.1	14.8	12.8	30.0	1	1	1	1	1	Eddy Correlation
45	Atlantic	Barbados	Sonic Anemometer	F.L.I.P.	-1.75	-0.64	7.7	5.4	30.0	22	22	22	22	22	Eddy Correlation
60	Atlantic	Wallops Island, U.S.	Cup-Vane and Hot Film Anemometer	Tower on Beach	Mixed		15.3	5.9	30.5	55	5	55	55	5	Eddy Correlation
61	Lake Huron	---	Gust Probe	Airplane	-1.29			---	31.0	-	1	1	-	-	Eddy Correlation
61	Carribbean	---	Gust Probe	Airplane	-0.08			---	30.0	-	1	1	-	-	Eddy Correlation
57	Atlantic	Barbados	Hot Wire and Sonic Anemometer	Airplane	-1.72		5.4		43.0	1	1	1	-	1	Eddy Correlation
60	Atlantic	Wallops Island, U.S.	Cup-Vane and Hot Film Anemometer	Tower on Beach	Mixed		17.0	5.9	45.7	52	2	52	52	3	Eddy Correlation

TABLE 1 (Continued)

Ref.	Location	Country	Instruments	Platform	z/L minimum	z/L maximum	U, m/s max.	U, m/s min.	z,m	Number of Observations Analyzed U	U*	σ_u	σ_v	σ_w	Method for Obtaining U*
57	Atlantic	Barbados	Hot Wire and Sonic Anemometer	Airplane	-0.31		10.8		49.0	1	1	1	-	1	Eddy Correlation
60	Atlantic	Wallops Island, U.S.	Cup-Vane and Hot Film Anemometer	Tower on Beach	Mixed		19.0	6.1	61.0	55	4	55	55	4	Eddy Correlation
60	Atlantic	Wallops Island, U.S.	Cup-Vane and Hot-Film Anemometer	Tower on Beach	Mixed		20.6	6.1	76.2	54	4	54	54	5	Eddy Correlation
28	Atlantic	Puerto Rico	Gust Probe	Airplane	-0.2	-0.1	16.0	14.8	90.0	2	-	2	2	2	-----
61	East China Sea	---	Gust Probe	Airplane	-4.13	-1.62	---		99.0	-	7	7	-	-	Eddy Correlation
61	East China Sea	---	Gust Probe	Airplane	-5.05	-1.57	---		110.0	-	6	6	-	-	Eddy Correlation
61	East China Sea	---	Gust Probe	Airplane	-3.77	-1.26	---		135.0	-	6	6	-	-	Eddy Correlation
57	Atlantic	Barbados	Hot Wire and Sonic Anemometer	Airplane	-1.73	-1.2	11.8	6.1	150.0	2	2	2	-	2	Eddy Correlation
28	Atlantic	Puerto Rico	Gust Probe	Airplane	-0.2	-0.1	16.5		200	3	-	3	3	3	-----

Table 2 Turbulence ratios σ_u/U^* and A_u

z,m	$(\frac{\sigma_u}{U^*})_{avg}$	± S.D.	$\sigma_u = A_u U^*$ A_u	S.D.	σ_u/U^* z/L = o	n	References	Stability U, N, S	Body of Water
1.9	2.69	0.39	2.64	0.10	-	20	37, 38	U	Ocean and Bay
2.3	2.70	0.25	2.69	0.04	2.81	8	39, 40	U	Coastal Inlet
2.7	3.06	0.42	3.00	0.05	-	5	16	U	Coastal Inlet
5.0	-	-	2.53	-	-	8	41	N	Coastal Inlet
5.0	2.88	0.05	2.92	-	-	5	15,37	U	Ocean and Bay
5.0	2.90	-	-	-	-	-	42	U	Ocean
8.0	2.88	0.39	2.83	0.09	2.65	29	44, 45	U	Ocean
8.4	2.33	0.23	2.32	-	2.28	30	47	U	Lake
8.5	2.92	0.17	2.89	0.04	2.45	7	44	U	Ocean
9.4	2.72	-	-	-	-	1	37	N	Bay
10.0	-	-	-	-	2.43	-	13	N	Ocean
10.0	2.42	0.21	2.48	0.08	-	52	17, 48	N	Ocean Beach
11.7	2.46	0.30	2.49	0.15	-	19	50	S	Ocean
13.0	-	-	-	-	2.68	-	51, 52	N	Ocean
13.5	2.63	0.25	2.60	0.14	2.70	19	53	N	Ocean
16.0	2.60	0.7	-	-	-	41	55	S	Ocean Beach
18.0	2.47	-	-	-	-	1	56	U	Ocean
18.0	2.21	-	-	-	-	1	57	U	Ocean
18.3	2.61	-	-	-	-	1	58	U	Ocean
20.0	2.34	-	-	-	-	1	57	U	Ocean
21.4	2.42	-	-	-	-	1	37	U	Bay
24.0	3.11	0.3	3.20	-	-	5	56	U	Ocean
30.0	2.75	0.6	2.72	0.12	-	24	28, 45	U	Ocean
30.5	2.29	0.22	2.39	-	-	5	60	S	Ocean Beach
30.5	2.61	-	-	-	-	2	61	U	Ocean and Lake
43.0	2.45	-	-	-	-	1	57	U	Ocean
45.7	2.40	-	-	-	-	3	60	S	Ocean Beach
49.0	2.23	-	-	-	-	1	57	U	Ocean
61.0	2.66	-	2.16	-	-	5	60	S	Ocean Beach
76.2	2.83	-	2.05	-	-	5	60	S	Ocean Beach
99.0	3.15	0.64	3.05	-	-	7	61	U	Ocean
110.0	3.05	0.38	2.98	-	-	6	61	U	Ocean
135.0	2.53	0.28	2.51	-	-	6	61	U	Ocean
150.0	2.05	-	-	-	-	2	57	U	Ocean

A_u is the slope of the straight line of best fit also through origin.

$$\frac{\sigma_u}{U^*} = m(\frac{z}{L}) + b$$

for $\frac{z}{L} = 0$ $\frac{\sigma_u}{U^*} = b$

Stability:
- U Unstable
- N Near Neutral
- S Stable
- n Number of Observations

Table 3 Turbulence ratios σ_v/U^* and A_v

z, m	$(\frac{\sigma_v}{U^*})_{avg}$	± S.D.	$\sigma_v = A_v U^*$ A_v	S.D.	σ_v/U^* z/L = o	n	References	Stability U, N, S	Body of Water
2.3	2.40	0.44	2.23	0.08	2.37	8	39, 40	U	Coastal Inlet
8	2.99	0.42	2.94	0.10	2.71	29	44, 45	U	Ocean
8.5	3.08	0.36	3.03	0.07	2.16	7	44	U	Ocean
10.0	--	--	--	--	1.70	-	--	N	Ocean
10.0	1.88	0.32	2.12	0.16	--	52	17, 48	N	Ocean Beach
11.7	2.08	0.38	2.04	0.12	--	19	50	S	Ocean
13.0	--	--	--	--	2.03	-	51,52	N	Ocean
13.5	2.27	0.28	2.28	0.18	2.24	19	53	N	Ocean
16.0	2.0	0.8	--	--	--	41	55	S	Ocean Beach
30.0	3.01	0.6	2.70	0.14	--	24	28, 45	U	Ocean
30.5	1.75	0.24	1.83	--	--	5	60	S	Ocean Beach
45.7	2.20	--	--	--	--	3	60	S	Ocean Beach
61.0	2.25	--	--	--	--	5	60	S	Ocean Beach
76.2	2.21	--	1.76	--	--	5	60	S	Ocean Beach

A_v is the slope of the straight line of best fit also through origin.

$\frac{\sigma_v}{U^*} = m\,(z/L) + b$

for $\frac{z}{L} = 0$ $\frac{\sigma_v}{U^*} = b$

Stability:

U Unstable

N Near Neutral

S Stable

n Number of observations

Table 4 Turbulence ratios σ_w/U^* and A_w

z,m	$(\frac{\sigma_w}{U^*})_{avg}$	± S.D.	$\sigma_w = A_w U^*$ A_w	S.D.	σ_w/U^* z/L = o	n	References	Stability U, N, S	Body of Water
1.9	1.51	0.23	1.52	0.06	-	19	37, 38	U	Ocean
2.3	1.40	0.09	1.39	0.02	1.43	8	39, 40	U	Coastal Inlet
2.7	1.36	0.12	1.30	0.02	-	5	16	U	Coastal Inlet
5.0	-	-	1.41	-	-	8	41	N	Coastal Inlet
5.0	1.45	0.55	1.19	-	-	5	15,37	U	Ocean and Bay
5.0	1.30	-	-	-	-	-	42	U	Ocean
5.2	1.22	0.07	1.19	-	1.20	12	43	N	Lake
8.0	1.32	0.12	1.30	0.03	1.20	29	44, 45	U	Ocean
8.5	1.33	0.08	1.31	0.02	1.14	7	44	U	Ocean
8.9	1.34	0.12	1.37	-	1.32	13	43	N	Lake
9.6	1.18	0.09	1.19	-	-	8	43	N	Lake
10.0	1.39	0.21	1.35	-	1.06	7	43	U	Lake
10.0	-	-	-	-	1.20	-	13	N	Ocean
10.0	1.21	0.10	1.17	0.04	1.07	55	17, 48	N	Ocean Beach
11.7	1.28	0.17	1.27	0.07	-	19	50	S	Ocean
13.0	1.24	0.10	-	-	1.25	196	51, 52	N	Ocean
13.5	1.43	0.14	1.40	0.09	1.43	19	53	N	Ocean
16.0	1.40	0.5	-	-	-	41	55	S	Ocean Beach
18.0	1.59	-	-	-	-	1	56	U	Ocean
18.0	1.19	-	-	-	-	1	57	U	Ocean
18.3	1.47	-	-	-	-	1	58	U	Ocean
20.0	1.38	-	-	-	-	1	57	U	Ocean
24.0	1.68	0.15	-	1.67	-	-	56	U	Ocean
30.0	1.68	0.26	1.58	0.05	-	24	28, 45	U	Ocean
30.5	1.27	0.11	1.32	-	-	5	60	S	Ocean Beach
43.0	2.01	-	-	-	-	1	57	U	Ocean
45.7	1.50	-	-	-	-	3	60	S	Ocean Beach
49.0	1.55	-	-	-	-	1	57	U	Ocean
61.0	1.45	-	-	-	-	5	60	S	Ocean Beach
76.2	1.41	-	-	-	-	5	60	S	Ocean Beach

A_w is the slope of the straight line of best fit also through origin.

$$\frac{\sigma_w}{U^*} = m(\frac{z}{L}) + b$$

for $\frac{z}{L} = 0$ $\frac{\sigma_w}{U^*} = b$

Stability:
- U Unstable
- N Near Neutral
- S Stable
- N Number of observations

TABLE 5

Turbulence Intensities, σ_u/U

z, m	$(\frac{\sigma_u}{U})_{avg}$	±SD	m'u	SD	m_u	b_u	SD	σ_u/U for z/L~0	n	References	Stability U, N, S	Velocity range (m/s)		Body of Water
1.9	0.117	0.011	0.116	0.079	0.114	+0.009	0.079	-	20	38	U	4.0	9.0	Ocean and Bay
2.7	0.104	0.010	0.106	0.050	0.132	-0.124	0.040	-	5	16	U	3.5	6.4	Coastal Inlet
5.0	0.079	-	-	-	-	-	-	-	8	41	N	7.0	12.0	Coastal Inlet
5.0	0.102	0.009	0.101	-	0.092	+0.075	-	-	5	15, 37	U	5.3	9.4	Ocean and Bay
8.0	0.105	0.012	0.104	0.070	0.088	+0.103	0.069	0.105	29	44, 45	U	3.9	7.5	Ocean
8.0	-	-	-	-	-	-	-	0.090	-	46	N	-	-	Ocean
8.4	0.090	0.009	0.092	-	0.140	-0.559	-	0.096	33	47	U	10.1	14.5	Lake
8.5	0.113	0.007	0.112	0.042	0.079	+0.198	0.032	0.102	7	44	U	4.8	6.8	Ocean
9.4	0.084	-	-	-	-	-	-	-	1	37	U	9.4	-	Bay
10.0	0.097	0.018	-	-	-	-	-	-	19	43	-	-	-	Lake
10.0	0.078	0.004	-	-	-	-	-	-	6	43	-	-	-	Lake
10.0	0.079	0.011	-	-	-	-	-	-	13	43	-	-	-	Lake
10.0	0.081	0.009	-	-	-	-	-	-	39	43	-	-	-	Ocean
10.0	0.080	0.008	0.080	0.058	0.092	-0.098	0.057	0.079	33	17, 48	N	5.6	10.0	Ocean Beach
10.0	0.102	0.012	0.106	0.166	0.145	-0.584	0.101	-	26	17, 48	N	10.0	21.2	
10.0	-	-	0.080	-	-	-	-	-	-	49	N	U <	12.0	Ocean
10.0	-	-	-	-	0.20	-1.5	-	-	-	49	N	U >	12.0	
11.5	0.114	0.021	0.104	-	0.049	0.376	-	-	4	37	-	4.0	10.0	Bay
11.7	0.086	0.007	0.086	0.068	0.091	-0.055	0.068	-	14	50	S	6.7	11.5	Ocean
11.7	0.101	0.011	0.103	0.168	0.185	-1.147	0.111	-	5	50	S	11.5	15.9	
13.0	0.092	0.018	-	-	-	-	-	-	195	51, 52	Mixed	6.0	19.3	Ocean
13.5	0.095	0.007	0.099	0.129	0.134	-0.545	0.079	-	19	53	N	10.1	20.0	Ocean
16.0	0.065	0.027	0.059	0.163	0.035	+0.164	0.154	-	17	54	S	2.5	10.8	Ocean Beach

TABLE 5 (CONTINUED)

Turbulence Intensities, σ_u/U

z,m	$(\frac{\sigma_u}{U})_{avg}$ ±SD		m_u	SD	m_u	b_u	SD	σ_u/U for z/L~0	n	References	Stability U, N, S	Velocity range (m/s)		Body of Water
18.0	0.084	-	-	-	-	-	-	-	1	56	N	5.0	-	Ocean
18.0	0.075	-	-	-	-	-	-	-	1	57	U	10.0	-	Ocean
18.3	0.070	-	-	-	-	-	-	-	1	58	U	8.5	-	Ocean
20.0	0.093	0.017	0.093	-	0.096	-0.04	-	-	11	37	U	7.5	16.8	Bay
21.4	0.069	-	-	-	-	-	-	-	1	37	-	10.2	-	Bay
24.0	0.100	0.009	0.105	-	0.097	0.055	-	-	5	56	U	4.0	9.0	Ocean
30.0	0.075	0.01	0.077	0.094	0.096	-0.153	0.085	0.073	24	28, 45	U	5.4	14.8	Ocean
30.5	0.071	0.010	0.073	0.089	0.103	-0.277	0.071	-	13	60	U			
30.5	0.070	0.006	0.071	0.070	0.081	-0.110	0.066	-	15	60	N	5.9	15.3	Ocean Beach
30.5	0.060	0.008	0.061	0.073	0.076	-0.135	0.066	-	27	60	S			
43.0	0.070	-	-	-	-	-	-	-	1	57	U	5.4	-	Ocean
45.7	0.065	0.009	0.067	0.084	0.098	-0.292	0.062	-	13	60	U			
45.7	0.063	0.006	0.064	0.087	0.069	-0.064	0.086	-	14	60	N	5.9	17.0	Ocean Beach
45.7	0.051	0.008	0.051	0.081	0.059	-0.080	0.078	-	25	60	S			
49.0	0.055	-	-	-	-	-	-	-	1	57	U	10.8	-	Ocean
61.0	0.062	0.006	0.063	0.067	0.083	-0.193	0.055	-	13	60	U			
61.0	0.058	0.007	0.059	0.107	0.064	-0.066	0.105	-	14	60	N	6.1	19.0	Ocean Beach
61.0	0.043	0.009	0.043	0.091	0.042	+0.018	0.091	-	27	60	S			
76.2	0.058	0.007	0.060	0.071	0.083	-0.233	0.055	-	13	60	U			
76.2	0.054	0.008	0.055	0.122	0.059	-0.057	0.121	-	14	60	N	6.1	20.6	Ocean Beach
76.2	0.038	0.009	0.038	0.098	0.042	0.046	0.097	-	27	60	S			
90.0	0.058	-	-	-	-	-	-	-	2	28	U	14.8	16.0	Ocean

m'_u is the slope of the straight line ($\sigma_u = m'_u U$) of best fit through the origin.
m_u and b_u are the slope and intercept of the straight line ($\sigma_u = m_u U + b_u$) of best fit
Stability: U Unstable
N Near Neutral
S Stable
n Number of Observations

TABLE 6

Turbulence Intensities, σ_v/U

z,m	$(\frac{\sigma_v}{U})_{avg}$	±SD	m'_v	SD	m_v	b_v	SD	σ_v/U for z/L~0	n	References	Stability U, N, S	Velocity range (m/s)		Body of Water
8.0	0.110	0.019	0.108	0.114	0.063	0.103	0.069	0.108	29	44, 45	U	2.9	7.5	Ocean
8.5	0.120	0.015	0.117	0.082	0.043	0.442	0.058	0.091	7	44	U	4.8	6.8	Ocean
10.0	0.093	0.030	-	-	-	-	-	-	19	43	-	-	-	Lake
10.0	0.078	0.040	-	-	-	-	-	-	6	43	-	-	-	Lake
10.0	0.066	0.012	-	-	-	-	-	-	13	43	-	-	-	Lake
10.0	0.067	0.014	-	-	-	-	-	-	39	43	-	-	-	Ocean
10.0	0.060	0.007	0.060	0.056	0.059	0.007	0.056	0.051	34	17 ,48	N	5.6	9.8	Ocean Beach
10.0	0.086	0.021	0.094	0.292	0.173	-1.203	0.104	-	26	17, 48	N	10.0	21.2	
10.0	0.080	-	-	-	-	-	-	-	-	49	-	U	< 12.0	Ocean
10.0	-	-	-	-	0.16	-1.06	-	-	-	49	-	U	> 12.0	
11.7	0.072	0.010	0.072	0.104	0.076	-0.045	0.104	-	14	50	S	6.7	11.5	Ocean
11.7	0.090	0.022	0.082	0.116	0.129	-0.663	0.084	-	4	50	S	11.5	15.9	
13.0	0.080	0.031	-	-	-	-	-	-	196	51, 52	-	6.0	19.3	Ocean
13.5	0.084	0.010	0.087	0.184	0.138	-0.826	0.130	-	19	53	N	10.1	20.1	Ocean
16.0	0.049	0.022	0.048	0.120	0.044	0.024	0.120	-	17	54	S	2.5	10.8	Ocean Beach
30.0	0.061	0.038	0.077	0.116	0.034	0.342	0.072	-	24	28, 45	U	5.4	14.8	Ocean
30.5	0.062	0.012	0.062	0.088	0.073	-0.096	0.086	-	13	60	U			
30.5	0.056	0.009	0.058	0.096	0.080	-0.248	0.079	-	15	60	N	5.9	15.3	Ocean Beach
30.5	0.049	0.009	0.051	0.092	0.070	-0.184	0.082	-	27	60	S			

TABLE 6 (CONTINUED)

Turbulence Intensities, σ_v/U

z,m	$(\frac{\sigma_v}{U})_{avg}$	±SD	m'_v	SD	m_v	b_v	SD	σ_v/U for z/L-0	n	References	Stability U, N, S	Velocity range (m/s)		Body of Water
45.7	0.058	0.011	0.058	0.080	0.068	-0.098	0.078	-	13	60	U			
45.7	0.049	0.008	0.051	0.089	0.068	-0.200	0.076	-	14	60	N	5.9	17.0	Ocean Beach
45.7	0.041	0.006	0.042	0.057	0.055	-0.131	0.048	-	25	60	S			
61.0	0.054	0.011	0.055	0.088	0.071	-0.157	0.083	-	13	60	U			
61.0	0.045	0.006	0.046	0.085	0.053	-0.087	0.083	-	14	60	N	6.1	19.0	Ocean Beach
61.0	0.035	0.007	0.036	0.080	0.044	-0.089	0.077	-	27	60	S			
76.2	0.052	0.011	0.052	0.085	0.060	-0.082	0.083	-	13	60	U			
76.2	0.042	0.007	0.043	0.104	0.045	-0.028	0.103	-	14	60	N	6.1	20.6	Ocean Beach
76.2	0.034	0.009	0.035	0.097	0.044	-0.111	0.092	-	27	60	S			
90.0	0.049	-	-	-	-	-	-	-	2	28	U	14.8	16.0	Ocean
200.0	0.036	-	-	-	-	-	-	-	2	28	U	16.5		Ocean

---

m'_v is the slope of the straight line ($\sigma_v = m'_v U$) of best fit through the origin.

m_v and b_v are the slope and intercept of the straight line ($\sigma_v = m_v U + b_v$) of best fit

Stability: U Unstable
N Near Neutral
S Stable
n Number of Observations

TABLE 7

Turbulence Intensities, σ_w/u

z,m	$(\frac{\sigma_w}{U})_{avg}$	±SD	m'_w	SD	m_w	b_w	SD	σ_w/U for z/L-0	n	References	Stability	Velocity range (m/s)		Body of Water
1.9	0.066	0.009	0.067	0.055	0.082	-0.102	0.050	-	19	38	U	4.0	9.0	Ocean
2.7	0.046	0.002	0.046	0.009	0.047	-0.003	0.009	-	5	16	U	3.5	6.4	Coastal Inlet
5.0	0.044	-	-	-	-	-	-	-	8	41	N	7.0	12.0	Coastal Inlet
5.0	0.048	0.010	0.045	-	0.013	0.241	-	-	4	15	U	5.3	9.4	Ocean
5.2	0.051	0.006	0.053	-	0.049	0.020	-	0.054	12	43	U	3.3	6.3	Lake
8.0	0.049	0.004	0.048	0.026	0.043	0.031	0.025	0.049	27	44, 45	U	3.9	7.5	Ocean
8.5	0.051	0.002	0.051	0.011	0.038	0.079	0.005	0.047	7	44	U	4.8	6.8	Ocean
8.9	0.044	0.007	0.048	-	0.060	-0.081	-	0.046	13	43	N	2.9	9.5	Lake
9.6	0.041	0.002	0.041	-	0.045	-0.029	-	-	8	43	-	4.4	10.0	Lake
10.0	0.049	0.008	0.047	-	0.009	0.243	-	0.037	7	43	U	5.3	7.8	Lake
10.0	0.044	0.007	-	-	-	-	-	-	19	43	-	-	-	Lake
10.0	0.043	0.004	-	-	-	-	-	-	6	43	-	-	-	Lake
10.0	0.042	0.009	-	-	-	-	-	-	13	43	-	-	-	Lake
10.0	0.045	0.006	-	-	-	-	-	-	39	43	-	-	-	Ocean
10.0	0.042	0.002	0.042	0.014	0.045	-0.024	0.014	0.041	33	17, 48	N	5.6	9.8	Ocean Beach
10.0	0.047	0.004	0.049	0.054	0.068	-0.18	0.036	-	26	17, 48	N	10.0	21.2	
10.0	0.046	-	-	-	-	-	-	-	-	49	O	U <	12.0	Ocean
10.0	0.053	-	-	-	-	-	-	-	-	49	-	U >	12.0	
11.7	0.046	0.005	0.046	0.049	0.041	0.047	0.049	-	14	50	S	6.7	11.5	Ocean
11.7	0.050	0.001	0.050	0.016	0.041	0.120	0.009	-	5	50	S	11.5	15.0	
13.0	0.046	0.006	-	-	-	-	-	-	196	51, 52	N	5.8	18.2	Ocean
13.5	0.053	0.006	0.054	0.086	0.072	-0.299	0.072	-	19	53	N	10.0	20.1	Ocean
16.0	0.031	0.020	0.033	0.125	0.087	-0.307	0.116	-	8	55	S	2.5	10.8	Ocean Beach
18.0	0.054	-	-	-	-	-	-	-	1	56	N	5.0		Ocean
18.0	0.040	-	-	-	-	-	-	-	1	57	U	10.0		Ocean

TABLE 7 (CONTINUED)

Turbulence Intensities, σ_w/u

z,m	$(\frac{\sigma_w}{U})_{avg}$	±SD	m'_w	SD	m_w	b_w	SD	σ_w/U for z/L-0	n	References	Stability	Velocity range (m/s)		Body of Water
18.3	0.039	-	-	-	-	-	-	-	1	58	U	8.5		Ocean
20.0	0.062	-	-	-	-	-	-	-	1	57	U	5.0		Ocean
24.0	0.053	0.007	0.055	-	0.059	-0.025	-	-	5	56	U	4.0	9.0	Ocean
30.0	0.046	0.003	0.045	0.031	0.036	0.073	0.024	0.046	24	28, 45	U	5.4	14.8	Ocean
30.5	0.032	0.006	-	-	-	-	-	-	5	60	S	6.0	9.3	Ocean Beach
43.0	0.057	-	-	-	-	-	-	-	1	57	U	5.4		Ocean
45.7	0.025	-	-	-	-	-	-	-	3	60	S	6.2	10.4	Ocean Beach
49.0	0.038	-	-	-	-	-	-	-	1	57	U	10.8		Ocean
61.0	0.024	-	-	-	-	-	-	-	4	60	S	6.5	11.4	Ocean Beach
76.2	0.020	-	-	-	-	-	-	-	5	60	S	6.7	10.8	Ocean Beach
90.0	0.036	-	-	-	-	-	-	-	2	28	U	14.8	16.0	Ocean

---

m'_w is the slope of the straight line ($\sigma_w = m'_w U$) of best fit through the origin.

m_w and b_w are the slope and intercept of the straight line ($\sigma_w = m_w U + b_w$) of best fit

Stability: U Unstable
N Near Neutral
S Stable
n Number of Observations

TABLE 8

Variation of σ_α with Velocity Below and Above the Critical Wind Speed

Reference	z,m	Velocity Range m/s	$\sigma_\alpha = m_\alpha U + b_\alpha$		$\sigma_\alpha = m'_\alpha U$	Body of Water
			m_u	b_u	m'_u	
47	8.4	10.1-14.5	0.140	-0.559	-	Lake Flavo, The Netherlands
17,48	10.0	5.6-10.0	0.092	-0.098	0.080	Atlantic Ocean,
		10.0-21.2	0.145	-0.584	-	Sable Island
49	10.0	<12.0	-	-	0.08	Atlantic Ocean
		>12.0	0.20	-1.5	-	5 km off Long Island
50	11.7	6.7-11.5	0.091	-0.055	0.086	Atlantic Ocean
		11.5-15.9	0.185	-1.15	-	
53	13.5	10.1-20.0	0.134	-0.545	-	Atlantic Ocean
			m_v	b_v	m'_v	
17,48	10	5.6-9.8	0.059	0.007	0.060	Atlantic Ocean
		10.0-21.2	0.173	-1.20	-	Sable Island
49	10	<12.0	-	-	0.08	Atlantic Ocean
		>12.0	0.16	-1.06	-	5 km off Long Island
50	11.7	6.7-11.5	0.076	-0.045	0.072	Atlantic Ocean
		11.5-15.9	0.129	-0.663	-	
53	13.5	10.1-20.1	0.138	-0.826	-	Atlantic Ocean
			m_w	b_w	m'_w	
17,48	10	5.6-9.8	0.045	-0.024	0.042	Atlantic Ocean
		10.0-21.2	0.068	-0.18	-	Sable Island
49	10	<12.0	-	-	0.046	Atlantic Ocean
		>12.0	-	-	0.053	5 km off Long Island
50	11.7	6.7-11.5	0.041	0.047	0.046	Atlantic Ocean
		11.5-15.0	0.041	0.120	0.050	
53	13.5	10.0-20.1	0.072	-0.299	0.054	Atlantic Ocean

TABLE 9

Turbulence Intensities, σ_α/U, for Mean Wind Speeds in Excess of the Critical Wind Speed

z,m	Intensities σ_α/U, %	Mean Velocity, U, m/s 10	12	14	16	18	20	References
8.4	σ_u/U	8.4	9.3	10.0	-	-	-	47
10.0	σ_u/U	8.7	9.6	10.3	10.9	11.3	11.6	17.48
	σ_v/U	6.0	7.3	8.7	9.8	10.6	11.3	
	σ_w/U	5.0	5.3	5.5	5.7	5.8	5.9	
10.0	σ_u/U	8.0	7.5	9.3	10.6	11.7	12.5	49
	σ_v/U	8.0	7.2	8.4	9.4	10.1	10.7	
	σ_w/U	4.6	5.3	5.3	5.3	5.3	5.3	
11.7	σ_u/U	8.6	8.9	10.3	11.3	-	-	50
	σ_v/U	7.2	7.4	8.2	8.8	-	-	
13.5	σ_u/U	8.0	8.9	9.5	10.0	10.4	10.7	53
	σ_v/U	5.5	6.9	7.9	8.6	9.2	9.7	
	σ_w/U	4.2	4.7	5.1	5.3	5.5	5.7	

TABLE 10

Summary of the turbulence intensities in the high-velocity range. Results are based on curve fits of the data presented in Figures 33 through 35. ($z = 13.5$ m)

U, m/s	Turbulence Component	Stability, Z/L		
		-0.2	0.0	+0.2
10	σ_u/U	10.6	8.6	6.6
13		11.6	9.6	7.6
16		12.2	10.2	8.2
19		12.8	10.8	8.6
10	σ_v/U	10.0	7.1	4.2
13		10.4	7.8	5.2
16		10.6	8.2	5.8
19		10.9	8.7	6.5
10	σ_w/U	4.8	4.5	4.2
13		5.0	4.95	4.9
16		5.3	5.35	5.4
19		5.4	5.6	5.8

TABLE 11

Summary of the Turbulence Ratios σ_α/U^* α = u, v and w

Source	σ_u/U^*	σ_v/U^*	σ_w/U^*
Fig. 39	2.71	2.22	1.39
Fig. 40	2.71	2.25	1.42
Fig. 41	2.66	2.19	1.33
Ref. 51 z = 13 m	2.63	2.19	1.25
$\lvert z/L \rvert < 0.1$ $z \leq 20$ m	2.64	2.17	1.37
Suggested averages over water	2.67	2.20	1.38
Suggested averages over land [11]	2.39	1.92	1.25

Water: $\frac{\sigma_u}{\sigma_w} = 1.93$ $\frac{\sigma_v}{\sigma_w} = 1.59$

Land: $\frac{\sigma_u}{\sigma_w} = 1.91$ $\frac{\sigma_v}{\sigma_w} = 1.54$

TABLE 12

Turbulence Integral Scales Measured Over Water

Height z,m	Scale	Magnitude, m	Reference
15	L_x^u	60 - 150	60
30	L_x^u	90 - 240	60
40	L_x^u	204	64
40	L_x^w	32	65
40	L_y^w	13	65
40	L_y^u	50	64
15	L_z^u	20 - 40	60
30	L_z^u	20 - 50	60
15	L_z^v	10 - 20	60
30	L_z^v	20 - 30	60
40*	L_x^w	14 - 20	67
40*	L_y^u	32	67
40*	L_y^v	35	67

*Integral scales obtained from spectra measured by aircraft.

END

FILMED

6-85

DTIC